PHARMACOKINETICS OF RESVERATROL, ITS MONOCONJUGATES AND ITS TRIMETHOXY ANALOG TMS

A Dissertation
Submitted to
the Temple University Graduate Board

In Partial Fulfillment
of the Requirements for the Degree
DOCTOR OF PHILOSOPHY

By
Satish Sharan
May, 2013

Examining Committee Members:

Dr. Swati Nagar, Advisory Chair, Pharmaceutical Sciences
Dr. Michael Borenstein, Pharmaceutical Sciences
Dr. Kenneth Korzekwa, Pharmaceutical Sciences
Dr. Cheryl L. Zimmerman, External Member, University of Minnesota

ABSTRACT

Resveratrol (RES) has been associated with numerous pharmacological effects. Yet its pharmacokinetics is not clearly understood. It is known to get extensively metabolized into its sulfated and glucuronidated metabolites and has very low circulating RES concentrations in plasma. Although the concentrations of conjugated metabolites of RES have been reported to be much greater than that of RES, they have not been evaluated. This also becomes important in light of positive biological activities reported for sulfated metabolites of RES. Conjugation is a complex process which can sometimes be a reversible process and needs comprehensive evaluation to better understand RES and its metabolites' disposition. There has been a debate among the researchers regarding the differences in kinetics of preformed versus *in vivo* formed metabolites in the light of guidelines issued by regulatory bodies regarding metabolites in safety testing (MIST). We have addressed the above questions in this work, in addition to evaluating brain permeability of a potent RES analog, trimethoxy-trans-stilbene (TMS).

Chapter 1 presents a detailed introduction, hypothesis and significance of my work. Chapter 2 includes the development and validation of a bioanalytical method for quantitation of RES and its metabolites on LC/MS/MS. We were able to develop and validate a robust bioanalytical method to quantitate RES and its four major metabolites resveratrol-4'-glucuronide (R4'G), resveratrol-3-glucuronide (R3G), resveratrol-4'-sulfate (R4'S) and resveratrol-3-sulfate (R3S).

In Chapter 3, lung as a possible metabolizing organ for RES was evaluated. This study was performed *in vivo* in mouse model using multiple site of administration and single site of sampling approach. *In vitro* studies were also performed to confirm the *in vivo* results. Inter species differences in RES pulmonary metabolism were also studied. We observed lungs to be the major metabolizing organs for RES with inter species differences in its metabolism.

Chapter 4 provides detailed pharmacokinetics of sulfated metabolites of RES, i.e. resveratrol-3-sulfate (R3S) and resveratrol-4'-sulfate (R4'S) in mouse model by both systemic and oral routes. *In vitro* studies were also conducted to test the desulfation in liver. Although we did not observe any significant RES in plasma, we observed from our *in vitro* studies that sulfated metabolites were desulfated in liver.

Chapter 5 explains the detailed pharmacokinetics of glucuronidated metabolites of RES i.e. resveratrol-3-glucuornide (R3G) after both systemic and oral route. R3G was observed to undergo enterohepatic circulation. Explanation of R3G disposition in hepatocytes and enterocytes were proposed based on our own and reported results.

In Chapter 6 we compared the differences in the kinetics of preformed versus *in vivo* formed metabolites using modeling and simulation approach. Individual models for disposition of RES, R3S and R3G were developed. These models were combined to give a global model for RES metabolism into R3S and R3G. Simulations were performed under two assumptions; preformed versus *in vivo* formed metabolite kinetics a) are same

and b) they are not same. Our results reported that preformed and *in vivo* formed metabolite kinetics are not same at least for hydrophilic phase II metabolites.

Chapter 7 includes method development and validation for quantitation of TMS in plasma and brain of mouse. Chapter 8 includes a steady state study to characterize the pharmacokinetic parameters of TMS, which was used to evaluate brain permeability of TMS.

In summary we developed a robust bioanalytical method for direct quantitation of RES and its metabolites, found the lung to be a major metabolizing organ for RES, delineated complex kinetics of conjugated metabolites of RES, and showed differences in preformed versus *in vivo* formed metabolite kinetics and better brain permeability of TMS.

ACKNOWLEDGEMENTS

There are very few decisions in our lives, which make us happy and proud about the choices we make for ourselves. The decision to pursue PhD at Temple University has been one of them. My journey in the pursuit of PhD at Temple began in Fall 2007 and from the beginning it had been an adventurous and rewarding one. It will be my honor to express my deepest gratitude towards people who have made this day possible for me.

At the outset, I would like to express my deepest gratitude towards my advisor Dr. Swati Nagar. This dissertation would not have been possible without her immense support and mentoring. She provided me with complete freedom in terms of creativity which was critical in development of my scientific skills. She had been a true inspiration to me as a scientist and as a leader. I still remember the conversation we had about PhD, when she made me realize that "PhD is not a doctorate in pharmacokinetics, it is in philosophy. It is given that you will do well in science but PhD is more than that. It should help you become a philosopher, thinker, leader and better citizen." Today, I get to realize the significance of her words. I truly value the opportunity to work with her and consider myself fortunate to have worked under her mentorship.

I would like to extend my heartfelt gratitude to all my thesis committee members, Dr. Michael Borenstein and Dr. Kenneth Korzekwa for their constructive comments and valuable suggestions during my entire course of PhD. I would especially like to thank Dr. Kenneth Korzekwa for being so humble and always ready to answer and help with our

scientific queries and naive questions. I have greatly valued his quantitative approach towards scientific problems and have learnt a lot from him. I would also like to thank our external advisor Dr. Cheryl L. Zimmerman for the useful interactions we had regarding the modeling and simulation project. Her stature as a renowned researcher in Pharmacokinetics has always inspired me.

I am thankful to Dr. James M. Gallo and his lab members for the learning opportunities I received from them during my initial days in PhD program, which helped me, develop my surgical and mass spectrometry skills. I would especially like to thank Dr. Silpa Nuthalapati for the useful discussions we had related to bioanalytical method development and validation. I should also mention Dr. Daniel Canney and our former graduate student Dr. Otito Iwuchukwu who synthesized the metabolites, without which this dissertation would not have been possible.

I am thankful to my current and past lab members for the useful interactions I had with them throughout my graduate years. I will especially like to thank Amir and Vaishnavi with whom I have shared my office space and spent most of my lab time discussing everything from science to world politics (Room 423A rocks!). I am also thankful to my roommates Bharat and Kabir for providing an enjoyable and friendly atmosphere at home, which helped me to cope up with the rigors of program.

I am thankful to the Dean and faculty members of school of Pharmacy for providing me with the financial and collegial support. I would like to thank all my friends, seniors and

juniors at school of Pharmacy for making my life at Temple a memorable and fun experience. I would also like to thank Mr. John Goodheart, evening supervisor at Ginsburg library who helped me immensely by giving me rides at midnight, whenever I had long experiments; without him my PhD would have definitely been much longer.

Love you Mom, Dad, Sanjay mamaji, Bhaiya, Bhabhi, Abhishek and Mohnish for being with me in every way possible and for showing so much of faith in me. It's your faith and love that gave me strength and confidence to complete my dissertation despite several ups and downs in life. At the end, I would like to welcome the youngest member in our family, my nephew Swarit and wish him a great future ahead.

DEDICATION

To My Family

Who unequivocally supported my ambition to seek knowledge!

My Teachers

Who nurtured and mentored me all along!

My Friends

Who made my life happy!

My Life/God

For giving invaluable experiences and positive attitude!

TABLE OF CONTENTS

LIST OF TABLES

LIST OF FIGURES

Figure Page

ABBREVIATIONS

APAP – acetaminophen

BBB - blood brain barrier

BCRP - breast cancer resistance protein

COX1 - cyclooxygenase 1

COX2 - cyclooxygenase 2

CS – calibration standards

DPPH - 2, 2-diphenyl-1-picrylhydrazyl

EHC - enterohepatic circulation

ER - endoplasmic reticulum

FDA - food and drug administration

i.a. – intra-arterial administration

IS – internal standard

i.v. – intravenous administration

Kow - octanol/water partition coeffecient

LC-MS/MS – liquid chromatography with tandem mass spectrometry

LOQ – limit of quantitation

MDCK - Madin-Darby canine kidney

MIST - metabolites in safety testing

MRP - multidrug resistance protein

MRM – multiple reaction monitoring

MWT - molecular weight

NO - nitric oxide

OATP - organic anion transporting polypeptide

OAT - organic anion transporter

Papp - apparent permeability

PAPS – 3'-Phospho-adenosine-5'-phosphosulphate

PK – pharmacokinetics

PSA - polar surface area

QC – quality control

QR1 - Quinone reductase 1

RES - Trans-3,5,4'-trihydroxystilbene; trans-resveratrol

R3G – trans-resveratrol-3-O-glucuronide

R4'G – trans-resveratrol-4'-O-glucuronide

R3S – trans-resveratrol-3-sulfate

R4'S – trans- resveratrol-4'-sulfate

ROS - reactive oxygen species

SULT - Sulfotransferase

TMS - 3,4',5-trimethoxy-trans-stilbene

UDPGA – Urindine 5'-diphosphoglucuronic acid

UGT - Urindine 5'-diphosphoglucuronosyltransferase

Uppercase UGT denotes human protein and lowercase Ugt denotes mouse protein

Uppercase SULT denotes human protein and lowercase Sult denotes mouse protein

Uppercase MRP and BCRP transporters denotes human protein and lowercase Mrp and Bcrp denotes mouse protein

CHAPTER 1

INTRODUCTION

1.1. Resveratrol (RES): *trans*-resveratrol (RES, *trans*-3,5,4'-trihydroxystilbene; Fig. 1.1) is a naturally occurring phytoalexin. Phytoalexins are compounds produced by higher plants in response to environmental stress or pathogenic attack (Baur and Sinclair, 2006). RES can be classified as a stilbenoid (a hydroxylated derivative of stilbene) or a polyphenol due to more than two hydroxyl groups in its structure.

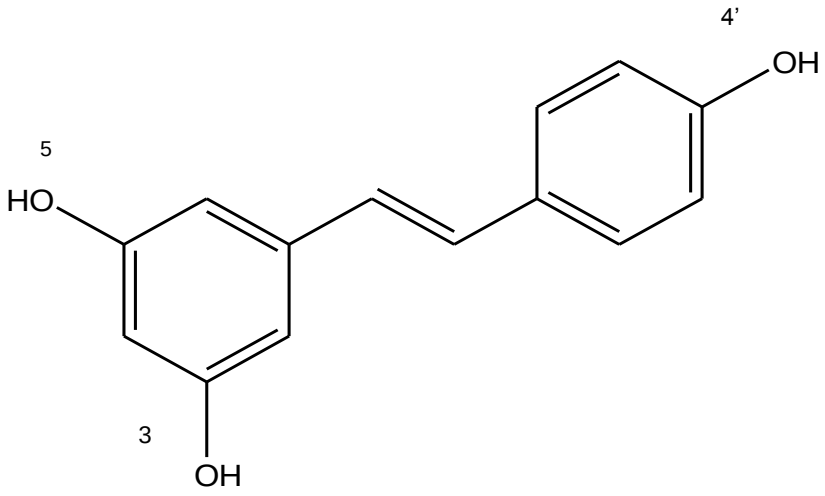

Fig 1.1: Structure of *trans*-3, 5, 4’-trihydroxystilbene (RES, *trans*-resveratrol)

1.1.1. Plant sources: RES has been initially reported to be isolated from the roots of white hellebore (*Veratrum grandiflorum O. Loes*) in 1940 and thereafter from the roots of *Polygonum cuspidatum* in 1963, which has been used in traditional Chinese and Japanese medicine (Baur and Sinclair, 2006). It is widely present in dietary sources like peanuts (Sanders et al., 2000) and grapes (Jang et al., 1997a). It is also reported to be found in

mulberries, blueberries, cranberries, bilberries and hops (Lyons et al., 2003; Baur and Sinclair, 2006). Red wine and white wine are good commercial sources of RES with red wine having higher content of RES than white wine (Baur and Sinclair, 2006; Buiarelli et al., 2007).

1.1.2. RES Pharmacological activity: RES is known to have beneficial health effects via numerous mechanisms (Baur and Sinclair, 2006). RES research globally was triggered after 1997, when Jang and colleagues published a seminal paper in the journal Science reporting the ability of RES to inhibit carcinogenesis at multiple stages (Jang et al., 1997a). Currently there are 62 clinical trials listed with either RES alone or in combination with other drugs for different indications (clinicaltrial.gov, assessed on 12th Jan 2013). These trials include evaluation of the potential of RES in the management of type 2 diabetes, cognitive disorders, Alzheimer's disease, cancer, obesity and several other indications. Some of these activities will be discussed below.

Cancer

RES has been shown to inhibit carcinogenesis at multiple stages by inhibiting tumor initiation, promotion and progression (Jang et al., 1997a). Angiogenesis is important to support the growth of solid tumors beyond 2-3 mm. It has been reported that RES inhibits angiogenesis by inhibiting tumor induced neovascularization (Kimura and Okuda, 2001; Tseng et al., 2004) and wound healing (Bråkenhielm et al., 2001). Cell cycle arrest and apoptosis are other mechanisms by which RES inhibits tumor formation (Aggarwal et al., 2004). Inhibition of cyclooxygenase (Jang et al., 1997a), ornithine decarboxylase (Khanduja et al., 2004), phase I metabolizing enzymes (Ciolino et al.,

1998; Chan and Delucchi, 2000; Chang et al., 2000; Piver et al., 2001; Yu et al., 2003) and induction of phase II metabolizing enzymes (Cao and Li, 2004; Hebbar et al., 2005) are other mechanisms by which RES has been shown to inhibit cancer.

Cardiovascular effects

It was observed that French have relatively lower risk of cardiovascular diseases despite having a diet rich in saturated fat, termed as the 'French Paradox' (Renaud and de Lorgeril, 1992; Renaud and Gueguen, 1998). This was credited to their regular consumption of red wine, which is known to be a good source of RES (Wu et al., 2001). RES has been reported to be involved in cardioprotection in humans (Magyar et al., 2012). Cardioprotection by RES has been reported to be mediated through inhibition of platelet aggregation (Demrow et al., 1995), suppression of atherosclerosis (Wang et al., 2005b), reduction of lipid peroxidation (Fuhrman et al., 1995), induction of vasorelaxation (Novakovic et al., 2006) and improvement of serum cholesterol and triglyceride concentrations (Frankel et al., 1993).

Anti-inflammatory effects

Inflammation is an important pathology of psoriasis, arthritis and can also play a role in the development of cancer and cardiovascular disease. RES is reported to inhibit cyclooxygenase activity *in vivo* (Jang et al., 1997a; Khanduja et al., 2004; Murias et al., 2004; Kang et al., 2009) a key enzyme catalyzing the synthesis of prostaglandins. RES has been shown to significantly reduce osteoarthritis (Elmali et al., 2005; Wang et al., 2012a) and lipopolysaccharide induced airway inflammation (Birrell et al., 2005). RES is

also reported to inhibit the inflammatory mediators of cytokines, such as tumor necrosis factor-α (TNF-α) and interleukin-1β (IL-1β) (Culpitt et al., 2003; Csiszar et al., 2006).

Other effects

RES has been reported to have numerous pharmacological effects. Apart from the effects listed above, RES has been reported to have antioxidant (Kensler et al., 1995), anti-aging (Valenzano et al., 2006; Milne et al., 2007), anti-obesity (Rayalam et al., 2008), cancer chemopreventive (Jang et al., 1997a; Aziz et al., 2003) and neuroprotective (Fonseca-Kelly et al., 2012; López-Miranda et al., 2012) effects.

1.1.3. *In vitro* metabolism:

In vitro glucuronidation of RES has been characterized in human liver and intestinal microsomes. R3G and R4'G were the major glucuronidated metabolites formed from RES (Aumont et al., 2001; Brill et al., 2006; Iwuchukwu and Nagar, 2008). The glucuronide conjugates were reported to be formed at higher levels in intestinal compared to liver microsomes (Brill et al., 2006). RES has been reported to be sulfated *in vitro* in human liver and intestine (De Santi et al., 2000; Walle et al., 2004; Miksits et al., 2005). The rate of sulfation was reported to be similar in both human liver and duodenum (De Santi et al., 2000).

1.1.4. Reaction phenotyping of RES metabolism:

RES has been reported to be glucuronidated at its 3-OH position via UGT1A1, UGT1A7, UGT1A9, UGT1A3, UGT1A6, UGT1A8, UGT1A10 and UGT2B7 (Fig 1.2) (Brill et al., 2006). UGT1A1, 1A7 and 1A9 are the major contributor for glucuronidation at 3 position. UGT1A9, UGT1A1, UGT1A8, UGT1A10 and UGT1A3 isoforms of UGT have been reported to be involved in the glucuronidation of RES at its 4' position (Fig 1.2) (Brill et al., 2006). UGT1A9 is the major contributor for glucuronidation of RES at its 4' position.

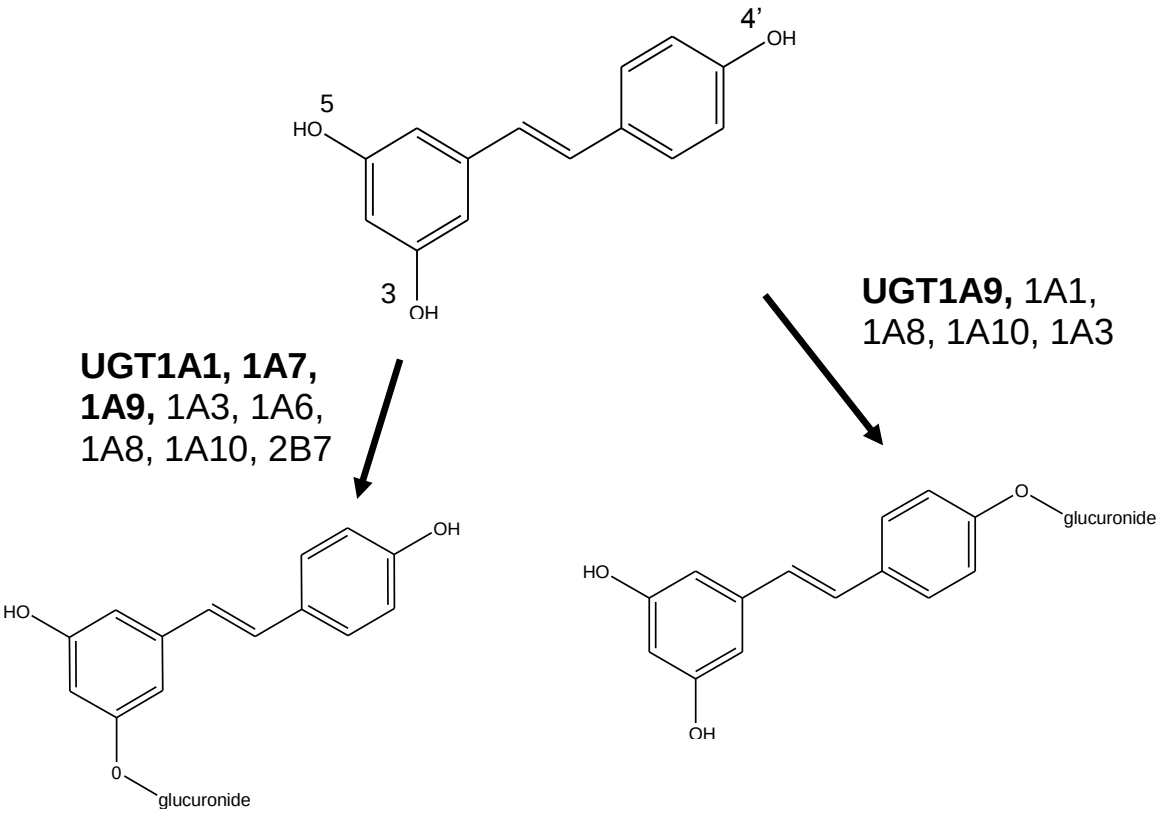

Fig 1.2: Chemical structure of trans-resveratrol (RES), glucuronidation at its 3 and 4' position to form resveratrol-3-glucuronide (R3G) and resveratrol-4'-glucuronide (R4'G) and reported major and minor UGT isoforms responsible for glucuronidation at those positions (Brill et al., 2006). Major isoforms are indicated in bold letters.

RES sulfation at its 3 -OH position has been reported to be mediated by sulfotransferase (SULT) SULT1A1, SULT1A2, SULT1A3, and SULT1E1, with SULT1A1 to be the major contributor (Miksits et al., 2005). Whereas RES sulfation at its 4'-OH position has been reported to be mediated by SULT1A1 and SULT1E1 isoforms, SULT1E1 is reported to be the major contributor (Miksits et al., 2005).

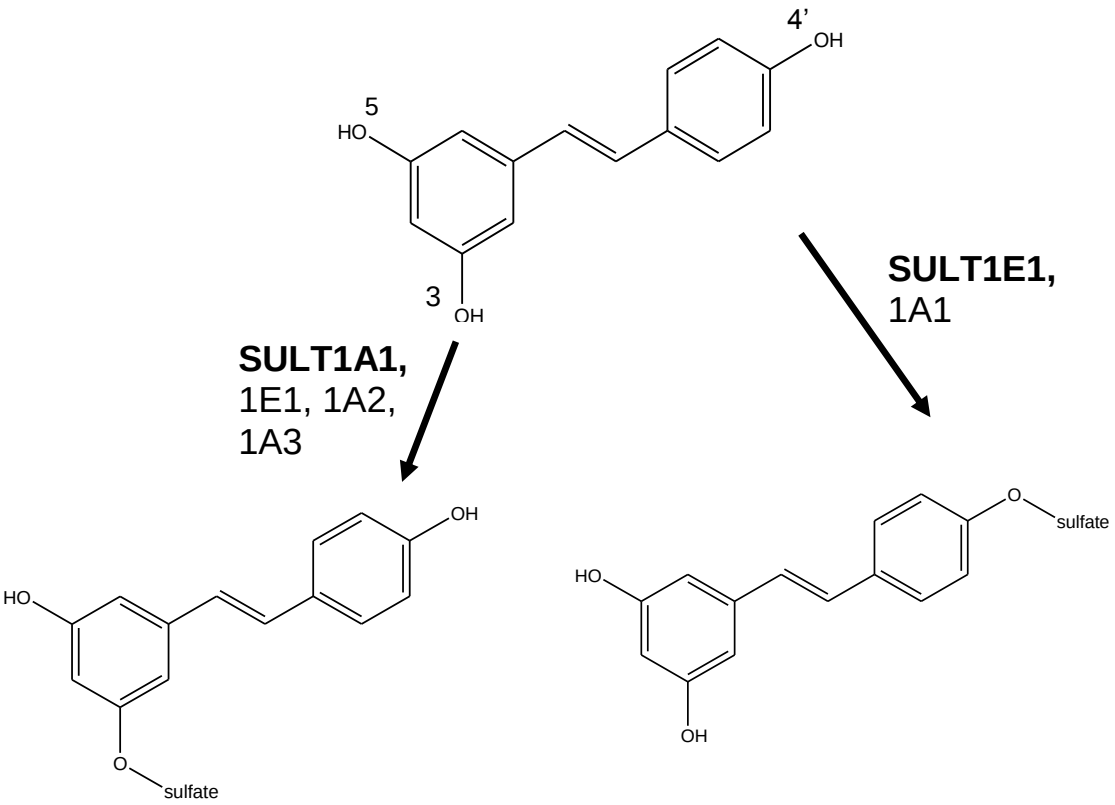

Fig 1.3: Chemical structure of trans-resveratrol (RES), sulfation at its 3 and 4' position to form resveratrol-3-sulfate (R3S) and resveratrol-4'-sulfate (R4'S) and reported major and minor SULT isoforms responsible for sulfation at those positions (Miksits et al., 2005). Major isoforms are indicated in bold letters.

Interestingly SULT1A2 has been reported to be present at mRNA level but not at the protein level so its *in vivo* relevance in RES sulfation is doubtful (Nowell et al., 2005). SULT1A3 has been shown to be expressed in large quantities in human gut but not in liver. Also, its ortholog in other species has not been identified indicating more relevance in humans compared to other species (Eisenhofer et al., 1999).

1.1.5. RES metabolites and their pharmacological activities: Sulfated metabolites of RES (R3S, R4'S) have been reported to exhibit positive biological activity *in vitro* (Calamini et al., 2010; Hoshino et al., 2010). Calamini and coworkers (Calamini et al., 2010) have shown that R4'S and RES inhibit cycloxygenase-1 (COX-1) and cycloxygenase-2 (COX-2) with similar efficacy, which is important as it has been shown that RES exhibits cardioprotective and anticancer effects by inhibiting COX-1 and COX-2 enzymes (Goldberg et al., 1995; Pace-Asciak et al., 1995; Jang et al., 1997b). Hoshino and coworkers (Hoshino et al., 2010) have shown that R3S causes quinine reductase 1 (QR1) induction, 2,2-diphenyl-1-picrylhydrazyl (DPPH) free radical scavenging, and exhibits COX-1 and COX-2 inhibitory activities. R4'S was shown to inhibit NFkB induction, as well as COX-1 and COX-2 activities (Hoshino et al., 2010). Induction of QR1 has been associated with cancer chemoprevention (Talalay et al., 1995; Kennelly et al., 1997) and NFkB has been associated with progression of cancer and several human elements (Hoshino et al., 2010). Chemopreventive activity of RES is also attributed to its ability to quench unstable free radicals and prevent damage to DNA caused by reactive oxygen species (ROS) (de la Lastra and Villegas, 2007; Qian et al., 2009). R3S has been shown to have free radical scavenging activity comparable to RES, whereas R4'S has

been shown to have lower free radical scavenging activity as compared to RES (Hoshino et al., 2010). The pharmacological activity of R3G has not been reported to date.

1.1.6. Pharmacokinetics:

Pharmacokinetics and metabolism of RES in *in vitro*, ex vivo, rodents and humans have been reviewed in detail (Wenzel and Somoza, 2005). RES has been found to be absorbed well with peak concentration found to be around 15 min after its oral administration in rats (Marier et al., 2002). RES and glucuronidated metabolites of RES have been shown to undergo enterohepatic circulation by a linked rat model (Marier et al., 2002). In a different study with i.v. administration of RES in rats, glucuronidated and sulfated metabolites of RES were observed in plasma as early as 1 min after the administration of RES showing extremely rapid metabolism of RES (Juan et al., 2010b). Glucuronides were observed to be the major metabolites as compared to sulfates in rats (Juan et al., 2010b). The tissue distribution of RES was highest in kidney followed by lungs, liver, brain and testes at 90 min after RES administration in rats. The glucuronide concentration was highest in kidney followed by testis, liver and lungs. Sulfates were found mainly in lungs, testis, liver and brain of rats (Juan et al., 2010b).

Clinical Studies:

Goldberg et al initially studied the pharmacokinetics of RES in humans in 3 different matrices (grape juice, white wine and V8 juice). They observed that RES was well absorbed and achieved its highest concentration at approximately 30 minutes after its administration (Goldberg et al., 2003). Walle et al examined the absorption,

bioavailability and metabolism of ^{14}C-RES after its oral and i.v. administration to healthy volunteers. They reported that absorption of RES was around 70% with negligible unchanged RES (< 5 ng/ml) detected in plasma, showing very poor systemic bioavailability (Walle et al., 2004). The poor systemic bioavailability is attributed to extensive metabolism of RES into its glucuronidated and sulfated metabolites. A secondary peak was also observed in this study at 6 h after the oral dose, indicating enterohepatic cycling of conjugated metabolites by reabsorption after intestinal hydrolysis (Walle et al., 2004). Boocock et al studied the pharmacokinetics of RES by administering it orally as single doses of 0.5, 1, 2.5 and 5 g in 10 healthy volunteers at each dose level (Boocock et al., 2007). R3S was found to be the most abundant metabolite of RES followed by glucuronides in this study (Boocock et al., 2007). Brown et al conducted a repeat dose study of the RES in healthy volunteers at 0.5, 1.0, 2.5, or 5.0 g daily for 29 days (Brown et al., 2010). RES was observed to be rapidly absorbed achieving peak concentration after 1hr of administration. Six metabolites of RES, R3S, R4'S, R3G R4'G, RES disulfate and RES sulfate glucuronides were identified in the plasma. R3S was reported to be the most abundant circulating metabolite. The respective AUClast of R3S, R4'G and R3G were reported to be 20.3 to 9.49, 7.61 to 4.88 and 5.00 to 5.39 fold higher than the AUC's for RES across the four doses. It is important to mention that direct quantitation of RES metabolites has not been conducted to date (Boocock et al., 2007; Brown et al., 2010; Juan et al., 2010b; Kapetanovic et al., 2011). Conjugates have been quantified after their hydrolysis utilizing a RES standard curve, or by assuming that the relationship between peak area ratio and concentration were the same for metabolites as for parent RES.

1.2. 3, 4', 5 trimethoxy-trans-stilbene (TMS): TMS (Fig 1.4) is a trimethoxy analogue of RES. It is also abbreviated as BTM-0512 and MR-3 in literature. TMS has been reported to be present in the bark of *Virola elongate* (MacRae and Towers, 1985) and *Virola cuspidata* (Blair et al., 1969). Reports of pharmacological activities of RES have led researchers to synthesize and evaluate analogues of RES. Although TMS was discovered earlier, its pharmacological evaluation has been reported recently. TMS has been shown to exhibit comparable or higher potency than RES in several cancer cells (Simoni et al., 2006; Bader et al., 2008; Pan et al., 2008; Wang et al., 2010; Weng et al., 2010). TMS is also reported to have anti-invasive and anti-angiogenic activities (Belleri et al., 2005; Yang et al., 2009; Alex et al., 2010; Weng et al., 2010) which can inhibit tumor metastasis. It is reported to have anti-allergic activity by significantly inhibiting antigen-induced release of TNF-α and IL-4 in RBL-2H3 cells (Matsuda et al., 2004). It has been also shown to inhibit high glucose induced cell senescence (Yuan et al., 2010), hepatoprotection (Rivera et al., 2008) and gastroprotection activities (Li et al., 2010).

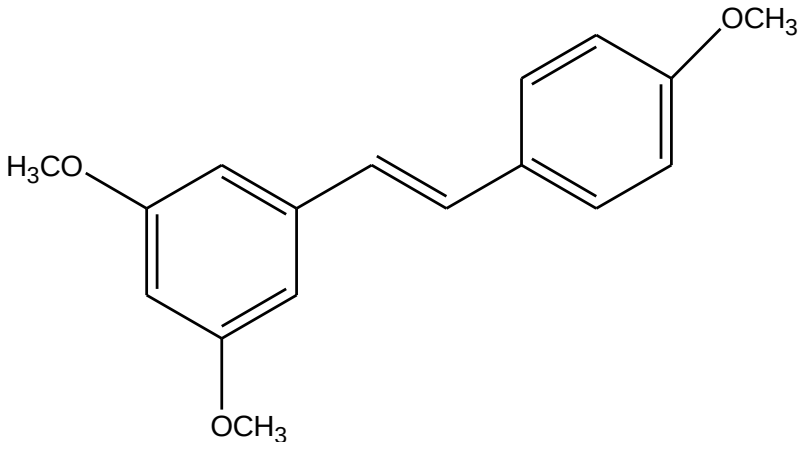

Fig 1.4: Structure of 3, 4', 5 trimethoxy-trans-stilbene (RES analogue; TMS)

It has been observed that RES exerts significant antitumor effects on subcutaneous (s.c.) glioma tumors showing slower tumor growth rate, longer survival time and higher survival rate in a rat model. However it was found that RES at a much higher dose only prolonged the survival time without improving the survival rate in rat bearing intracranial glioma tumors (Tseng et al., 2004). One of the main reasons for lack of improvement in the survival rate in rats bearing intracranial glioma tumors can be due to decreased permeability of RES in brain due to the restrictions at the BBB or efflux by transporters at the BBB.

For these reasons there was a need to test analogues of RES which are more potent and have better physicochemical properties for permeation through the blood-brain-barrier (BBB). Physicochemical properties have been long used by medicinal chemists to design compounds with better BBB permeability. Several suggestions based on the molecular structure and properties of compounds have been proposed which can give better brain permeability (Kelder et al., 1999; Norinder and Haeberlein, 2002; Lipinski, 2004; Gleeson, 2008) . Certain physicochemical properties of compounds suggested to be positively associated with their ability to have good BBB permeability are listed below.

1.2.1. Physicochemical properties:

Molecular weight (MWT): It has been observed that the molecules with molecular weight below 400 are more favorable to cross BBB (Gleeson, 2008).

Octanol/water partition coefficient (Kow): It has been shown that with increase in lipophilicity (up to a certain limit) there is an increase in the permeation through BBB (Lanevskij et al., 2009).

Polar Surface Area (PSA): Polar surface area is defined as the sum of surfaces of polar atoms in a molecule. PSA shows good correlation with passive molecular transport through membranes (Ertl et al., 2000). It has been reported that lower PSA leads to enhanced BBB penetration (Gleeson, 2008) and PSA value less than 60 – 70 are likely to be CNS active compounds (Kelder et al., 1999).

It has been also reported that if N + O (number of nitrogen and oxygen atoms) in a compound is less than or equal to five and if log P – (N + O) is positive then the compound is considered favorable to enter the brain (Norinder and Haeberlein, 2002; Lipinski, 2004).

TMS has all the favorable physicochemical properties to cross the BBB.

Table 1.1: Physicochemical properties of TMS (CambridgeSoft):

	Mol Wt.	**tPSA**	**logP**	**(N+O)**	**log P -(N+O)**
TMS	270.32 (< 400)	27.69 (< 60)	3.85	3 (< 5)	0.85 (+ve)

1.3. Significance:

RES has been shown to exhibit numerous pharmacological activities. The amount of research being done on RES can be inferred from the fact that a Pubmed search with resveratrol resulted in 5281 hits (assessed on 2nd Feb 2013). There is a dedicated global conference on Resveratrol conducted every alternate year to discuss the research related to this molecule. There are 62 clinical trials listed with either RES alone or in combination with other drugs for different indications (clinicaltrial.gov, assessed on 12th Jan 2013).

Although RES has been shown to have numerous biological effects, its plasma concentrations have been reported to be low (Wenzel et al., 2005; Wenzel and Somoza, 2005). RES is known to get extensively metabolized into its sulfated and glucuronidated metabolites (Goldberg et al., 2003; Walle et al., 2004). There is a mismatch between pharmacological effects of RES achieved with its high concentration in-vitro to its low levels in plasma. But interestingly RES administration in animals models have led to therapeutic effects despite its low plasma concentrations (Carbó et al., 1999; Tessitore et al., 2000; Banerjee et al., 2002; Li et al., 2002). This has given rise to the idea that metabolites themselves might be active or can deconjugate to give parent RES at the target tissue (Vitrac et al., 2003; Wenzel et al., 2005; Hoshino et al., 2010). Sulfated metabolites of RES i.e. R3S and R4'S have been shown to biologically active *in vitro* (Calamini et al., 2010; Hoshino et al., 2010). The other possibility of conjugated metabolites getting deconjugated to give parent RES has not been evaluated. It has been earlier shown that estrone sulfate gets desulfated in liver to form estrone (Tan et al.,

2001). Similarly there is a possibility that sulfated conjugates of RES can undergo desulfation in tissues to give back parent RES and can act as depot for RES. It has been also reported that SN-38 glucuronide (metabolite of irinotecan) formed in liver is eliminated into the bile and deconjugated in gut by β-glucuronidase leading to diarrhea (Araki et al., 1993; Ma and McLeod, 2003). Similarly RES glucuronides which have been shown to be eliminated into the bile (Marier et al., 2002) can also undergo deconjugation in the gut by β-glucuronidase which generates parent RES locally.

A proper understanding of the disposition of RES conjugated metabolites is needed to answer all of these questions. The pharmacokinetic studies to date have mainly focused on the plasma concentration of the parent compound RES. There are some studies reporting levels of metabolites but none of them have measured metabolites directly using standards. Currently there are no reported studies examining the role of metabolites of RES on RES pharmacokinetics. These observations warrant us to examine the metabolite kinetics of RES conjugated metabolites in detail. This has also assumed greater significance in the light of reports of positive biological activities of sulfated metabolites of RES i.e. R3S and R4'S (Calamini et al., 2010; Hoshino et al., 2010).

Formation of active and toxic metabolites in drug development demands a thorough understanding of metabolite kinetics (Pang, 1985). Many primary metabolites can be further metabolized and this metabolism can occur in the organ responsible for its formation, e.g. liver. Identification of the site of metabolite formation is of paramount importance for the examination of metabolite kinetics, especially when the drug is

eliminated by many organs. The role of gut as extrahepatic site for metabolite formation of RES has been known (Kuhnle et al., 2000; van de Wetering et al., 2009). However, the role of an important first pass organ, e.g. the lungs has not been evaluated. Lungs are third in series of three potential biotransformation organs which a compound needs to cross before being available for systemic distribution after oral administration. The lungs also receive the entire cardiac output and can have great influence on drug disposition (Collins and Dedrick, 1982).

In this research project we have made an effort to understand the complex kinetics of RES metabolites. Metabolite kinetics in itself is a very complicated process. The pharmacokinetics of metabolites can be completely different from their parent compounds. They can exhibit interconversion as a function of reversible metabolism or can get further metabolized to secondary metabolite by sequential metabolism. The metabolites themselves can act as a depot to generate parent compound in the target organ, e.g. liver or gut. Enterohepatic cycling (EHC) of conjugated metabolites can also happen and lead to their futile cycling. EHC can influence the pharmacokinetics of parent drug, by increasing bioavailability and prolonging elimination (Roberts et al., 2002).

Additionally disposition of RES and its conjugated metabolites can be complicated by other factors, e.g. tissue distribution of drug metabolizing enzymes, presence of efflux or uptake drug transporters. Role of transporters in the disposition of RES and its metabolites has been widely reported (Maier-Salamon et al., 2008; van de Wetering et al., 2009; Juan et al., 2010a). We have tried to explain the disposition of RES and its

metabolites in major first pass metabolizing organ i.e. gut, liver and lungs based on findings of our studies and reported literature on transporters and drug metabolizing enzymes involved in RES disposition. A comprehensive explanation of the disposition of RES and its metabolites based on expression of various isoforms of metabolizing enzymes, their tissue distribution and influence of uptake and efflux transporters have been presented. This information can be useful in predicting any anticipated drug interactions with dietary products containing RES.

One important issue we have tried to address in this work is the controversy regarding differences between the kinetics of preformed versus *in vivo* formed metabolites. This topic has received increasingly more attention after the guidance issued by Food and Drug Administration (FDA) in February 2008 the *Guidance for Industry on Safety Testing of Drug Metabolites.* This guidance under certain circumstances requires safety evaluation studies to be performed as early as possible during the clinical development program by administration of preformed metabolites in pre clinical models. This has been a topic of debate. The preformed and *in vivo* formed metabolites can have different pharmacokinetics due to differences in their physicochemical properties or differences in their interaction with transporters, drug metabolizing enzymes or binding proteins. It is important to better understand the kinetic behavior of preformed versus *in vivo* formed metabolites before conducting resource intensive testing of toxicity of drug metabolite. Modeling and simulation are an important tool which can be helpful in discerning the differences between preformed versus *in vivo* formed metabolite kinetics and should be explored.

Currently, there is a lot of focus on synthesizing potent analogs of RES, which might have better bioavailability than RES. Trimethoxy stilbene (TMS) is one of the analogs of RES, where the hydroxyl groups of RES are substituted by methoxy groups. TMS is reported to be comparable or more potent than RES. We additionally hypothesized that based on its favorable physicochemical properties it can have better blood-brain-barrier (BBB) permeability. This needs to be evaluated experimentally before proceeding to *in vivo* pharmacological studies.

1.4. Hypothesis:

Based on our in-vivo experiments we expect to test the hypothesis that a) RES will undergo pulmonary metabolism and its sulfated and glucuronidated metabolites will be deconjugated systemically and in the gut to give RES; and b) TMS, an analog of RES will exhibit good brain permeability.

1.5. Specific Aims:

1.5.1. Development and validation of a bio-analytical method for direct quantitation of RES and its sulfated (R3S, R4'S) and glucuronidated (R3G, R4'G) metabolites:

Pharmacokinetic studies reported to date have quantified RES metabolites indirectly. RES metabolites have been either quantified after their hydrolysis utilizing a RES standard curve or by assuming that relationship between peak area ratio and concentration were the same for metabolites and for parent RES. To be able to correlate metabolite exposure to any observed pharmacological activity a robust bioanalytical method for direct quantification of RES and its metabolites is essential. This is also important in the light of the positive biological activity of sulfated metabolites of RES. We have achieved this objective by developing a robust bioanalytical method for quantification of RES, R3S, R4'S, R3G and R4'G on LC-MS/MS (API4000). This work has been presented in chapter two of this dissertation.

1.5.2. Pharmacokinetics of Resveratrol and its pulmonary metabolism: The lungs are an important site of metabolism as the entire cardiac output (approximately four times liver blood flow) perfuses the lung and can play an important role in drug disposition (Davies and Morris, 1993). Phenolic compounds have been shown to undergo pulmonary metabolism. Although the role of gut and liver is well known in the metabolism of RES (Kuhnle et al., 2000; Miksits et al., 2005; Brill et al., 2006; Iwuchukwu and Nagar, 2008; van de Wetering et al., 2009), the role of the lungs has not been evaluated in the metabolism of RES. Additionally we have observed a very high clearance of RES, much higher than the hepatic blood flow in rodents (Marier et al., 2002), indicating the possibility of extrahepatic conjugation of RES. These results led us to investigate the lung as a possible metabolizing organ for RES. This also becomes important in the light of positive pharmacological effects of RES seen in human lung adenocarcinoma cells (Alex et al., 2010; Zhang et al., 2011; Zhang et al., 2012b) and lung cancer chemopreventive activity (Mollerup et al., 2001).

The contribution of pulmonary metabolism of RES *in vivo* was studied by using multiple sites of administration and a single site of sampling (Cassidy and Houston, 1980) approach. *In vivo* findings in mouse were further confirmed by *in vitro* experiments using lung fractions of mouse. *In vitro* studies using human lung fractions were also performed to compare mouse versus human RES pulmonary conjugation. This work has been presented in chapter three of the dissertation.

1.5.3. Characterization of the pharmacokinetics of preformed sulfated and glucuronidated metabolites: Sulfated metabolites of RES, i.e. R3S and R4'S have been recently shown to have positive biological activity *in vitro* (Calamini et al., 2010; Hoshino et al., 2010). Although no biological activity has been reported for the glucuronidated metabolite (R3G) of RES to date, there are several examples of pharmacologically active glucuronides (Osborne et al., 1988; Kroemer and Klotz, 1992; Sperker et al., 1997). Additionally R3G has been shown to be biliarily eliminated and subject to enterohepatic circulation (Marier et al., 2002). R3G eliminated in gut by biliary elimination can be deglucuronidated by β-glucuronidase enzymes present in the gut to give RES locally. Researchers have also hypothesized that conjugated metabolites of RES can be deconjugated in the target organ e.g liver to give RES (Wenzel et al., 2005; Hoshino et al., 2010).

We carried out a detailed pharmacokinetic study by administering preformed sulfated (R3S, R4'S) and glucuronidated metabolite (R3G) by oral and intra-arterial (i.a.) routes of administration. The hypothesis that sulfated metabolite can regenerate RES at the target tissue, the liver, was also evaluated by performing *in vitro* studies with R3S and mouse/human liver fractions. This study also provided a better understanding of the influence of the disposition of the sulfated and glucuronidated metabolites disposition on RES pharmacokinetics. Detailed pharmacokinetics of preformed sulfated metabolites (R3S, R4'S) and *in vitro* studies with R3S have been presented in chapter four. Chapter five gives detailed pharmacokinetics of the preformed glucuronidated metabolite (R3G).

1.5.4. Preformed versus *in vivo* formed metabolite kinetics: Attention has increasingly focused on the issue of drug metabolites in safety testing (MIST) by both pharmaceutical companies and regulatory agencies. Regulatory guidelines were recently published on this topic (Center for Drug Evaluation and Research (U.S.), 2008; International Conference on Harmonisation, 2009). These guidances recommend metabolite safety evaluation studies to be performed as early as possible during the clinical development program. The recommendation is to synthesize the metabolite and to evaluate it in preclinical toxicity studies. One major assumption underlying metabolite toxicity evaluation studies is that the kinetic behavior of a preformed metabolite is the same as that of the metabolite formed *in vivo* following administration of parent compound. This has been a topic of debate (Prueksaritanont et al., 2006; Pang et al., 2008; Pang, 2009). Metabolites are generally more polar than their precursors. A polar preformed metabolite may experience diffusional barriers to its penetration into an eliminating organ, and hence its elimination clearance may be less than that of *in vivo* generated metabolite, whose entry into the eliminating organ is in the form of a more lipophilic parent.

We compared the metabolite kinetics of preformed and *in vivo* generated metabolites by modeling and simulation under two assumptions: i) assuming similar PK of preformed versus *in vivo* formed metabolite, ii) assuming dissimilar PK of preformed versus *in vivo* formed metabolite. The first approach assumes that the systemic or elimination clearance of *in vivo* formed and preformed metabolites are similar, whereas the second approach does not make this assumption. RES and its two major metabolites, R3S and R3G were used as model substrates. This work has been presented in chapter six of this dissertation.

1.5.5. Pharmacokinetics and brain permeability of 3, 4', 5 Trimethoxy trans stilbene (TMS): TMS has favorable physicochemical properties to cross the blood brain barrier (BBB) indicated by its lower molecular weight (270.32), favorable log P (3.85) and lower tPSA (27.69) (CambridgeSoft). It also satisfies Lipinski's rule of five (Lipinski et al., 2001) in addition to its comparable or higher potency than RES. Its hydroxyl groups are also protected by methoxy groups which might lead to its decreased metabolism and enhanced exposure compared to RES. Better brain permeability of TMS if proved might open a new avenue to screen TMS for indications involving brain where RES has also shown positive biological activity e.g. alzheimer's disease (Marambaud et al., 2005), and brain tumors (Tseng et al., 2004).

A pharmacokinetic study of TMS was conducted in the mouse model and the pharmacokinetic (PK) parameters obtained from this study were used to design a steady state PK study. Brain penetration of TMS was evaluated at steady state. For conducting this study we required a robust bioanalytical method to quantitate TMS in plasma and brain. Therefore, a bioanalytical method for quantification of TMS in plasma and brain was developed and validated. Bioanalytical method development and validation for quantification of TMS in plasma and brain is presented in chapter seven. Chapter eight includes the evaluation of *in-vivo* brain permeability of TMS in mouse model.

CHAPTER 2

DEVELOPMENT AND VALIDATION OF AN LC-MS/MS METHOD FOR THE QUANTIFICATION OF RESVERATROL AND ITS METABOLITES

2.1 Rationale

The comprehensive study of RES and its metabolites *in vivo* requires a validated bioanalytical assay with low detection capability in order to quantitate low circulating levels of RES and its metabolites. While methods have been reported for the quantitation of RES and qualitative identification of its metabolites (Juan et al., 2010b), to our knowledge direct quantitation of RES metabolites has not been conducted to date. RES metabolites have previously been evaluated by hydrolysis and against a RES standard curve. Our aim in this study was to develop and validate an LC-MS/MS assay for quantitation of RES and each of its monoconjugates by using synthetic standards.

2.2 Assay development

2.2.1. Preparation of stock solutions, calibration standards (CS) and quality control (QC) samples

Stock solutions of RES, R4'G, R3G, R4'S, R3S and APAP (IS) were prepared separately in DMSO. CS samples were prepared by spiking stock standard working solutions into heparinized mouse plasma to give eight CS in the concentration range of 2.46 – 2460 ng/ml for R3S, 3.57 – 3570 ng/ml for R4'S and 10 – 10000 ng/ml for R4'G, R3G and RES. Similar to calibration standards, QC samples were prepared in replicates (n = 3 and n = 5 for the inter-day and intra-day validation respectively) at five concentration levels

representing the entire range of concentrations (10, 20, 50, 1000 and 10000 ng/ml for RES, R4'G, and R3G; 3.57, 7.15, 17.9, 357 and 3570 ng/ml for R4'S and 2.46, 4.93, 12.3, 246 and 2460 ng/ml for R3S).

2.2.2. Sample preparation

RES, R4'G, R3G, R4'S, and R3S were isolated from plasma with protein precipitation. To 10 uL of plasma sample, 2.5 uL of 15 % ascorbic acid was added and vortexed for 1 min. Then 30 uL of methanol containing 78 ng/ml APAP (internal standard) was added and again vortexed for 1 min and centrifuged at 15,000 rpm for 15 min at room temperature. Supernatant (10 µL) was injected into the liquid chromatography tandem mass spectrometry system.

2.2.3. LC-MS/MS conditions

The LC-MS/MS assay was carried out on an Agilent series 1100 high-performance liquid chromatography system equipped with a binary pump, autosampler and degasser coupled to an API 4000 triple-quadrupole tandem mass spectrometer from ABSciex with ESI source operated in the negative ion mode. Analyst software version 1.4.2 (ABSciex) was used for instrument control, data acquisition and data processing for both chromatography and mass spectrometry. The chromatographic separation system consisted of a guard column (Zorbax SB-C18, 5 um, 4.6 × 12.5 mm; Agilent Technologies), an analytical column (Zorbax SB-C18, 5 um, 4.6 × 150 mm; Agilent Technologies) and a gradient mobile phase of A: 5mM ammonium acetate and B: methanol. The elution started with 90% A at 0 min to 80% at 2 min, 65% at min 10, 40%

at min 12 to min 17 and 90% at min 19. Flow rate of the mobile phase was 1ml/min and the flow from the column was split 1:3 into an ABSciex API4000 triple quadrupole mass spectrometer equipped with a Turbo ionspray source operating at 450°C. The column temperature was maintained at 35°C. The ESI instrument settings were optimized for the analysis and the appropriate multiple reaction monitoring (MRM) transitions and MS/MS parameters were determined for individual compounds by direct infusion into the mass spectrometer. Nitrogen was used as the curtain, collision and ion source gas.

2.3. Assay validation

The method was validated according to published recommendations for bioanalytical method validation (Shah et al., 2000). Calibration curves were constructed from the peak area ratios of each analyte to internal standard versus plasma concentrations with linear least squares regression calculation and a weighting factor of $1/X^2$. Solvent (methanol) and blank samples were run after every two samples. Intra-day accuracy and precision were determined by analyzing five replicates of QC samples. Inter-day accuracy and precision were evaluated on five separate days. Precision was expressed as the relative standard deviation of the determined concentrations. Accuracy was calculated with the following equation: Accuracy = [(mean measured concentration – nominal concentration)/nominal concentration] × 100. Recovery of metabolites was investigated by analyzing five individual plasma samples at low, medium and high concentrations. These concentrations were: 20, 1000, and 10000 ng/ml for R3G and R4'G; 4.93, 246, and 2460 ng/ml for R3S; and 7.15, 357, and 3570 ng/ml for R4'S. The recovery was

determined by comparing analyte: IS peak area ratio upon extraction from spiked plasma to analyte: IS peak area ratio from post extracted plasma sample.

2.4. Results

2.4.1. LC-MS/MS assay for quantitation of RES and its metabolites

ESI operated in negative ion mode was used for the LC-MS/MS analysis to provide optimum sensitivity and selectivity. The optimized tandem mass spectrometry conditions are summarized in Table 2.1.

Table 2.1: Optimized ESI-MS/MS operating, MRM and MS/MS parameters for RES, R4'G, R3G, R4'S, R3S and APAP (IS).

Operating parameters	Setting			
Collision gas (psi)	6			
Curtain gas (psi)	40			
Ion source gas 1 (psi)	55			
Ion source gas 2 (psi)	55			
Ion spray voltage (V)	-4500			
Temperature (°C)	450			
EP (V)	-10			
Run duration (min)	19			
	RES	R4'G/R3G	R4'S/R3S	APAP(IS)
Precursor ion (m/z)	227	403	307	150
Product ion (m/z)	185	113	227	107
Dwell time (ms)	400	400	400	400
DP (V)	-70	-65	-40	-40
CE (V)	-26	-24	-32	-24
CXP (V)	-11	-5	-5	-5

The following precursor-product ion transitions were observed: m/z 227→185 for RES, m/z 150→107 for acetaminophen (APAP, internal standard IS), 403→113 for R4'G and R3G and 307→227 for R4'S and R3S with a dwell time of 400 ms for each ion transition. The daughter ion for sulfated metabolites (227) corresponds to the RES moiety and the daughter ion for glucuronidated metabolites (113) corresponds to the glucuronide moiety fragment (Wang et al., 2005a). The retention time was ~ 5 min for APAP, ~ 5.9 min for R4'G, ~ 7.3 min for R3G, ~ 9.2 min for R4'S, ~ 10.2 min for R3S and ~ 14.2 min for RES. A representative chromatogram is presented in Figure 2.1.

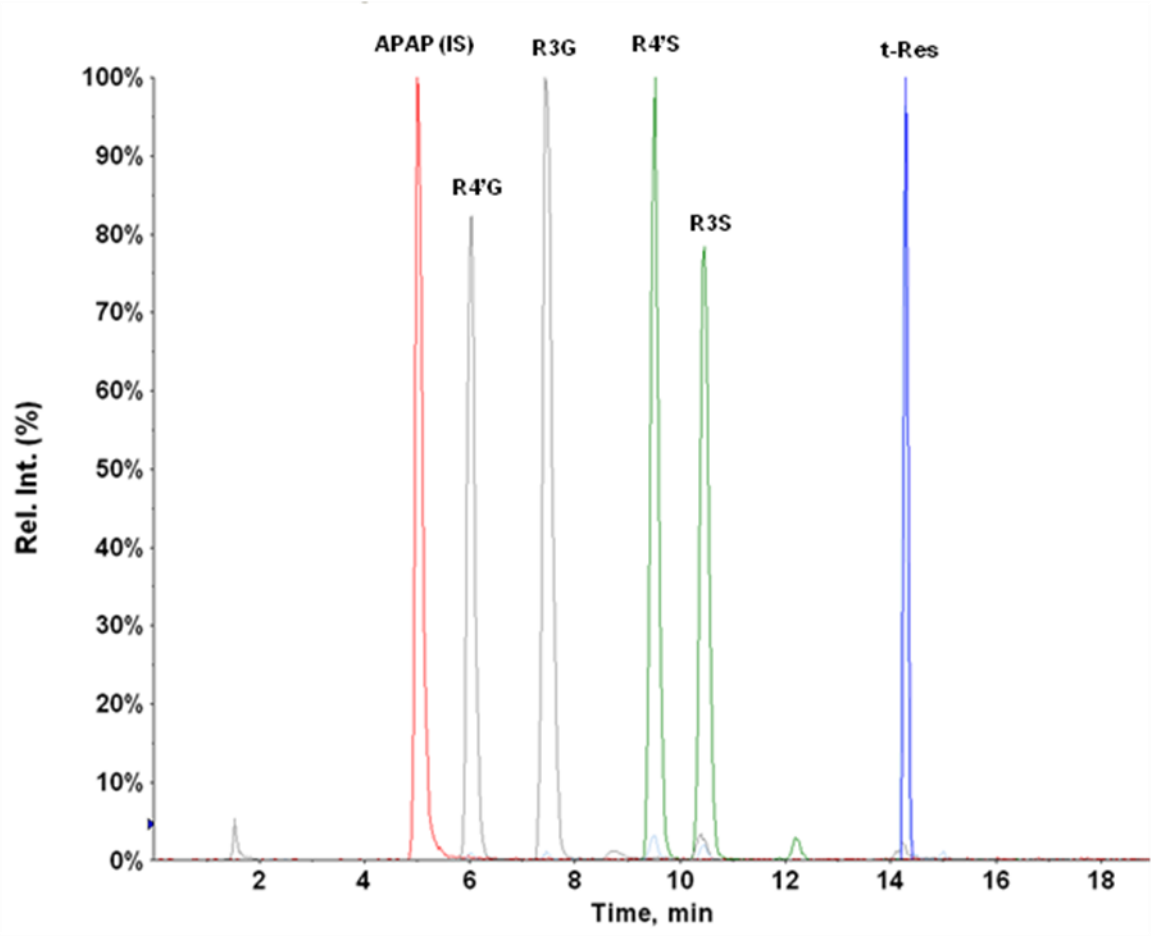

Fig 2.1: Representative chromatograms of RES, APAP (IS), R4'G, R3G, R4'S and R3S

In this study, the calculated peak area ratios of RES, R4'G, R3G, R4'S and R3S to APAP versus their respective nominal concentration displayed a good linear relationship with coefficients of determination ≥ 0.99 over the concentration range of 10 – 10000 ng/ml for RES, R4'G, and R3G, and 3.57 to 3570 for R4'S and 2.46 to 2460 ng/ml for R3S using a weighting factor of $1/X^2$. The LOQs were established at the lowest point of each standard curve, i.e. 3.57 ng/ml for R4'S, 2.46 ng/ml for R3S and 10 ng/ml for R4'G, R3G and RES. Representative standard curve of RES, R4'G, R3G, R4'S and R3S is presented in Fig 2.2 to 2.6.

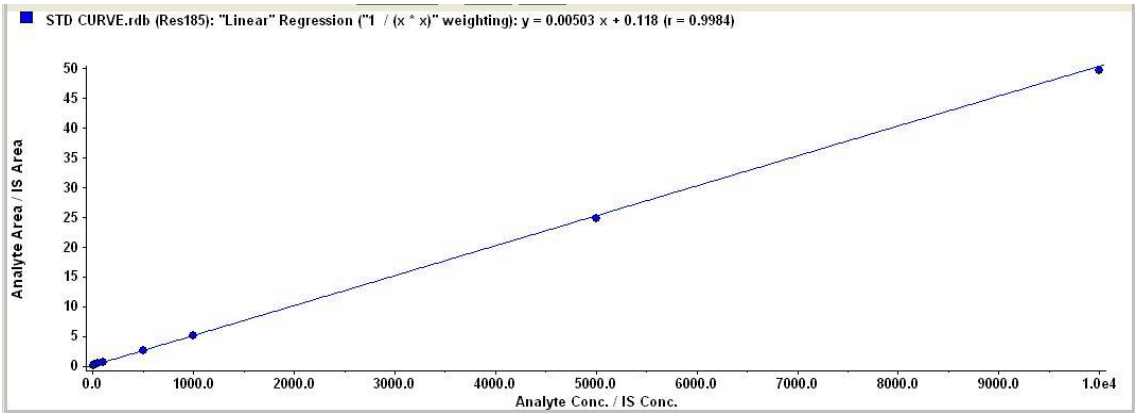

Fig 2.2: Representative calibration curve of RES. Substrate concentrations range from 10 – 10000 ng/ml, using a weighting factor of $1/X^2$.

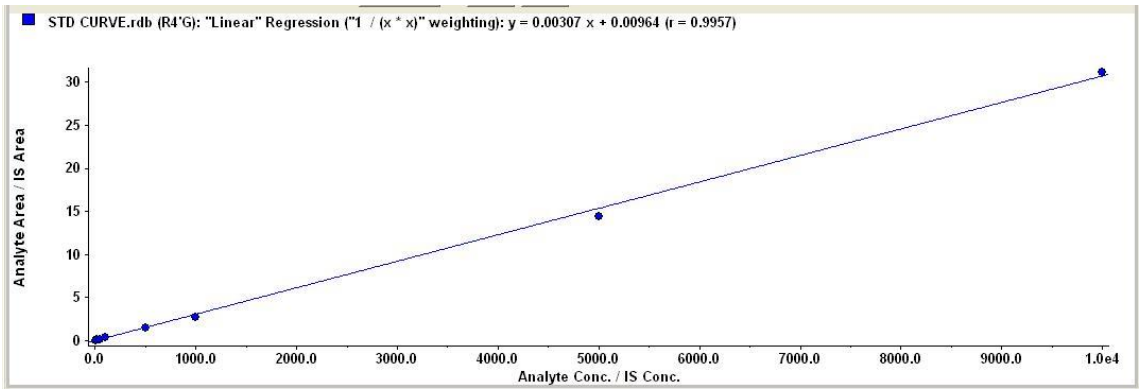

Fig 2.3: Representative calibration curve of R4'G. Substrate concentrations range from 10 – 10000 ng/ml, using a weighting factor of $1/X^2$.

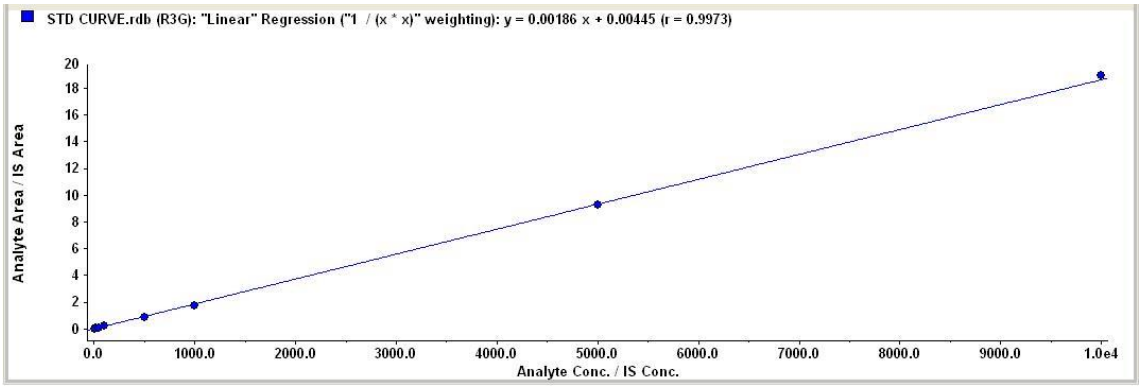

Fig 2.4: Representative calibration curve of R3G. Substrate concentrations range from 10 – 10000 ng/ml, using a weighting factor of $1/X^2$.

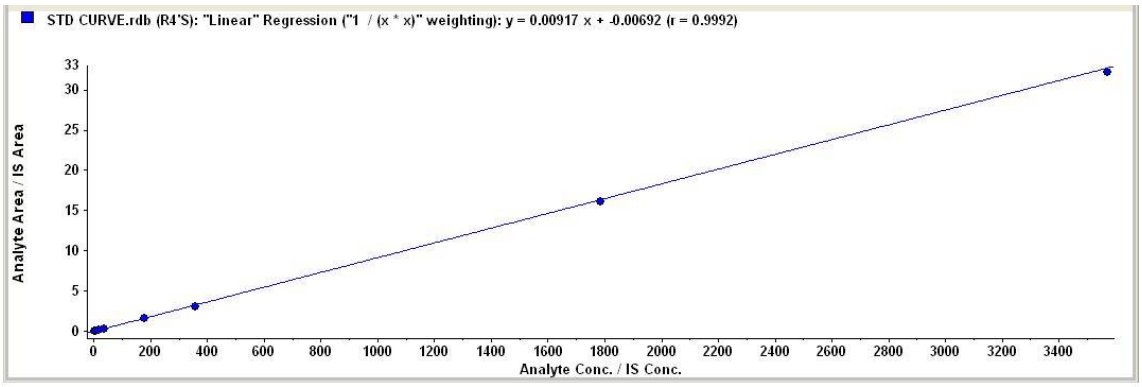

Fig 2.5: Representative calibration curve of R4'S. Substrate concentrations range from 3.57 – 3570 ng/ml, using a weighting factor of $1/X^2$.

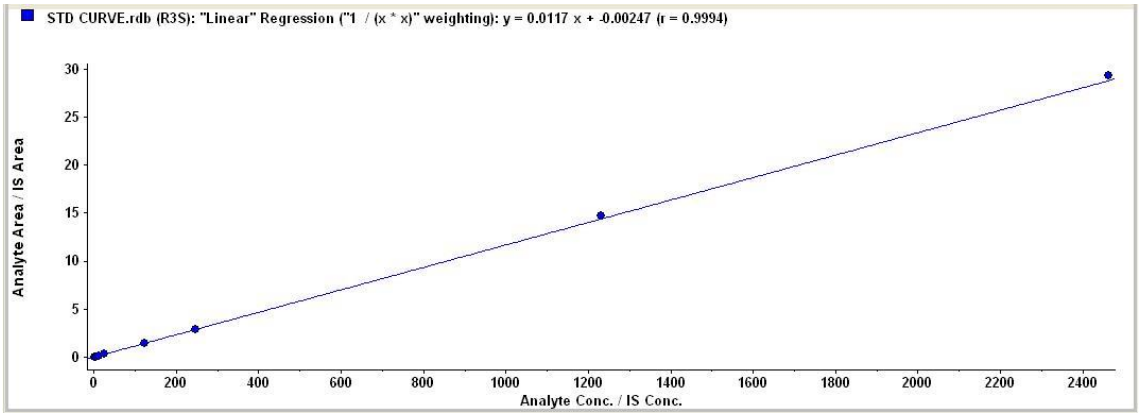

Fig 2.6: Representative calibration curve of R3S. Substrate concentrations range from 2.46 – 2460 ng/ml, using a weighting factor of $1/X^2$.

The results of inter-day and intra-day accuracy and precision are presented in Table 2.2 and 2.3 respectively. The intra- and inter-day precision for all the analytes was less than 15%. The recovery of R3G and R4'G at low (20 ng/ml), medium (100 ng/ml) and high (10000 ng/ml) concentrations was 79.58, 91 and 90.98 % for R3G and 89.93, 86.15 and 94.83% for R4'G respectively. Recovery of R3S at low (4.93 ng/ml), medium (246

ng/ml) and high (2460 ng/ml) concentration was 105.13, 99.21 and 96.11 % respectively. R4'S recovery at low (7.15 ng/ml), medium (357 ng/ml) and high (3570 ng/ml) concentration was 97.31, 108.71 and 103.61 % respectively. The results indicate that the recovery, precision and accuracy of this method were adequate for bioanalytical purposes.

Table 2.2: **Inter-day (n = 5) precision and accuracy for RES, R4'G, R3G, R4'S and R3S in mouse plasma.**

Analytes	Nominal Concentration (ng/ml)	Inter-day validation		
		Measured concentration (ng/ml)	Precision (%)	Accuracy (%)
RES	10	9.83 ± 0.89	9.02	-1.7
	20	20.80 ± 1.70	8.16	3.99
	50	50.70 ± 4.18	8.24	1.41
	1000	1020.32 ± 59.84	5.86	2.03
	10000	10038.27 ± 780.66	7.78	0.38
R4'G	10	9.69 ± 0.83	8.52	-3.09
	20	19.64 ± 1.25	6.34	-1.82
	50	47.73 ± 3.00	6.28	-4.55
	1000	1058.11 ± 23.5	2.22	5.81
	10000	10202.8 ± 471.46	4.62	2.03
R3G	10	9.64 ± 0.56	5.84	-3.58
	20	19.09 ± 1.21	6.33	-4.56
	50	46.49 ± 1.91	4.12	-7.03
	1000	1075.65 ± 27.76	2.58	7.57
	10000	10351.20 ± 429.35	4.15	3.51
R4'S	3.57	3.73 ± 0.25	6.82	4.46
	7.15	7.12 ± 0.41	5.7	-0.41
	17.9	17.63 ± 1.35	7.68	-1.5
	357	378.68 ± 11.89	3.14	6.07
	3570	3826.93 ± 114.03	2.98	7.2
R3S	2.46	2.42 ± 0.14	5.97	-1.63
	4.93	4.83 ± 0.28	5.88	-2
	12.3	11.79 ± 0.82	6.98	-4.15
	246	259.01 ± 3.62	1.4	5.29
	2460	2610 ± 162.48	6.23	6.1

Table 2.3: Intra-day (n = 5) precision and accuracy for RES, R4'G, R3G, R4'S and R3S in mouse plasma.

Analytes	Nominal Concentration (ng/ml)	Intra-day validation		
		Measured concentration (ng/ml)	Precision (%)	Accuracy (%)
RES	10	9.34 ± 0.93	10	-6.64
	20	19.66 ± 1.81	9.2	-1.7
	50	54.82 ± 1.92	3.52	9.16
	1000	1017.6 ± 81.99	8.06	1.76
	10000	10218 ± 501.12	4.9	2.18
R4'G	10	9.01 ± 0.91	10.07	-9.88
	20	18.68 ± 1.23	6.59	-6.6
	50	48.96 ± 2.11	4.32	-2.08
	1000	1053.20 ± 33.78	3.21	5.32
	10000	10254 ± 422	4.12	2.54
R3G	10	9 ± 0.35	3.83	-9.96
	20	17.64 ± 0.42	2.39	-11.8
	50	47 ± 1.96	4.16	-6
	1000	1047.60 ± 44.03	4.2	4.76
	10000	10366 ± 426.36	4.11	3.66
R4'S	3.57	3.55 ± 0.32	8.89	-0.5
	7.15	7 ± 0.71	10.19	-2.07
	17.9	17.76 ± 0.75	4.24	-0.78
	357	359.40 ± 12.18	3.39	0.67
	3570	3708 ± 164.07	4.42	3.87
R3S	2.46	2.30 ± 0.25	10.88	-6.5
	4.93	5.03 ± 0.44	8.78	1.95
	12.3	12.38 ± 0.40	3.25	0.65
	246	255.40 ± 8.02	3.14	3.82
	2460	2740 ± 140.36	5.12	11.38

2.5. Discussion and conclusion

There are reports of synthetic RES metabolites used as qualitative standards, but no study to date has directly quantitated these metabolites (Yu et al., 2002; Wenzel and Somoza, 2005; Boocock et al., 2007). Studies to date have utilized a RES standard curve to quantitate its conjugates after their hydrolysis. Hydrolysis of conjugated metabolites to convert them to parent RES adds uncertainty to their quantitation due to experimental issues such as incomplete deconjugation, degradation, and error introduced due to additional sample preparation steps. Thus, quantitation of RES conjugates directly against their synthetic standards is a vast improvement. Table 2.2 and 2.3 shows the validation of our assay for the parent as well as all monoconjugates analytes. The LC method reported here was modified from a previously published method (Hoshino et al., 2010). Our modified method had a shorter run time (19 min versus 30 min), and included an internal standard (APAP). The sensitivity of the present assay is greatly increased (2.46 ng/ml for R3S) as compared to the earlier method (100 ng/ml for R3S). This improved sensitivity is critical to evaluation of low levels of metabolites formed *in vivo*. The most important distinction in our assay is the resolution of R3S and R4'S metabolites, and quantitation of each metabolite against its synthetic standard. Given the purported activity of R4'S in cell-based assays (Calamini et al., 2010), it is especially important to analyze this metabolite and understand its *in vivo* disposition. Finally, the direct quantitation of RES glucuronides has not been previously reported. The present method offers a major advantage over previous methods in being a highly sensitive and specific assay for concomitant determination of RES and all 4 of its monoconjugated metabolites.

Copyright Notice

The work in this study has been published in the following article:

Otito F. Iwuchukwu*, **Satish Sharan*,** Daniel J. Canney, Swati Nagar. Analytical method development for synthesized conjugated metabolites of trans-resveratrol, and application to pharmacokinetic studies. Journal of Pharmaceutical and Biomedical Analysis. 63 (2012) 1 – 8; doi:10.1016/j.jpba.2011.12.006 **(*Authors contributed equally)**

ELSEVIER LICENSE
TERMS AND CONDITIONS

Jan 30, 2013

This is a License Agreement between Satish Sharan ("You") and Elsevier ("Elsevier") provided by Copyright Clearance Center ("CCC"). The license consists of your order details, the terms and conditions provided by Elsevier, and the payment terms and conditions.

All payments must be made in full to CCC. For payment instructions, please see information listed at the bottom of this form.

Supplier	Elsevier Limited The Boulevard,Langford Lane Kidlington,Oxford,OX5 1GB,UK
Registered Company Number	1982084
Customer name	Satish Sharan
Customer address	3307 North Broad Street, Room No. 423 Philadelphia, PA 19140
License number	3070960099139
License date	Jan 16, 2013
Licensed content publisher	Elsevier
Licensed content publication	Journal of Pharmaceutical and Biomedical Analysis
Licensed content title	Analytical method development for synthesized conjugated metabolites of*trans*-resveratrol, and application to pharmacokinetic studies
Licensed content author	Otito F. Iwuchukwu,Satish Sharan,Daniel J. Canney,Swati Nagar
Licensed content date	7 April 2012
Licensed content volume number	63
Licensed content issue number	None
Number of pages	8
Start Page	1
End Page	8
Type of Use	reuse in a thesis/dissertation
Portion	full article
Format	both print and electronic
Are you the author of this Elsevier article?	Yes
Will you be translating?	No
Order reference number	None
Title of your thesis/dissertation	Pharmacokinetics of resveratrol, its monoconjugates, and its trimethoxy analog TMS
Expected completion date	Feb 2013
Estimated size (number of pages)	200
Elsevier VAT number	GB 494 6272 12
Permissions price	0.00 USD

CHAPTER 3

PHARMACOKINETICS OF RESVERATROL AND ITS PULMONARY METABOLISM

3.1. Rationale:

RES exhibits very low bioavailability due to its extensive conjugative metabolism. Human studies indicate that systemic exposure of RES is predominantly in the form of its conjugated metabolites (Boocock et al., 2007; Almeida et al., 2009). This has led to the hypothesis that the conjugates of RES might themselves be active, and therefore need to be evaluated. Sulfated metabolites of RES, R3S and R4'S have recently been shown to be biologically active in *in vitro* studies (Calamini et al., 2010; Hoshino et al., 2010). Although glucuronides have generally been assumed to be pharmacologically inactive, there are some studies showing some of them to be pharmcologically active (Osborne et al., 1988; Kroemer and Klotz, 1992; Sperker et al., 1997), but no biological activity of R3G has been reported to date. Finally, *in vitro* activity does not always translate to *in vivo* activity. Knowledge of systemic levels of metabolites is necessary in order to correlate metabolite exposure to any observed pharmacological activity.

The knowledge of extrahepatic metabolism in drug disposition is also important. Extrahepatic drug metabolism can modify the systemic as well as tissue exposure of drug/metabolites and, and this becomes especially important in cases of active metabolite formation and certain disease states. For example, in severe cirrhosis of the liver,

extrahepatic metabolic pathways might compensate for the impaired hepatic elimination of a drug (Patwardhan et al., 1981). Tissue levels of drug/active metabolites might change depending upon the site of metabolism. For example in case of irinotecan, its active metabolite SN-38 is conjugated to SN-38 glucuronide in liver. This is eliminated via the bile and metabolized by β-glucuronidase in gut to regenerate SN-38 which causes diarrhea (Araki et al., 1993; Takasuna et al., 1996; Michael et al., 2004). Thus, information about sites of metabolism is important for appropriately selecting dosage regimens for various clinical conditions, as well as selection of an appropriate route of drug administration.

The route of drug administration can significantly change the disposition of parent drug and metabolites if extrahepatic eliminating organs are involved. Although a bioavailability of 100% is assumed upon intravenous administration of a drug, pulmonary metabolism can decrease the bioavailability even upon i.v. administration. Similarly, compounds administered orally must cross the gut and lungs in addition to the liver before reaching the arterial blood supply for distribution to tissues. The lung as a site of metabolism assumes significance as the entire cardiac output (approximately four times liver blood flow) perfuses the lung and can play an important role in drug disposition (Davies and Morris, 1993). It has been shown that phenolic compounds e.g. harmol (Mulder et al., 1984) and phenol (Cassidy and Houston, 1984) undergo pulmonary metabolism. Although the role of gut and liver is well known in the metabolism of RES (Kuhnle et al., 2000; Miksits et al., 2005; Brill et al., 2006; Iwuchukwu and Nagar, 2008; van de Wetering et al., 2009), the role of the lungs has not been evaluated in the

metabolism of RES. RES has been shown to induce apoptosis in human lung adenocarcinoma cells (Alex et al., 2010; Zhang et al., 2011; Zhang et al., 2012b). It has been also shown to have lung cancer chemopreventive activity by altering the expression of genes involved in the phase I metabolism of polycyclic hydrocarbons (Mollerup et al., 2001). RES is known to be extensively metabolized into its two major metabolites i.e. trans-resveratrol-3-sulfate (R3S) and trans-resveratrol-3-glucuronide (R3G) in humans as well as rodents (Yu et al., 2002; Meng et al., 2004; Hoshino et al., 2010; Sharan et al., 2012). In previous studies (Marier et al., 2002; Iwuchukwu et al., 2012; Sharan et al., 2012) we have observed that clearance of RES was much higher than hepatic blood flow in rodents, indicating the possibility of extrahepatic conjugation of RES. These results led us to investigate the lung as a possible metabolizing organ for RES.

We studied the contribution of pulmonary metabolism of RES *in vivo* by using multiple sites of administration and a single site of sampling (Cassidy and Houston, 1980), which exploits the anatomical arrangement of lungs. When administered i.v., RES enters the right atrium of the heart and crosses the lungs in a relatively undiluted form prior to reaching the general arterial system for distribution throughout the body. In contrast, when given i.a. into the right carotid artery, RES is available immediately for tissue distribution. By comparison of plasma concentration time profiles following administration of RES by both routes, we calculated the contribution of lungs in the first pass metabolism of RES across the lungs. *In vivo* findings in mouse were further confirmed by *in vitro* experiments using lung fractions of mouse. *In vitro* studies using

human lung fractions were also performed to compare mouse versus human RES pulmonary conjugation.

In this study we aim to evaluate if a) lungs contribute towards RES metabolism *in vivo*, b) if yes, then confirm the lung conjugation *in vitro*.

3.2. Materials and Methods

3.2.1. Animals: Male C57BL/6 mice weighing between 20 and 25 g were supplied by Jackson labs and maintained in the American Association for the Accreditation of Laboratory Animal Care-accredited University Laboratory Animal Resources of Temple University. Animals were fed a normal diet and water was continuously available. Animals were housed in rooms with a standard 12 hr dark/light cycle. Animals were acclimatized for four days before the procedure. All animal studies were approved by the Temple University Institutional Animal Care and Use Committee.

3.2.2. Catheterization: Right carotid artery cannulation was performed under anesthesia using EZ-ANESTHESIA (serial no. EZ388) apparatus with 1.5 % isoflurane and 2 L/min oxygen. An incision was made right of midline in the neck and the right carotid artery was isolated. The right carotid artery was ligated, a small cut was made and a medical grade vinyl catheter tubing (0.28-mm i.d. × 0.64 mm o.d., SCI, Lake Havasu City, Arizona) with heparin-saline (50 IU/ml, APP Pharmaceuticals, LLC, Schaumburg, IL) was inserted with the cannula tip in the right carotid artery. Similarly the right jugular vein was cannulated for animals receiving i.v. drug administration. The cannulas were tied in place, exteriorized at the back of the neck and the incision was sutured. Animals were allowed to recover from the surgery. Animals regained full consciousness and started moving freely after 15 minutes of surgery.

3.2.3. Drug administration and blood sampling: RES was solubilized in 20% 2-hydroxypropyl-β-cyclodextrin (HP-β-CD) in saline (Juan et al., 2010b). The carotid

artery cannula was used for i.a. and jugular vein cannula for i.v. drug administration. Blood was sampled from carotid artery cannula. Heparin-saline (20 uL, 50 IU/ml) was used to flush the cannula after systemic administration or blood sampling. RES was administered i.a. at the dose of 15 mg/kg and 60 mg/kg, i.v. at the dose of 15 mg/kg and orally at 60 mg/kg. Blood (20 uL) was serially sampled at 2.5, 5, 10, 15, 45, 90, 180, 300, 420 and 600 min. For animals with functional cannulas, 24-h and 48-h collection were also taken. Blood samples were centrifuged at 14,000 rpm for 2 min, the harvested plasma was collected and stored at -80 °C until LCMS/MS analysis.

3.2.4. *In vitro* pulmonary glucuronidation: RES glucuronidation was determined in pooled mouse lung S9 fraction and in pooled human lung microsomes. For the mouse lung S9 glucuronidation assay, conditions of protein and time linearity were optimized in preliminary studies. The incubation mixture consisted of mouse lung S9 fraction (final concentration, 0.5 mg/ml), substrate RES (0.01 uM to 5 mM) solubilized in HP-β-CD (final HP-β-CD concentration 2%), alamethicin (final concentration 10 ug/ml), $MgCl_2$ (final concentration 5 mM), and made up to final incubation volume (20 uL) with Tris-HCl buffer (100 mM, pH 7.4, 37°C). The reaction mixture was preincubated for 3 min in a shaking water bath at 37°C. The reaction was started by adding 2 uL (50 mM stock) of the cofactor UDPGA (uridine 5'-diphosphoglucuronic acid, final concentration 5 mM). To 20 uL of the reaction mixture, 5 uL of ascorbic acid (15%) and 60 uL of ice cold methanol containing acetaminophen (APAP) as internal standard (IS) were added at the end of 60 min to stop the reaction. All reactions were performed in triplicate.

Appropriate negative control experiments were performed under the same conditions but without UDPGA.

For human lung glucuronidation assay, the incubation was performed at 0.1, 0.5 and 2.5 mg/ml (final concentration) of human lung microsomes with substrate RES (0.5 mM) solubilized in HP-β-CD (final HP-β-CD concentration 2%). Preliminary studies showed minimal glucuronidation in human lung microsomes, hence kinetic assays were not conducted.

3.2.5. *In vitro* pulmonary sulfation: RES sulfation activity was determined in pooled mouse lung S9 fraction and in pooled human lung S9 fraction. Conditions of protein and time linearity were optimized in preliminary studies. The incubation mixture consisted of mouse lung S9 fraction (final concentration, 1 mg/ml) or, human lung S9 fraction (final concentration, 0.5 mg/ml), the substrate RES (0.01 uM to 5 mM) solubilized in HP-β-CD (final HP-β-CD concentration 2%), $MgCl_2$ (5 mM final concentration), and made up to final incubation volume (20 uL) with potassium phosphate buffer (10 mM, pH 6.5, 37°C). The reaction mixture was preincubated for 3 min in a shaking water bath at 37°C. The reaction was started by adding 2 uL (stock 10 mM) of the cofactor PAPS (3'-phospho-adenosine-5'-phosphosulphate, final concentration 1 mM) and incubated in a shaking water bath for 60 min at 37°C. To 20 uL of the reaction mixture, 5 uL of ascorbic acid and 60 uL of ice cold methanol containing APAP (IS) were added at the end of 60 min to stop the reaction. All reactions were performed in triplicate. Appropriate negative control experiments were performed under the same conditions but without PAPS.

3.2.6. Protein Binding Assay: Equilibrium dialysis was performed using a 96-well equilibrium dialyzer with a MW cutoff of 5K (Harvard Apparatus, Holliston, MA) which was placed in a dual-plate rotator set to maximum speed (Harvard Apparatus, Holliston, MA), and placed in a 37° C incubator with 10% CO_2 atmospheric environment. Frozen mouse plasma was thawed and its pH was adjusted to 7.4 with 1N hydrochloric acid (HCl). RES, R3G, R3S, R4'G and R4'S protein binding assay was performed at concentrations of 1, 5 and 20 uM. The protein binding assay was performed (Kochansky et al., 2008). In brief, 200 uL of plasma samples and buffer were added to the respective sides of 96-well dialysis plate and the wells were capped. The plate was then placed in the rotator and incubator and was allowed to dialyze for 22 hr. After 22 hr of dialysis, 25 uL of buffer and plasma were removed from each side of dialysis plate and mixed with 25 uL of the opposite matrix. Samples were then stored at -20°C till analysis. Samples were analyzed as explained below except the standard and quality control samples (QCs) were prepared in plasma diluted with an equal volume of buffer.

3.2.7. Pharmacokinetic Analysis

The area under the plasma concentration-time curves (AUC) was calculated by the linear trapezoidal method with extrapolation of $AUC_{0\text{-}inf}$. Clearance was calculated as CL = Dose/$AUC_{0\text{-}inf}$. Volume of distribution based on the terminal phase was calculated as Vd = (Dose)/($\lambda n \times AUC_{0\text{-}inf}$). Volume of distribution at steady state was calculated as Vss = $CL \times MRT_{0\text{-}inf}$. Mean residence time was calculated as MRT = ($AUMC_{0\text{-}inf}/AUC_{0\text{-}inf}$), where AUMC is the first moment of the serum concentration-time curve (Yamaoka et al., 1978). The terminal half-life ($t_{1/2}$) was calculated as 0.693/k, where k is the slope of the

terminal regression line. C_{max} (maximum plasma concentration) and T_{max} (time to reach the maximum plasma concentration) were also estimated. Phoenix WinNonlin 5.1 software was used for non-compartmental analysis. The bioavailability (F) of RES after i.a. and oral administration was calculated with the following equation:

$$F = [\text{mean } AUC_{0\text{-inf, oral}}]/ [\text{mean } AUC_{0\text{-inf, i.a.}}] \times [Dose_{i.a.}]/[Dose_{oral}] \times 100 \quad \text{[Eq 3.1]}$$

where $AUC_{0\text{-inf}}$ is the AUC from time 0 to infinity.

The use of multiple sites input can be used to calculate the extraction of the organ during the first pass through that organ (Mistry and Houston, 1985). Administration of drug into an efferent blood vessel results in rapid passage to the heart and simultaneous distribution to all the tissues of the body according to their particular quota of cardiac output. By comparison following input via an afferent blood vessel, a drug must cross the organ as a single bolus and be metabolized before mixing with the venous return and undergoing distribution throughout the body. First pass loss of RES across the organ may be assessed from the AUC measurements. The bioavailability (f_L) of RES after i.v. and i.a. administration can be calculated with the following equation (Cassidy and Houston, 1980):

$$f_L = [\text{mean } AUC_{0\text{-inf, i.v.}}]/ [\text{mean } AUC_{0\text{-inf, i.a.}}] \times 100 \quad \text{[Eq 3.2]}$$

3.2.8. Data analysis for enzyme kinetics: All data were transformed and Eadie-Hofstee curves were plotted before nonlinear regression analysis. The Michaelis-Menten model was fit only to data which showed linear Eadie-Hofstee plots. The following equation

was used to fit the data showing linear Eadie-Hofstee plots and Michaelis-Menten parameter estimates were determined (Segel, 1993) by:

$$v = Vmax * [S]/(Km + [S]) \quad \text{[Eq 3.3]}$$

where v is the rate of the reaction, Vmax is the maximum velocity estimate, [S] is the substrate concentration, and Km is the Michaelis-Menten constant.

The following equation was used to fit the data exhibiting substrate inhibition profile (Hutzler and Tracy, 2002; Tracy and Hummel, 2004):

$$v = Vmax * [S]/(Km + [S] + \left(\frac{[S]^2}{Ki}\right)) \quad \text{[Eq 3.4]}$$

where Ki is the substrate inhibition constant. Nonlinear regression was performed with GraphPad Prism for Windows (version 4.03; GraphPad Software Inc., San Diego, CA).

3.2.9. Statistics: Student's unpaired t test was used, with $p < 0.05$ set as the significance level. GraphPad Prism for Windows (version 4.03; GraphPad Software Inc., San Diego, CA) was used to perform statistical analysis.

3.3. Results:

3.3.1. Pharmacokinetics of RES: The pharmacokinetic profiles of RES and its metabolites after administration of RES are shown in Fig 3.1 to 3.4. R3G and R3S were the major metabolites and R4'G and R4'S were minor metabolites based on the plasma exposure by i.a, i.v. and oral routes of administration. The results of the noncompartmental pharmacokinetic analysis of i.a. and oral routes are summarized in Table 3.1. Four metabolites R3G, R4'G, R3S and R4'S exhibited early peak plasma concentration after oral and i.a. RES administration. The mouse i.a. studies indicated that RES exhibits a high clearance and a high volume of distribution in mice. The high clearance is likely due to the rapid metabolism of RES. Interestingly, the values for total body clearance (118.77 ml/min/kg or 251.14 ml/min/kg; Table 3.1) greatly exceed the values for hepatic blood flow rate (90 ml/min/kg) in mouse (Davies and Morris, 1993). Even when the hepatic extraction ratio of RES is assumed to be unity, hepatic clearance would exhibit a maximum value of hepatic blood flow (90 ml/min/kg). Extrahepatic clearance was calculated as the difference between total body clearance (118.77 ml/min/kg for 15mg/kg i.a. dose or 251.14 ml/min/kg for 60 mg/kg i.a. dose) and hepatic clearance (90ml/min/kg) as 28.77 and 161.14 ml/min/kg respectively, which represents 24.22% and 64.16% of total body clearance respectively. This shows that extrahepatic clearance, possibly extrahepatic conjugation plays a major role in the overall clearance of RES (Mulder et al., 1984). The oral bioavailability of RES was found to be 55% (calculated using 15mg/kg, i.a. and 60mg/kg, oral data).

RES exposure (294.98 ± 137.87 min*uM) and half life (101.30 ± 43.41 min) after i.v. administration were significantly lower than its exposure (591.08 ± 167.29 min*uM) and half life (190.58 ± 69.65 min) after i.a. administration (AUC: $p = 0.01$, $t_{1/2}$: $p = 0.04$). The bioavailability (f_L) of RES after i.v. administration was found to be 49.90 %. The clearance and volume of distribution at steady state of RES after i.v. administration were not statistically significantly different compared to i.a. administration (CL: $p = 0.05$, Vss: $p = 0.85$). Interestingly, it was observed that the exposure of R3G (2268.35 ± 517.00 min*uM) after i.v. administration of RES increased significantly compared to R3G exposure (921.23 ± 457.07 min*uM) after RES i.a. administration ($p = 0.004$). No significant change was observed in the exposure of R3S after RES administration by both routes ($p = 0.67$).

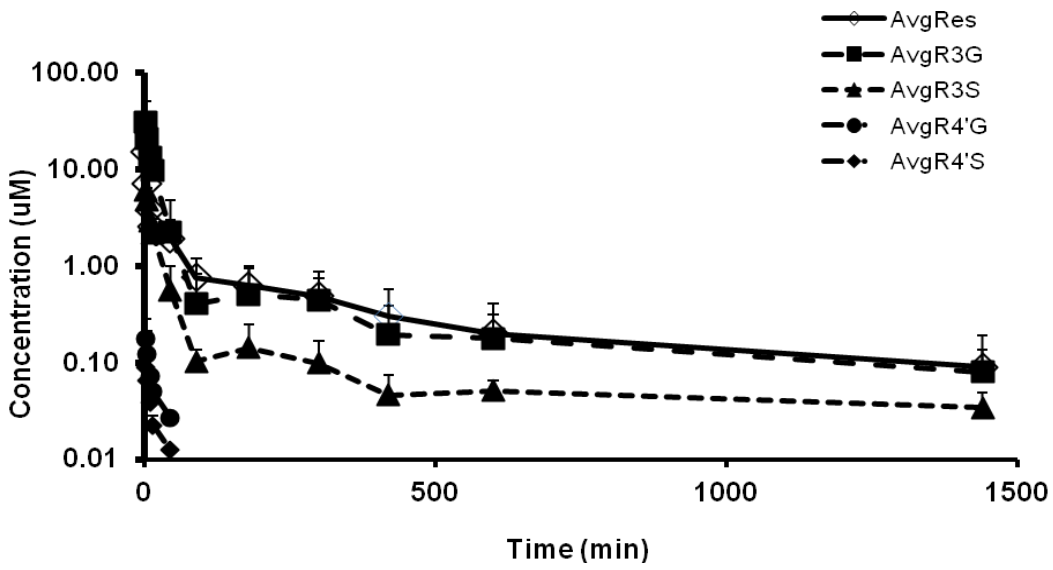

Fig 3.1: Plasma concentration time profile of RES and its metabolites after RES 15 mg/kg (i.a.) administration as a short 10 sec infusion (n = 5). Data are mean + SD.

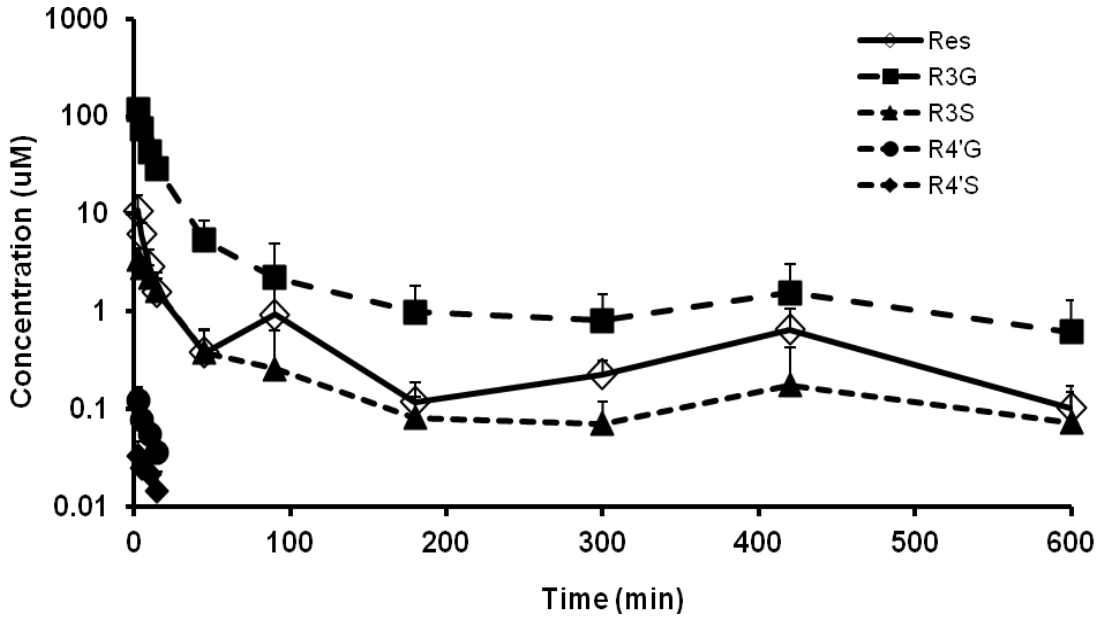

Fig 3.2: Plasma concentration time profile of RES and its metabolites after RES 15 mg/kg (i.v.) administration as a short infusion, 10 sec dose (n = 5). Data are mean + SD.

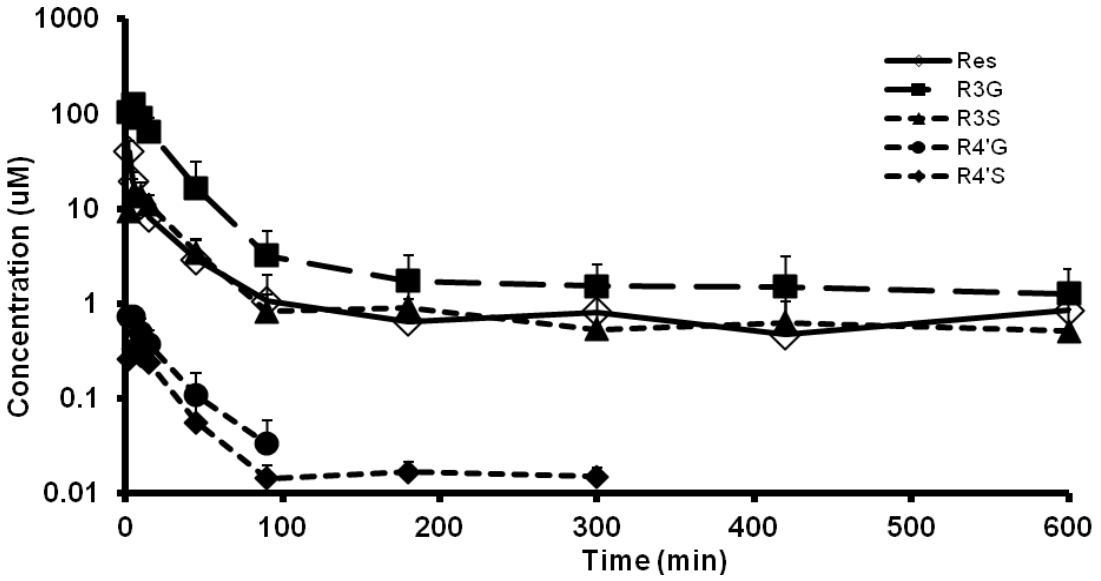

Fig 3.3: Plasma concentration time profile of RES and its metabolites after RES 60 mg/kg (i.a.) administration as a short infusion, 10 sec dose (n = 6). Data are mean + SD.

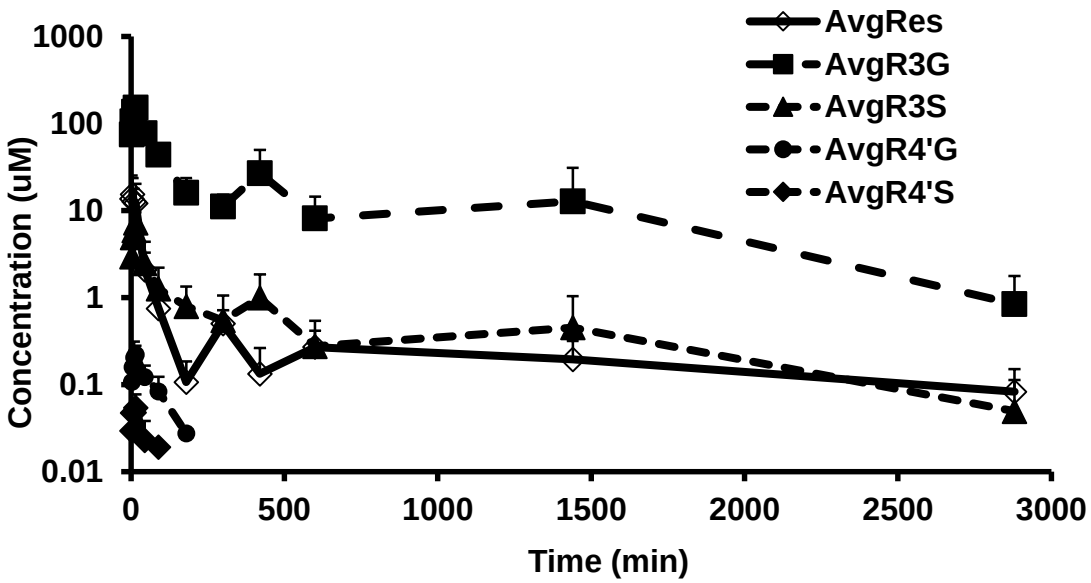

Fig 3.4: Plasma concentration time profile of RES and its metabolites after RES 60 mg/kg (oral) administration (n = 4). Data are mean + SD.

Table 3.1: Pharmacokinetic parameters of RES and its metabolites after 15 mg/kg (i.a.), 60 mg/kg (i.a.) and 60 mg/kg (oral) of RES administration.

RES	60 mg/kg (i.a.) n = 6	15 mg/kg (i.a.) n = 5	60 mg/kg (oral) n = 4	Units
AUC_{0-t}	1065.93 ± 394.89	510.01 ± 105.54	1005.23 ± 626.86	min*uM
AUC_{0-inf}	1206.87 ± 475.51	591.08 ± 167.29	1299.28 ± 603.28	min*uM
Cl	251.14 ± 109.08	118.77 ± 33.36	233.88 ± 95.32	ml/min/kg
Vss	38.35 ± 13.56	37.59 ± 23.70	546.53 ± 409.14	L/kg
$t_{1/2}$	109.75 ± 22.90	190.58 ± 69.65	2130.32 ± 1463.80	min
Cmax	50.10 ± 26.77	15.27 ± 9.07	16.69 ± 9.56	uM
Tmax	2.5 ± 0	2.5 ± 0	6.88 ± 5.54	min
MRT	178.79 ± 93.69	302.80 ± 130.52	2153.80 ± 1306.79	min
R3G				
AUC_{0-t}	3891.47 ± 1179.42	857.36 ± 396.17	36136.71 ± 20187.12	min*uM
AUC_{0-inf}	4191.01 ± 1297.29	921.23 ± 457.07	36998.33 ± 19539.31	min*uM
$t_{1/2}$	174.02 ± 96.69	264.75 ± 248.66	573.43 ± 192.65	min
Cmax	139.03 ± 14.98	59.26 ± 48.13	159.16 ± 21.97	uM
Tmax	5.42 ± 2.46	2.5 ± 0	13.75 ± 2.50	min
MRT	141.02 ± 66.93	251.23 ± 198.15	776.98 ± 286.96	min
R3S				
AUC_{0-t}	823.80 ± 214.63	163.87 ± 42.38	1347.56 ± 561.84	min*uM
AUC_{0-inf}	1023.86 ± 352.44	174.94 ± 45.75	1384.96 ± 554.18	min*uM
$t_{1/2}$	217.57 ± 99.78	201.12 ± 158.12	528.43 ± 107.20	min
Cmax	15.23 ± 5.22	6.11 ± 1.93	7.52 ± 1.73	uM
Tmax	8.33 ± 4.08	2.5 ± 0	13.75 ± 2.17	min
MRT	278.35 ± 163.05	217.75 ± 128.98	752.20 ± 202.04	min
R4'G				
AUC_{0-t}	17.49 ± 7.30	2.03 ± 1.78	15.38 ± 7.61	min*uM
AUC_{0-inf}	18.78 ± 7.61	2.61 ± 1.87	18.03 ± 6.99	min*uM
$t_{1/2}$	17.93 ± 6.34	14.11 ± 5.98	47.46 ± 5.97	min
Cmax	0.82 ± 0.13	0.18 ± 0.11	95.73 ± 33.80	uM
Tmax	5.42 ± 2.46	2.5	12.50 ± 2.89	min
MRT	22.80 ± 7.76	19.28 ± 7.06	70.78 ± 7.66	min
R4'S				
AUC_{0-t}	11.27 ± 3.75	0.83 ± 0.39	3.25 ± 2.72	min*uM
AUC_{0-inf}	12.17 ± 4.39	1.07 ± 0.43	4.99 ± 4.32	min*uM
$t_{1/2}$	41.54 ± 26.90	8.85 ± 4.37	118.2 ± 142.07	min
Cmax	0.36 ± 0.09	0.09 ± 0.02	0.07 ± 0.02	uM
Tmax	6.25 ± 2.80	3.0 ± 1.12	11.25 ± 4.79	min
MRT	51.95 ± 32.08	13.34 ± 5.32	179.76 ± 225.86	min

Note: CL and Vss in case of oral data are CL/F and Vss/F

Table 3.2: Noncompartmental pharmacokinetic analysis upon a single 15 mg/kg (i.a.) RES and 15 mg/kg (i.v.) RES . Data is presented as estimate ± SD.

RES	RES 15 mg/kg i.a. (n = 5)	RES 15 mg/kg i.v. (n = 5)	Units
$AUC_{0\text{-}inf}$	591.08 ± 167.29[a]	294.98 ± 137.87[a]	min*uM
Cl	118.77 ± 33.36	280.04 ± 158.25	ml/min/kg
Vss	37.59 ± 23.70	34.90 ± 20.10	L/kg
$t_{1/2}$	190.58 ± 69.65[a]	101.30 ± 43.41[a]	min
R3G			
$AUC_{0\text{-}inf}$	921.23 ± 457.07[a]	2268.35 ± 517.00[a]	min*uM
R3S			
$AUC_{0\text{-}inf}$	174.94 ± 45.75	157.21 ± 77.77	min*uM

[a] Denotes statistically significant parameters ($p < 0.05$, Student's unpaired t test).

Note: CL in case of i.v. data is CL/F

3.3.2. *In vitro* plasma protein binding of RES and its metabolites: The plasma protein binding of RES, R3G, R3S, R4'G and R4'S was measured at three concentrations of 1 uM, 5 uM and 20 uM substrate in plasma (Table 3.3). RES and its sulfated metabolites (R3S, R4'S) exhibited high plasma protein binding (86 – 94 %) whereas the glucuronidated metabolites (R3G, R4'G) exhibited lower plasma protein binding (39 - 70 %). It's interesting that the glucuronides have lower binding than sulfates.

Table 3.3: Extent of binding of RES, R3G, R3S, R4'G and R4'S to mouse plasma proteins (mean ± SD), n =3 for each concentration.

% Bound in plasma	1 uM	5 uM	20 uM
RES	ND	86.06, 83.88*	91.95 ± 0.99
R3G	65.77 ± 10.09	70.42 ± 2.56	66.75 ±1.56
R3S	94.50 ± 0.13	93.26 ± 0.44	87.24 ± 4.89
R4'G	44.88 ± 6.65	39.04 ± 10.33	51.80 ± 3.28
R4'S	93.08 ± 1.17	90.97 ± 0.70	88.36 ± 1.17

ND – Not detected; dialysate (unbound) concentration fell below the LLOQ of analytical method.
* Range is listed for n=2.

3.3.3. *In vitro* pulmonary metabolism: The glucuronidation and sulfation of RES was studied in mouse and human lung fractions. When RES was incubated with 0.1 and 0.5 mg/ml human lung microsomes, no R3G was observed above LOQ (10 ng/ml for R3G) at the end of 60 min incubation. Therefore no further RES glucuronidation kinetic studies were performed with human lung microsomes. Formation of R3G and R3S was linear with respect to time and protein concentration in mouse and human lung S9 fraction (Fig 3.5 to 3.7). Fig 3.8 (A) shows the formation rate of R3G in mouse lung fraction with its Eadie-Hofstee (E-H) plot shown as inset. The R3G profile exhibited substrate inhibition. This was determined by fitting the data to the substrate inhibition equation (Eq 3.4) and by visual examination of E-H plot. The E-H plot showed a hook in the upper quadrant typical of substrate inhibition kinetic profile (Fig 3.8 (A) inset) (Hutzler and Tracy, 2002). Enzyme kinetic parameters are presented in Table 3.4. Fig 3.8 (B) and 3.8 (C) show the formation kinetics of R3S in mouse and human lung fractions with its Eadie-Hofstee (E-H) plots as insets respectively. R3S formation in both mouse and human lung fractions showed substrate inhibition (Hutzler and Tracy, 2002).

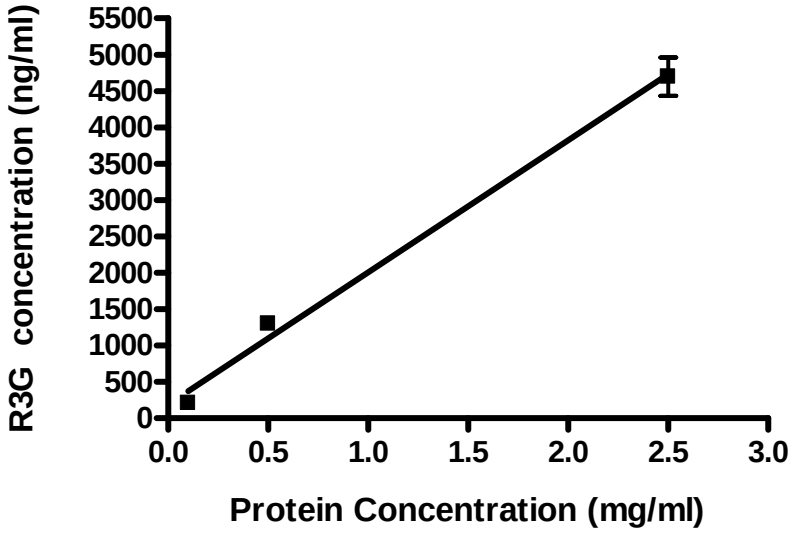

Fig 3.5 (A)

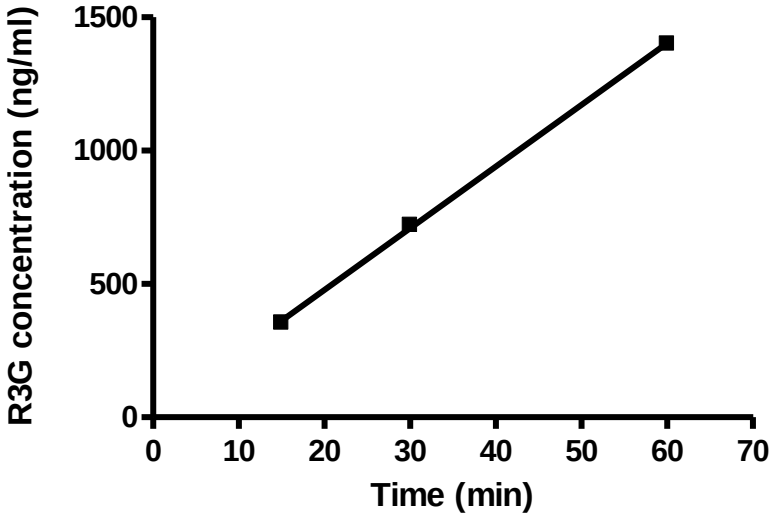

Fig 3.5 (B)

Figure 3.5: Linearity of formation for R3G in mouse lung S9 fraction (n = 3); A) Protein linearity over a 0.1 – 2.5 mg/ml concentration range using an incubation time of 60 mins B) Time linearity over 0 - 60 min time period with 0.5 mg/ml final protein concentration.

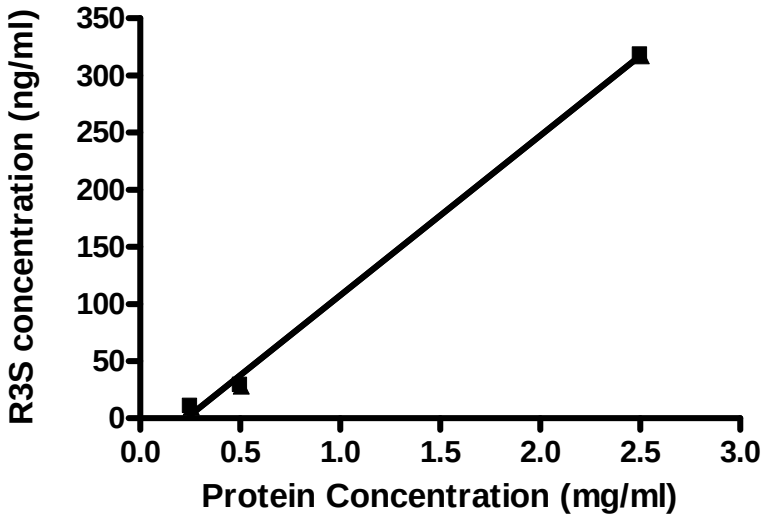

Fig 3.6 (A)

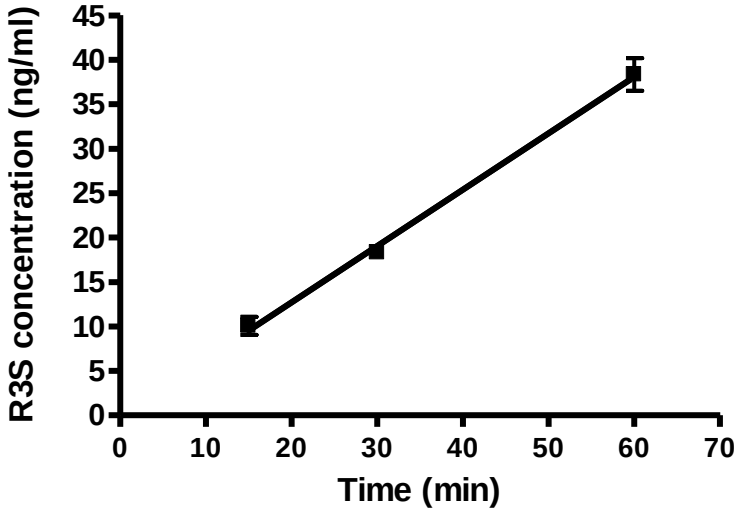

Fig 3.6 (B)

Figure 3.6: Linearity of formation for R3S in mouse lung S9 fraction (n = 3); A) Protein linearity over a 0.1 – 2.5 mg/ml concentration range using an incubation time of 60 mins B) Time linearity over 0 - 60 min time period with 0.5 mg/ml final protein concentration.

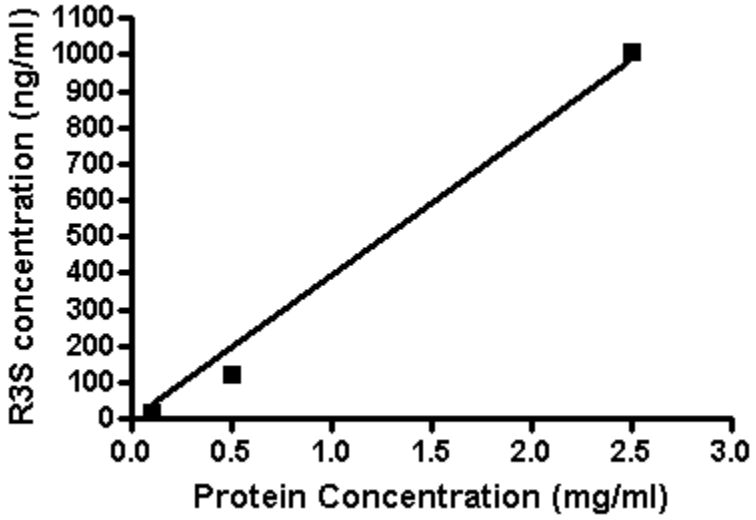

Fig 3.7 (A)

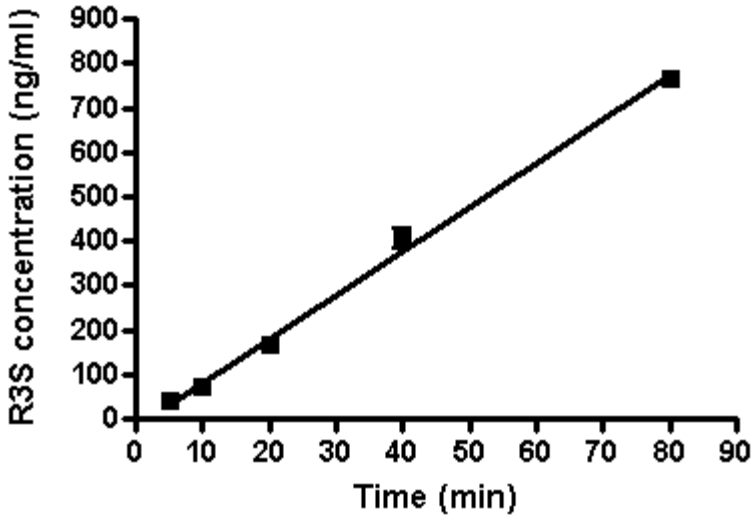

Fig 3.7 (B)

Figure 3.7: Linearity of formation for R3S in human lung S9 fraction; A) Protein linearity over a 0.1 – 2.5 mg/ml concentration range using an incubation time of 60 mins (n = 2) B) Time linearity over 0 - 80 min time period with 0.5 mg/ml final protein concentration (n = 3).

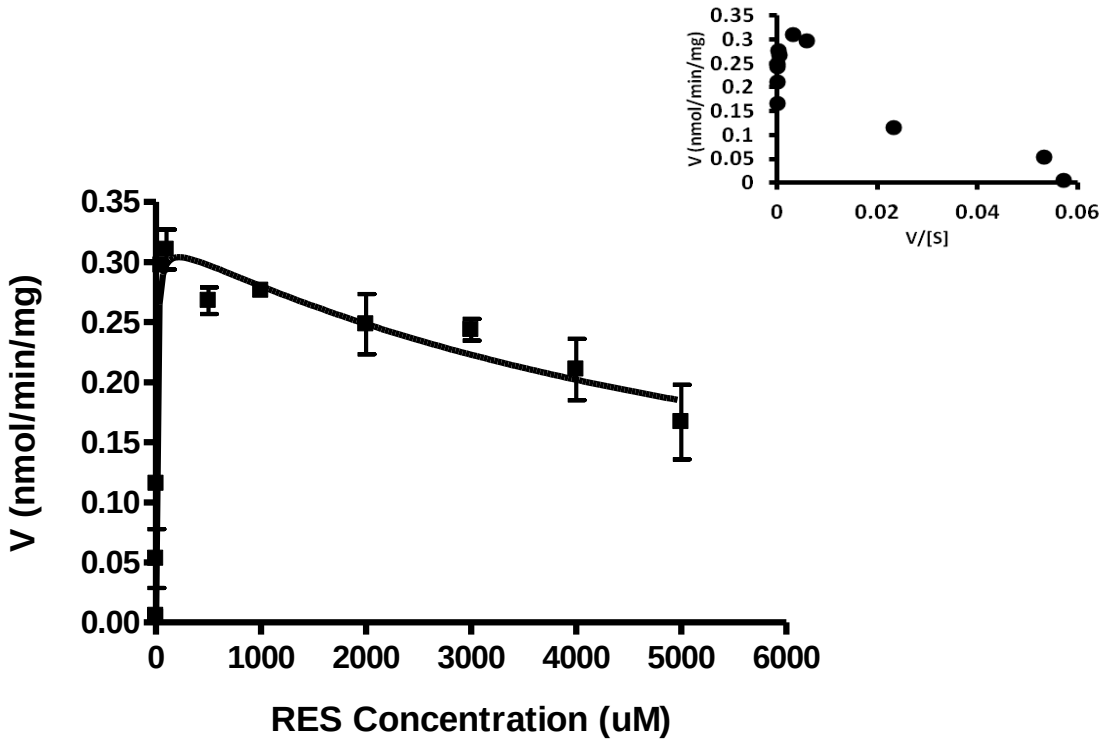

Fig 3.8 (A)

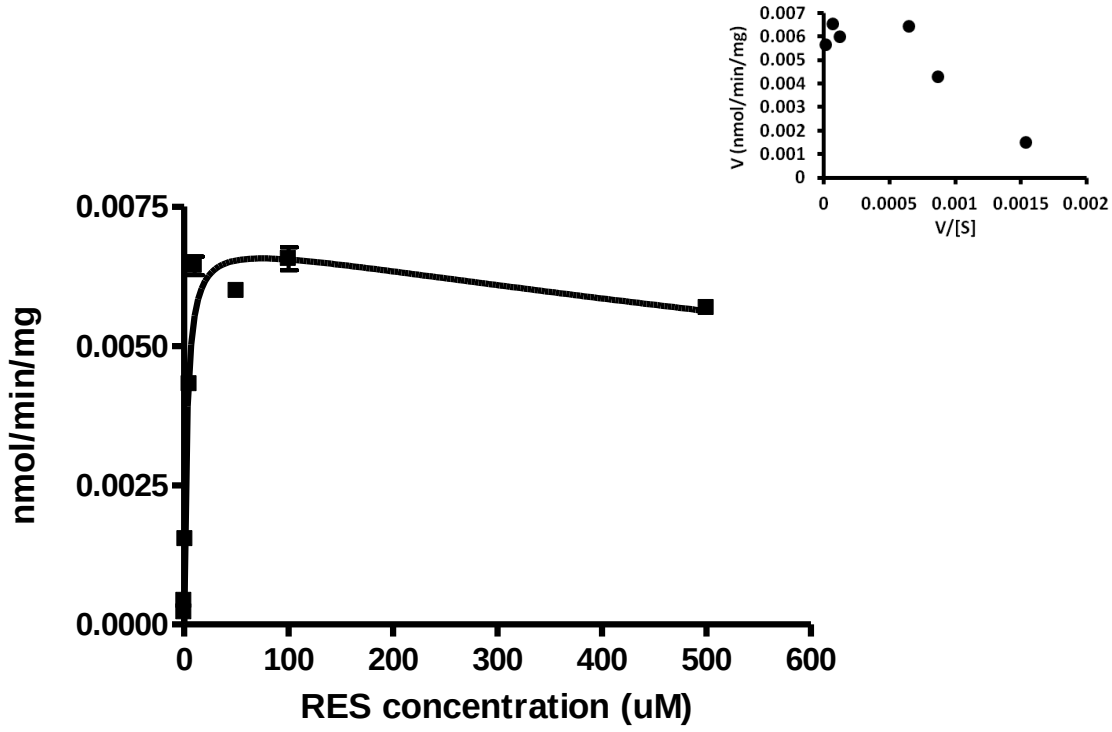

Fig 3.8 (B)

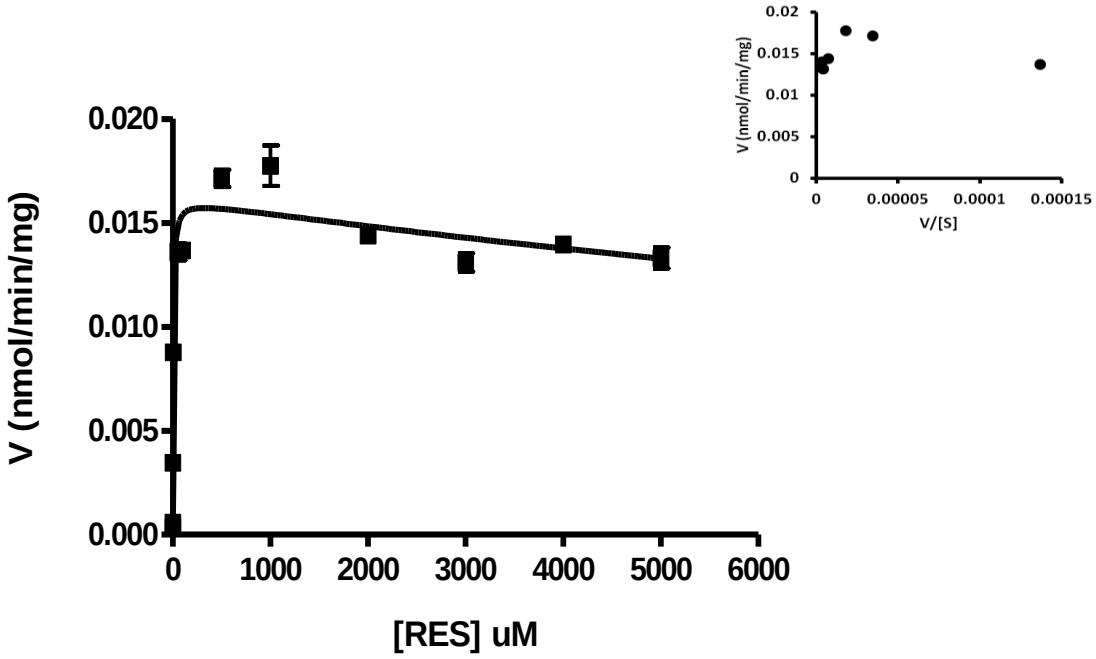

Fig 3.8 (C)

Fig 3.8: Kinetics of A: R3G formation in mouse lung S9 fraction, B: R3S formation in mouse lung S9 fraction, C: R3S formation in human lung S9 fraction. Data reported as mean ± standard deviation, (n = 3). The solid line represents curve fitting with the substrate inhibition equation (Eq 3.4); the figure in the inset represents the Eadie-Hofstee plot.

Table 3.4: Kinetic parameter estimates for the sulfation and glucuronidation of RES and R3S by human and mouse lung fractions. Data are expressed as estimates ± SD; n = 3. Estimate units are as follows: Vmax: nanomoles per minute per milligram total protein; Km, Ki : micromolar.

Substrate	Conjugation product	Protein source	Vmax (pmol/min/mg)	Km (uM)	Ki (uM)	Goodness of Fit (r^2)	Type of Fit
RES	R3G	Mouse lung S9	324.40 ± 13.05	7.34 ± 1.60	6632 ± 1198	0.93	Partial substrate inhibition
RES	R3S	Mouse lung S9	7.05 ± 0.28	2.69 ± 0.45	2021 ± 717.6	0.96	Partial substrate inhibition
RES	R3S	Human lung S9	16.15 ± 0.48	4.45 ± 0.79	23238 ± 7305	0.95	Partial substrate inhibition

3.4. Discussion and Conclusion:

The pharmacokinetics of RES are complex. RES has been shown to undergo extensive metabolism primarily to its glucuronidated and sulfated conjugates (Walle et al., 2004; Brown et al., 2010; Juan et al., 2010b; Iwuchukwu et al., 2012; Sharan et al., 2012). RES administration by i.a., i.v. and oral routes led to the formation of R3G and R3S as major metabolites and R4'G and R4'S as minor metabolites (Fig 3.1 to 3.4). Reentry peaks of RES, R3G and R3S in the plasma, likely due to enterohepatic recirculation, occurred at 5 to 7 hours after oral administration of 60 mg/kg of RES. Although no clear reentry peak for RES was observed after i.a. administration of RES, it has been confirmed (Marier et al., 2002) in bile cannulated rats that RES and R3G undergoes enterohepatic recirculation. Very high Vss for RES is also observed, partly because the enterohepatic cycling (EHC) loop behaves as an additional distributional compartment in the pharmacokinetic system as also explained by Herman and co workers (Herman et al., 1989). By bringing the RES and its metabolites back into systemic circulation by EHC, an extra area is added at the end of the concentration-time profile and their half lives are enhanced. Herman and co workers suggested that for drugs undergoing EHC, intestine changes from an eliminating to a holding, or only partially eliminating, organ and as such becomes integrated as a factor in the apparent volume of drug distribution (Herman et al., 1989). This might be one of the reasons for the very high volume of distributions for RES.

The very high clearance of RES (i.a), higher than hepatic blood flow, indicates extra-hepatic conjugation in the mouse. It has been shown that intestine, liver and lung

contribute to phenol metabolism (Cassidy and Houston, 1980). These indications led us to investigate the lung as a possible metabolizing organ for RES. Lungs are the third in a series of three potential biotransformation sites (the other two being the gut and liver) which orally ingested RES must cross prior to entering the general circulation. First pass metabolism by gut, liver and lungs in series can increase total body clearance of RES. Although the role of gut and liver in the metabolism of RES is known (Miksits et al., 2005; Brill et al., 2006; Iwuchukwu and Nagar, 2008), contribution of lungs in the metabolism of RES has not been evaluated. In the present study, contribution of lungs in the metabolism of RES was evaluated using multiple site of administration and single site of sampling design (Cassidy and Houston, 1980) in a mouse model. The *in vivo* study clearly demonstrated the contribution of lungs in the glucuronidation of RES to R3G in mice. The *in vivo* results were corroborated by *in vitro* results in mouse lung fractions.

Because species dependent differences in metabolism are known, *in vitro* studies were also conducted in human lung fractions to see if reliable extrapolation of data can be made between mice and humans. Interestingly, no significant glucuronidation of RES was observed in human lung fractions, implying that contribution of pulmonary glucuronidation in the metabolism of RES is quantitatively less important in humans. The species difference in RES glucuronidation at its 3-OH position can be explained by differential expression of urindine 5'-diphosphoglucuronosyltransferase (UGT) isoforms in mouse and human lungs. RES has been reported to be glucuronidated at its 3-OH position via UGT1A1, UGT1A7, UGT1A9,UGT1A3, UGT1A6, UGT1A8, UGT1A10 and UGT2B7 (Brill et al., 2006). Ugt1a6 has been shown to be expressed well in mouse

lung (Buckley and Klaassen, 2007). Thus, Ugt1a6 might be responsible for RES glucuronidation in mouse lungs. There are conflicting reports about the presence of UGT enzymes in human lung tissues. UGT1A1 and UGT1A10 have been reported in the lung cancer samples (Oguri et al., 2004). UGT 2B isozymes (4, 7, 10, 11, 15 and 17) have been reported to be present in human lungs (Turgeon et al., 2001). UGT activity has been reported to be highly expressed in the tissues of upper respiratory tract in human subjects (Zheng et al., 2002) which is of more importance to the inhaled compounds. In contrast, other studies have shown low or no UGT activity in normal human lung tissue (Zheng et al., 2002; Somers et al., 2007; Nakamura et al., 2008). In the present study, the absence of R3G formation in human lung fraction is consistent with the low expression or absence of UGT isoforms in normal human lung tissue (Nakamura et al., 2008) which are responsible for RES glucuronidation (Brill et al., 2006).

Sulfation experiments showed that RES is sulfated by both mouse as well as human lungs. RES sulfation at its 3-OH position has been reported to be mediated by sulfotransferase (SULT) SULT1A1, SULT1A2, SULT1A3 and SULT1E1 isoforms (Miksits et al., 2005). Mouse lungs express Sult1a1, with very low expression of Sult1e1 (Alnouti and Klaassen, 2006). SULT1A1, SULT1A3, SULT1E1, SULT2A1 and SULT1B1 have been found to be expressed in human lungs, and SULT1A1, SULT1A3 and SULT1E1 account for around 80 percent of all SULTs expressed in human lungs (Riches et al., 2009). Therefore, our results indicate that Sult1a1 and Sult1e1 in mouse lungs and SULT1A1, SULT1A3 and SULT1E1 in human lungs might be responsible for R3S formation. Steroid sulfatase activity have been reported in human (Milewich et al.,

1983) and mouse lung tissue (Milewich et al., 1984) with highest activity in microsomal fraction of human lung tissue homogenate (Milewich et al., 1983). Steroid sulfatase can desulfate R3S to give RES locally in the lung cells. This futile cycling of RES/R3S by the combined activity of sulfatase and sulfotransferase enzyme can lead to increase in the retention of the RES/R3S within the lung. This can be important since RES and R3S both have been shown to have pharmacological activity (Hoshino et al., 2010).

Transporters in conjunction with metabolizing enzymes play an important role in the disposition of drug and its metabolites. R3G and R3S disposition has been shown to be influenced by transporters. R3G has been shown to be a high affinity substrate for MRP2 (ABCC2), MRP3 (ABCC3) and BCRP (ABCG2) transporters (Maier-Salamon et al., 2008; van de Wetering et al., 2009; Juan et al., 2010a). Although the role of MRP1 (ABCC1) in R3G transport has not been evaluated, there are reports of MRP1-mediated transport of glucuronides such as 17β-estradiol-glucuronide (Jedlitschky et al., 1996), etoposide glucuronides, SN-38 glucuronide (Deeley and Cole, 2006) and β-O-glucuronide conjugate of the tobacco specific carcinogen 4-(methyl-nitrosamino)-1-(3-pyridyl)-1-butanol (NNAL) (Leslie et al., 2001). BCRP and MRP2 are involved in the transport of R3S (van de Wetering et al., 2009; Juan et al., 2010a). MRP4 (ABCC4) and MRP1 (ABCC1) have not been studied for R3S transport but there are reports which show both MRP4 and MRP1 to be involved in the transport of sulfo-conjugates such as dehydroepiandrosterone sulfate (Zelcer et al., 2003) and estrone 3-sulfate (Qian et al., 2001) for MRP1. Mouse lungs have been shown to express Mrp1, Mrp3 and Mrp4

transporters (Maher et al., 2005). It is interesting that mouse lungs did not express Mrp2 and Bcrp transporter (Scheffer et al., 2002; Maher et al., 2005).

Cellular distribution and localization of transporters in mouse lungs is unknown although cellular distribution and localization of MRP1, MRP2 and BCRP in human lungs are reported. MRP1, 3, 4 are basolateral transporters while MRP2 and 5 are located in the apical membrane of the cells (Toyoda et al., 2008). MRP 1 is expressed on basolateral membrane whereas MRP2 and BCRP are expressed towards apical membrane in human lungs (Bosquillon, 2010).

Based on the present results and previous reports, (Maher et al., 2005; Bosquillon, 2010) a simplified schematic pathway for disposition of RES, R3S and R3G in mouse lung cells has been proposed (Fig 3.9A). RES when administered i.v., can diffuse into mouse lung cells and can either get metabolized by SULT enzymes present in the cytosol or UGT enzymes present in the endoplasmic reticulum. Additionally, R3S formed from RES can get desulfated by sulfatase enzymes in the endoplasmic reticulum to give RES, which can further get glucuronidated to R3G. R3G formed can get transported into the cytoplasm and be transported into the blood by MRP3 and possibly MRP1. This also correlates well with our observation that even after sulfation of RES in lungs (based on our *in vitro* results) we did not observe any significant difference in the plasma exposure of R3S, when RES was administered by i.v. route compared to i.a. route. Similarly a schematic pathway for disposition of RES in human lungs has been proposed (Fig 3.9B). RES when presented to human lung cells gets sulfated to R3S in the cytoplasm. R3S formed can be

eliminated in the pulmonary lumen by MRP2 and BCRP transporters or blood by possibly MRP1 and MRP4 transporters. Additionally it can be desulfated by steroid sulfatase enzymes present in endoplasmic reticulum to give back RES. Since no activity of UGT was observed in human lung tissue, RES formed in endoplasmic reticulum can act as depot or diffuse back into cytoplasm to again get sulfated to R3S. This futile cycling of RES/R3S can prolong the presence of RES/R3S in human lung tissue and can be of pharmacological significance as both RES and R3S have been shown to have pharmacological activity (Hoshino et al., 2010).

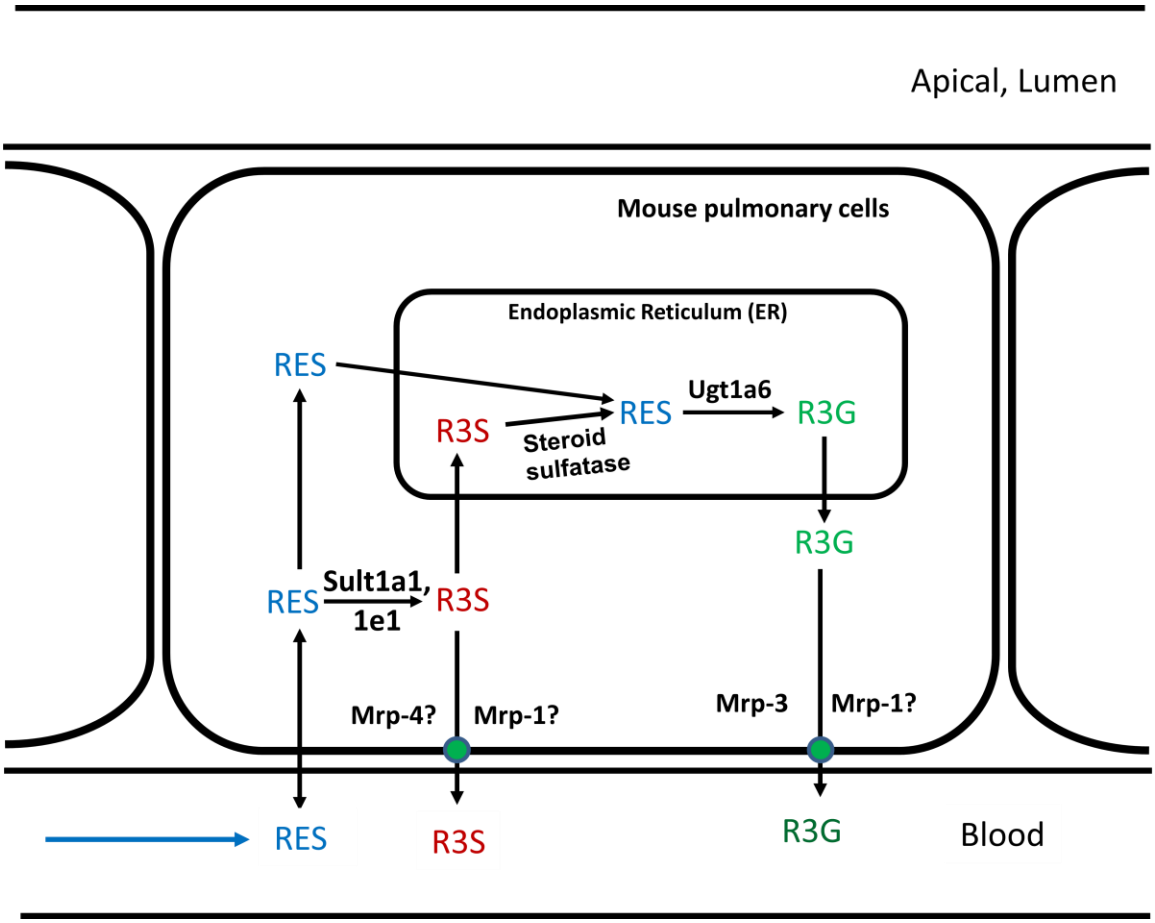

Figure 3.9 (A)

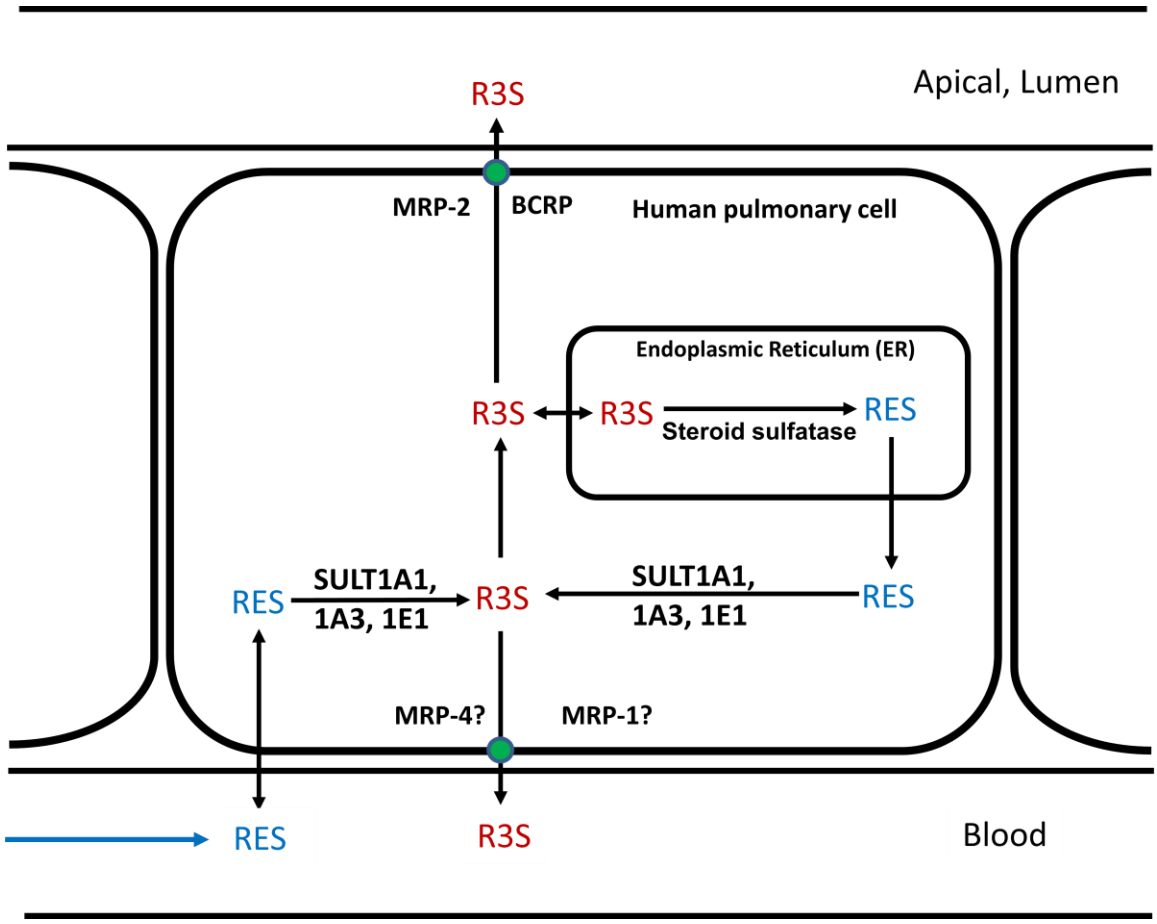

Figure 3.9 (B)

Figure 3.9: Proposed schematic representation of RES metabolism in **A)** mouse lung cell, **B)** human lung cell. Solid line represents pathways based on results in this manuscript and published literature reports for RES, R3S and R3G. Transporters followed by "?" indicates that the role of these transporters are not known for transport of R3S and R3G, but is based on findings of transport of other sulfated and glucronidated substrates.

The pulmonary metabolism of RES can have implications for local tissue level of parent and metabolites as well as in the systemic plasma level of RES and its metabolites. The absence of pulmonary glucuronidation in human lung as compared to extensive

pulmonary glucuronidation in mouse lungs can be one possible reason for the observed difference in pharmacokinetics of RES in rodents as compared to humans. In rodents, R3G has been observed as the major metabolite (Juan et al., 2010b; Colom et al., 2011; Iwuchukwu et al., 2012; Sharan et al., 2012) as compared to R3S in humans (Boocock et al., 2007; Brown et al., 2010). Benzo[a]pyrene is a polycyclic aromatic hydrocarbon (PAH) present in tobacco smoke and is considered as a procarcinogen. Its metabolic activation by aldo-keto reductases leads to the formation of benzo[a]pyrene-7,8-catechol, which undergoes autooxidation to yield benzo[a]pyrene-7,8-dione, generating reactive oxygen species (ROS). Benzo[a]pyrene-7,8-dione in the presence of nicotinamide adenine dinucleotide phosphate (NADPH) is reduced back to the catechol leading to futile redox-cycles and in turn amplifying ROS. Sulfation of benzo[a]pyrene-7,8-catechol has been suggested to be a detoxification pathway for benzo[a]pyrene-7,8-dione by limiting its ability to enter the redox cycle (Zhang et al., 2012a). By serving as substrates for SULTs, there is a possibility that RES might interfere with the detoxification of cigarette smoke toxicants. However there is also a possibility that the increased RES/R3S presence due to futile cycling in lung will lead to enhanced quenching of unstable free radicals, thereby reducing damage to DNA by reactive oxygen species (ROS) produced by cigarette smoke toxicants, as RES/R3S have been shown to have a comparable ability to quench the 2,2-diphenyl-1-picrylhydrazyl (DPPH) free radical (Hoshino et al., 2010).

In conclusion, R3G and R3S were found to be the major metabolites and R4'G and R4'S to be the minor metabolites in mouse irrespective of the route of administration. A significantly higher R3G exposure was observed in mouse when RES was administered

by i.v. route compared to i.a. route. Extensive glucuronidation and sulfation of RES was observed in mouse lung fractions. Human lung fractions, on the other hand, showed only sulfation of RES.

CHAPTER 4

PHARMACOKINETICS OF SULFATED METABOLITES OF RESVERATROL: RESVERATROL-3-SULFATE (R3S) AND RESVERATROL-4'-SULFATE (R4'S)

4.1. Rationale:

Resveratrol has been shown to undergo extensive metabolism and majority of RES detected in serum or urine after oral or systemic RES administration is in the form of its glucuronide and sulfate conjugates (Goldberg et al., 2003; Walle et al., 2004; Brown et al., 2010; Juan et al., 2010b; Iwuchukwu et al., 2012; Sharan et al., 2012). Low plasma concentrations of RES *in vivo* have led to the idea that metabolites might themselves be active. Recently two papers have been published where researchers have shown positive biological activity for sulfated metabolites of RES. This also assumes importance as it has been shown that sulfated metabolites are the major metabolites in humans (Boocock et al., 2007; Brown et al., 2010). Calamini and coworkers (Calamini et al., 2010) have shown that R4'S and RES inhibit COX-1 and COX-2 with similar efficacy, which is important as it has been shown that RES causes cardioprotective and anticancer effects by inhibiting COX-1 and COX-2 enzymes (Goldberg et al., 1995; Pace-Asciak et al., 1995; Jang et al., 1997b). Induction of QR1 has been reported to be associated with cancer chemoprevention (Talalay et al., 1995; Kennelly et al., 1997) and also coincides with the induction of detoxifying phase II metabolizing enzymes (Song et al., 1999). R3S has been shown to be a more potent QR1 inducer than RES (Hoshino et al., 2010). In work published by Hoshino and coworkers (Hoshino et al., 2010), it was reported that R3S and R4'S exhibited 2,2-diphenyl-1-picrylhydrazyl (DPPH) free radical scavenging

activities and comparable COX-1 and COX-2 inhibitory activities. The free radical scavenging activity of R3S was comparable and R4'S lower than that of RES. At least part of the chemopreventive activity of RES is also attributed to its ability to quench unstable free radicals and prevent damage to DNA by reactive oxygen species (ROS) (de la Lastra and Villegas, 2007; Qian et al., 2009). R3S and R4'S also inhibited nitric oxide (NO) production by inducible nitric oxide synthase (iNOS) and NFkB induction, although their activity was lower than that of RES (Hoshino et al., 2010).

In light of the recent findings of the above mentioned biological activity of R3S and R4'S, this study was undertaken to characterize the pharmacokinetic profile of preformed R3S and R4'S in an *in vivo* mouse model after direct administration of the metabolite following oral and i.a. administration. This study aimed at providing a better understanding of the influence of sulfated metabolites disposition on RES pharmacokinetics. This study also evaluated the hypothesis postulated by several researchers that metabolites can act as depot of RES and can be desulfated to give back RES at the tissue level, e.g. liver.

4.2. Materials and Methods:

4.2.1. Drug administration and blood sampling: R3S and R4'S were solubilized in saline. Details about surgery and cannulation have been provided in section 3.2.2. of chapter 3. Carotid artery cannula was used for systemic drug administration and blood sampling. Heparin-saline (20 uL, 50 IU/ml) was used to flush the cannula after systemic administration or blood sampling. Sulfated metabolites were synthesized and provided by

Dr. Daniel Canney's lab (Iwuchukwu et al., 2012). R3S was administered at a dose of 5, 10 or 20 mg/kg i.a. and 10 mg/kg orally. The lower dose of 5 mg/kg was selected by performing pilot studies which gave R3S exposures (AUCs) in the range comparable to R3S observed upon 15 mg/kg RES (i.a.) administration. The higher dose of 20 mg/kg was selected as it was equimolar dose to 15 mg/kg of RES dose. R4'S was administered at a dose of 5 or 20 mg/kg i.a. and 20 mg/kg orally. The higher dose of 20 mg/kg for R4'S was selected as it was equimolar dose to 15 mg/kg of RES dose. Blood (20 uL) was serially sampled at 2.5, 5, 10, 15, 45, 90, 180, 300, 420, 600 min and 24 hrs. Blood samples were centrifuged at 14,000 rpm for 2 min, and harvested plasma was collected and stored at -80 °C until LC-MS/MS analysis. PK analysis was performed as explained in section 3.2.7. of chapter 3.

4.2.2. Hepatic Glucuronidation Assay: Glucuronidation of R3S after its desulfation was determined in mouse liver microsomes and pooled human liver microsomes. Conditions of protein and time linearity were optimized in preliminary studies. The incubation mixture consisted of mouse liver microsomes or human liver microsomes (final concentration, 0.5 mg/ml) for their respective studies, the substrate R3S (final concentration range of 0.01 uM to 1 mM of R3S) solubilized in water, alamethicin (10 ug/ml), $MgCl_2$ (5 mM final concentration), and made up to final incubation volume (20 uL) with Tris-HCl buffer (100 mM, pH 7.4, 37°C). The reaction mixture was preincubated for 3 min in a shaking water bath at 37°C. The reaction was started by adding appropriate volume of the cofactor UDPGA (final concentration 5 mM) and incubated in a shaking water bath for 60 min at 37°C. Appropriate negative control

experiments were performed under the same conditions but without the cofactor UDPGA. All reactions were performed in triplicate. Additional incubations were conducted with and without the steroid sulfatase inhibitor STX64 (25 uM final concentration) at 0.5 mM R3S concentration. For all incubations, 5 uL of ascorbic acid (15%) and 60 uL of ice cold methanol containing APAP (IS) were added to 20 uL of reaction mixture at the end of 60 min to stop the reaction.

4.2.3. Data analysis for enzyme kinetics: All data were transformed and Eadie-Hofstee curves were plotted before nonlinear regression analysis. The Michaelis-Menten model was fit only to data which showed linear Eadie-Hofstee plots. The following equation was used to fit the data showing linear Eadie-Hofstee plots and Michaelis-Menten parameter estimates were determined (Pearson and Wienkers, 2009):

$$v = Vmax * [S]/(Km + [S]) \quad (4.1)$$

where v is the rate of the reaction, V_{max} is the maximum velocity estimate, [S] is the substrate concentration, and Km is the Michaelis-Menten constant.

The following equation was used to fit the data exhibiting substrate inhibition profile (Hutzler and Tracy, 2002; Tracy and Hummel, 2004):

$$v = Vmax * [S]/(Km + [S] + \left(\frac{[S]^2}{Ki}\right)) \quad (4.2)$$

where Ki is the substrate inhibition constant. Nonlinear regression was performed with GraphPad Prism for Windows (version 4.03; GraphPad Software Inc., San Diego, CA).

4.2.4. Permeability study:

MDCK cells were cultured and transport experiments were conducted (Korzekwa et al., 2012). Cells were maintained in DMEM supplemented with 10% FBS, penicillin (100 U/ml) and streptomycin (100 ug/ml) at 37°C in a humidified incubator with 5% CO_2. All cells were seeded at a density of 60,000 cells/cm^2 onto collagen-coated, microporous, polycarbonate membranes in 12-well Transwell® plates. Cells were used between passages 10 and 14. The culture medium was changed 24 hr after seeding to remove cell debris and dead cells; afterwards the medium was changed 24 hr after seeding to remove cell debris and dead cells; afterward the medium was changed every other day for 6 days. The permeability assay buffer was Hank's balanced salts solution (HBSS) containing 10 mM hydroxyethylpiperazineethane sulfonic acid (HEPES) and 15 mM glucose at pH 7.4 (Hank's balanced transport buffer). The test compounds were prepared in HBSS buffer to a final concentration of 20 uM each. R3S and R4'S stock solutions in DMSO were diluted in Hank's balanced transport buffer (pH 7.4) (Mediatech, Herndon, VA) to give a final DMSO concentration of 1 percent. R3S and R4'S (20 uM final concentration) were dosed on either the apical side (A-B transport) or the basolateral side (B-A transport) and incubated in a humidified atmosphere at 37°C with 5% CO_2. Samples were collected at 0, 5, 10, 20, 40 and 80 minutes for experiments in each direction. All experiments were conducted in duplicate and an average of the data was used. Lucifer yellow test was conducted to ensure the integrity of cell monolayer (Wang et al., 2008). The acceptance criteria for each batch of cell monolayer was a P_{app} of less than 0.4×10^{-6} cm/s (Wang et al., 2008). The apparent permeability coefficient, P_{app}, was calculated as follows:

$$P_{app} = (\Delta Qr/\Delta t)/(A\times C_0) \qquad (4.3)$$

Efflux ratio = P_{app} (B to A)/P_{app} (A to B) (4.4)

where $\Delta Qr/\Delta t$ is the cumulative amount in the receiver compartment versus time; A is the area of the cell monolayer; C_0 is the initial concentration of the dosing solution.

4.3. Results:

4.3.1. Pharmacokinetics of R3S

The pharmacokinetic profiles of R3S and its metabolites after R3S administration at different dose levels and through different routes are shown in Fig. 4.1 through Fig 4.3. R3G was the major metabolite based on the plasma exposure by both i.a. and oral routes of administration. The results of noncompartmental pharmacokinetic analysis are summarized in Table 4.1. We detected RES in few plasma samples at low concentrations. However in one mouse at 10 mg i.a. dose study we observed high RES concentrations (0.45, 2.88 and 38.64 uM at 90, 180 and 300 min respectively). Due to paucity of data points the kinetic parameters of RES could not be calculated. We observed in the mouse i.a. studies that R3G concentration initially declined rapidly until 90 min and then an abrupt increase in its systemic concentration was observed around 180 min onward. The mouse i.a. studies indicated that R3S exhibits a high clearance and a high volume of distribution in mice. The high clearance is likely due to rapid metabolism of R3S into R3G. The differences in clearance for R3S at 5, 10 and 20 mg/kg was not statistically significant ($p < 0.05$), indicating linear PK in this dose range.

Peak concentration (Cmax) of 0.65 ± 0.45 uM was observed after oral R3S dose between 2.5 to 15 min except for one mouse for which it occurred at 180 min, indicating that R3S was absorbed fast orally. Reentry peaks of R3G were clearly observed in R3S i.a. administration studies indicating enterohepatic recycling of R3G. The oral bioavailability of R3S was found to be poor (28 % at 10 mg/kg). The cause of poor oral bioavailability, in addition to poor absorption of R3S, might be sequential first pass elimination of R3S into R3G in liver with R3G being cleared by liver through the biliary route. Interestingly

two mice in the 10 mg/kg oral administration group exhibited the formation of R3G and R4'S as major metabolites. R4'S was not observed in any other mice besides these two animals. This variability can be attributed to the variability in the gut flora of animals which might lead to varied metabolism of R3S.

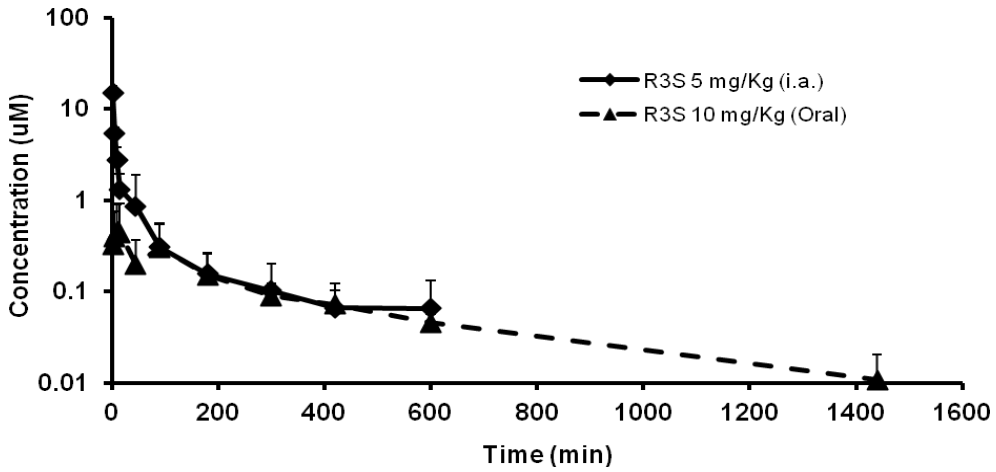

Fig 4.1: Plasma concentration time profile of R3S after R3S 5 mg/kg (i.a.) and 10 mg/kg (oral) administration (n = 4). Data presented as mean + SD.

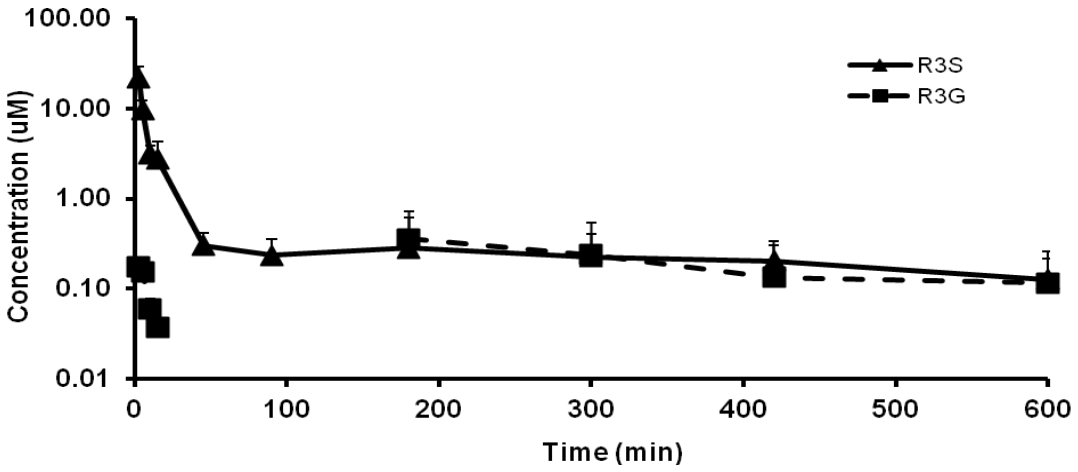

Fig 4.2: Plasma concentration time profile of R3S and its metabolite R3G after R3S 10 mg/kg (i.a.) administration (n = 4). Data presented as mean + SD.

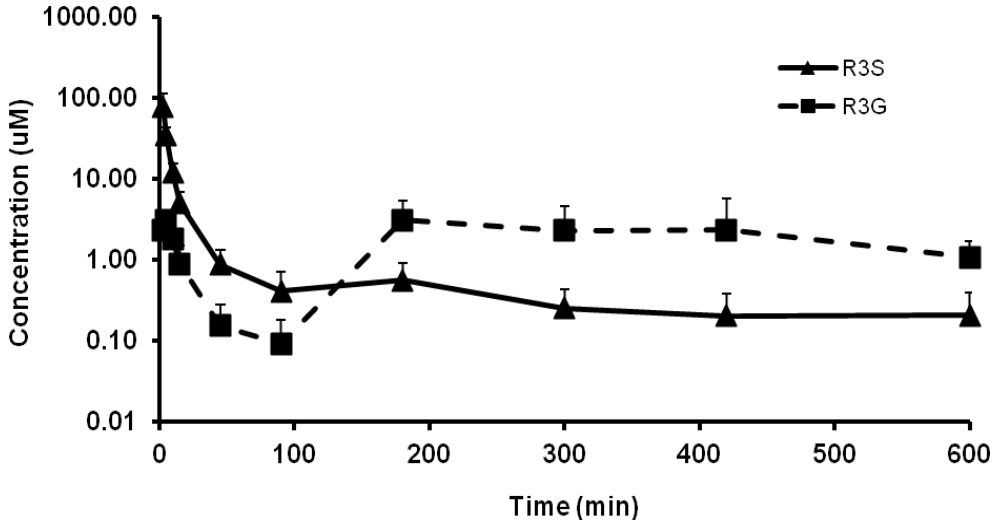

Fig 4.3: Plasma concentration time profile of R3S and its metabolite R3G after R3S 20 mg/kg (i.a.) administration (n = 3). Data presented as mean + SD.

Table 4.1: Pharmacokinetic parameters of R3S and its metabolites after 5, 10, 20 mg/kg (i.a.) and 10 mg/kg (oral) R3S administration.

R3S	5 mg/kg, i.a. (n = 4)	10 mg/kg, i.a. (n = 4)	20 mg/kg, i.a. (n = 3)	10 mg/kg, oral (n = 5)	Units
AUC_{0-t}	243.29 ± 113.10	407.80 ± 168.53	1031.81 ± 355.06	109.42 ± 39.04	min*uM
AUC_{0-inf}	255.84 ± 124.98	448.90 ± 188.02	1208.91 ± 195.76	126.14 ± 52.11	min*uM
Cl	76.29 ± 37.07	84.56 ± 41.49	54.69 ± 9.06	294.34 ± 115.05	ml/min/kg
Vd	13.58 ± 5.39	32.68 ± 10.89	14.83 ± 3.83	120.75 ± 61.83	L/kg
Vss	6.37 ± 2.36	23.22 ± 10.67	9.71 ± 7.05	128.35 ± 89.18	L/kg
$t_{1/2}$	128.08 ± 26.21	281.65 ± 40.19	186.42 ± 18.57	283.8 ± 68.82	min
Cmax	14.79 ± 3.15	21.54 ± 7.45	78.57 ± 33.58	0.65 ± 0.45	uM
Tmax	2.5	2.50 ± 0	2.50 ± 0	42.50 ± 77.01	min
MRT	96.30 ± 46.85	320.70 ± 204.92	132.57 ± 51.15	418.22 ± 137.95	min
R3G					
AUC_{0-t}	24.53 ± 16.08	98.60 ± 68.75	1101.06 ± 1042.91	165.40, 294.70*	min*uM
AUC_{0-inf}	38.79 ± 9.59	159.70 ± 132.00	1298.41 ± 1087.91	193.61, 329.47*	min*uM
$t_{1/2}$	256.75 ± 239.25	216.62 ± 157.28	184 ± 139.60	191.27, 355.41*	min
Cmax	0.21 ± 0.07	0.55 ± 0.25	4.14 ± 2.03	0.79, 0.35*	uM
tmax	167.5 ± 119.27	166.25 ± 121.48	143.33 ± 239.6	180, 600*	min
MRT	483.34 ± 445.68	463.97 ± 295.49	476.14 ± 197.61	370.49, 753.47*	min
R4'S					
AUC_{0-t}	NA	NA	NA	2026.19, 119.48*	min*uM
AUC_{0-inf}	NA	NA	NA	2033.70, 217.45*	min*uM
$t_{1/2}$	NA	NA	NA	470.23, 909.36*	min
Cmax	NA	NA	NA	29.06, 0.57*	uM
tmax	NA	NA	NA	90.00, 5.00*	min
MRT	NA	NA	NA	108.18, 1575.44*	min

All results are reported as estimate ± SD, * n = 2.

Note: CL, Vd and Vss in oral data are CL/F, Vd/F and Vss/F.

4.3.2. Pharmacokinetics of R4'S

The pharmacokinetic profiles of R4'S and its metabolites after R4'S administration at 20 mg/kg i.a. and 20 mg/kg oral dose are shown in Fig. 4.4 and 4.5 respectively. We also performed a PK study at 5 mg/kg i.a dose, but R4'S concentrations fell below LLOQ after 90 mins. So, we did not use this study to calculate the PK parameters for R4'S. The data from R4'S, i.a. (5 mg/kg) study has been included in appendix. R3G was the major metabolite based on the plasma exposure by both i.a. and oral route of administration. The results of the noncompartmental pharmacokinetic analysis are summarized in Table

4.2. We did not observe any RES in the systemic circulation after R4'S administration by both oral and i.a. routes. We observed in the i.a. dosing studies that R3G concentration initially declined rapidly until 90 min and then an abrupt increase in its systemic concentration was observed around 180 to 300 min. The i.a. dosing studies indicated that R4'S exhibits a very high clearance and a high volume of distribution in mice. The high clearance is likely due to rapid metabolism of R4'S into R3G and R3S. Interestingly, the values for total body clearance of 129.05 ml/min/kg greatly exceed the values for hepatic blood flow rate (90 ml/min/kg) in mouse (Davies and Morris, 1993). Even when the hepatic extraction ratio of RES is assumed to be unity, hepatic clearance would be expected to approach hepatic blood flow (90 ml/min/kg). Extrahepatic clearance was calculated as the difference between total body clearance (129.05 ml/min/kg for 20mg/kg ia dose) and hepatic blood flow (90ml/min/kg) and found to be 39.05 ml/min/kg, which represents 30% of total clearance. This shows that extrahepatic conjugation plays a major role in the metabolism of R4'S (Mulder et al., 1984). Peak concentration (C_{max}) of 0.25 ± 0.03 uM was observed after oral R4'S dose at 5 to 10 min. Post-dose this indicates that R4'S is being rapidly absorbed orally. Reentry peaks of R3G were clearly observed in R4'S i.a. administration studies indicating enterohepatic recycling of R3G. The oral bioavailability of R4'S was found to be poor (10 % at 20 mg/kg). The cause of poor oral bioavailability might be extensive metabolism of R4'S rather than poor absorption of R4'S as evident from Fig 4.5. First pass elimination of R4'S by conversion into R3G and R3S in liver with subsequent elimination through the biliary route can lead to very poor R4'S concentrations systemically which in turn might lead to its poor bioavailability. The half life of R4'S when given orally is very long i.e. 1060.28 ± 441.98 min compared to

154.32 ± 44.03 min when given systemically. Pronounced enterohepatic recycling might lead to prolonged elimination phase of R4'S.

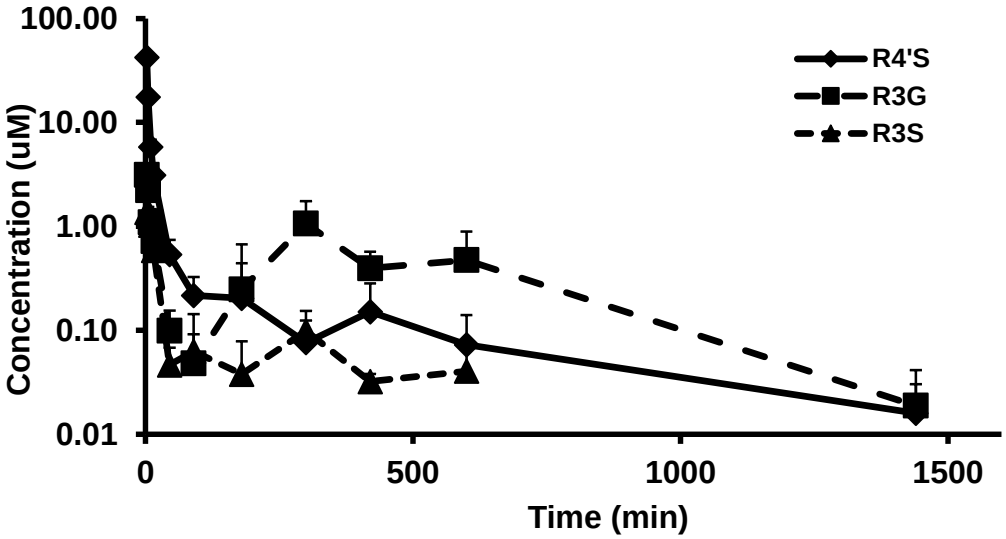

Fig 4.4: Plasma concentration time profile of R4'S and its metabolites after R4'S 20 mg/kg (i.a.) administration (n = 4) Data presented as mean + SD.

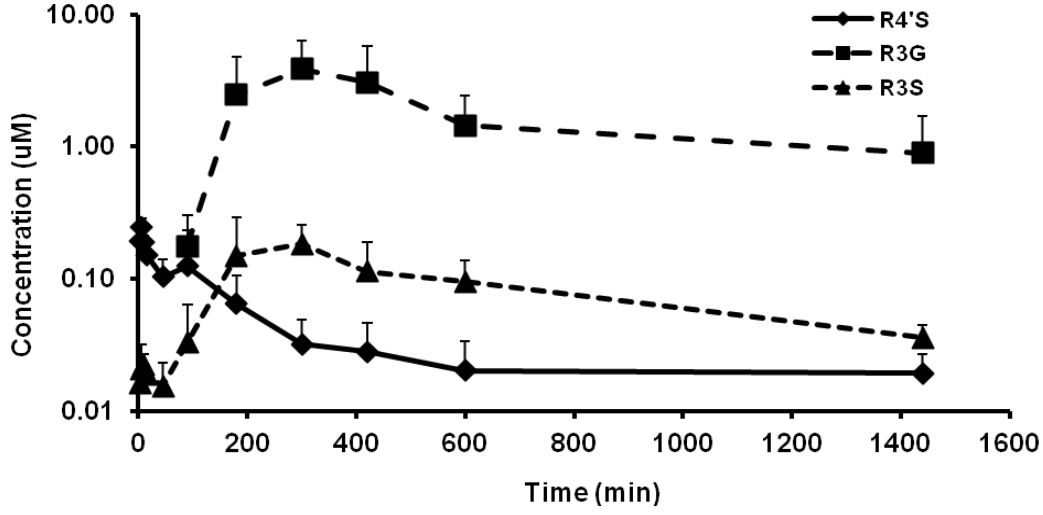

Fig 4.5: Plasma concentration time profile of R4'S and its metabolites after R4'S 20 mg/kg (oral) administration (n = 3). Data presented as mean + SD.

Table 4.2. Pharmacokinetic parameters of R4'S and its metabolites after 20 mg/kg, i.a. and 20 mg/kg, oral R4'S administration.

R4'S	**20 mg/kg, i.a. (n = 4)**	**20 mg/kg, oral (n = 3)**	**Units**
AUC_{0-t}	496.53 ± 42.34	50.68 ± 4.83	min*uM
AUC_{0-inf}	506.31 ± 45.00	77.12 ± 10.89	min*uM
Cl	129.05 ± 12.11	852.45 ± 111.45	ml/min/kg
Vd	29.19 ± 10.40	1311.42 ± 633.08	L/kg
Vss	13.96 ± 6.19	1106.69 ± 191.66	L/kg
$t_{1/2}$	154.32 ± 44.03	1060.28 ± 441.98	min
Cmax	42.20 ± 4.69	0.25 ± 0.03	uM
Tmax	2.5	6.67 ± 2.89	min
MRT	105.94 ± 35.67	1306.60 ± 217.60	min
R3G			
AUC_{0-t}	451.46 ± 293.35	2305.39 ± 1621.52	min*uM
AUC_{0-inf}	490.01 ± 270.36	3371.22 ± 2661.50	min*uM
$t_{1/2}$	212.45 ± 44.87	734.18 ± 255.90	min
Cmax	3.13 ± 0.51	4.10 ± 2.70	uM
tmax	2.5	340 ± 69.28	min
MRT	460.17 ± 97.19	1186.11 ± 400.67	min
R3S			
AUC_{0-t}	54.21 ± 8.53	121.56 ± 45.93	min*uM
AUC_{0-inf}	65.37 ± 12.66	160.14 ± 32.52	min*uM
$t_{1/2}$	185.92 ± 53.78	853.83 ± 571.90	min
Cmax	1.56 ± 0.34	0.21 ± 0.10	uM
tmax	5.63 ± 3.15	260 ± 69.28	min
MRT	282.25 ± 104.63	1188.96 ± 663.99	min

Results are reported as estimate ± SD.

Note: Cl, Vd and Vss for oral data are Cl/F, Vd/F and Vss/F.

4.3.3. *In vitro* hepatic metabolism:

Preliminary experiments showed that the reactions with R3S were linear up to 60 min and 2.5 mg/ml of total protein for each enzyme source (Fig 4.6 and Fig 4.7). Fig 4.8A shows the formation kinetics of R3G in mouse liver microsomes. The R3G profile showed Michaelis-Menten kinetics in mouse liver microsomes. Its apparent enzyme kinetic parameters were estimated by fitting equation 4.1 to the data. Fig 4.8B shows the formation kinetics of R3G in human liver microsomes with its Eadie-Hofstee (E-H) plot shown as inset. R3G formation in human liver microsomes showed a substrate inhibition profile (Hutzler and Tracy, 2002). Its apparent enzyme kinetic parameters were estimated by fitting equation 4.2 to the data (Table 4.3). *In vitro* incubation of R3S with mouse and human liver microsomes led to the formation of RES, which was further glucuronidated to R3G. To establish the rate of enzymatic hydrolysis of R3S to RES, incubations were performed with STX64 a (steroid sulfatase inhibitor). After incubation with STX64, a low concentration of R3G was observed in both mouse (36.70 ± 6.54 ng/ml) as well as human (79.60, 74.10 - 85.10 ng/ml, represented as mean and range) liver microsomes incubations compared to the incubations without STX64 in mouse (1077.67 ± 91.19 ng/ml) and human (11500.00 ± 400.00 ng/ml) liver microsome incubations.

A)

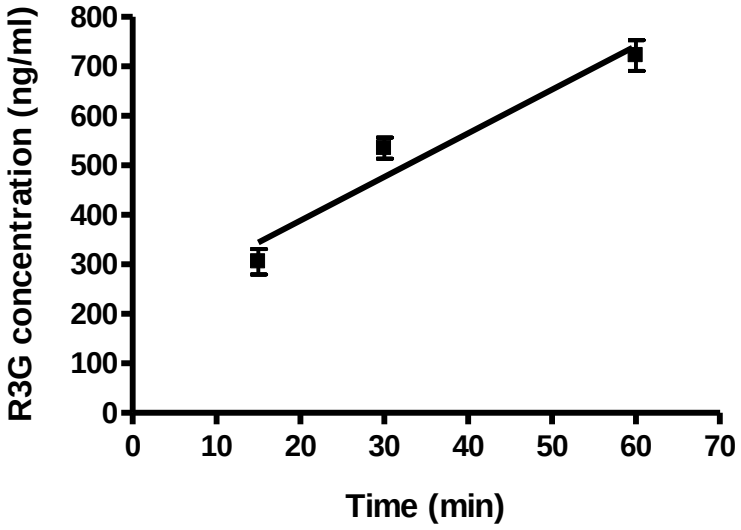

B)

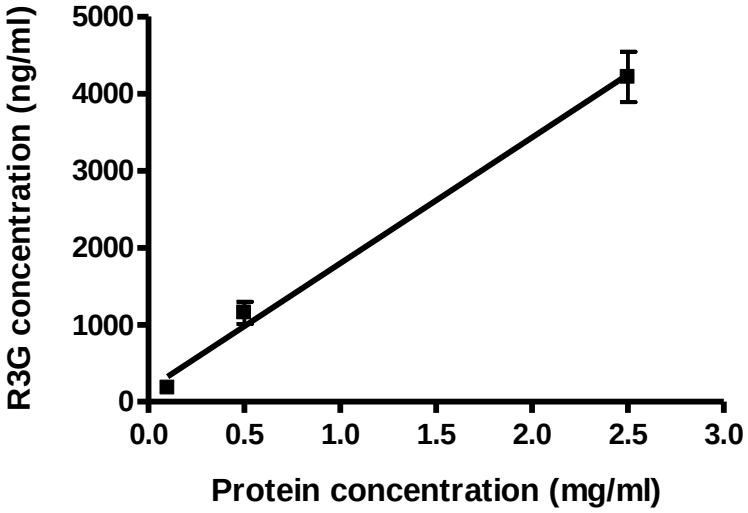

Fig 4.6: Linearity of formation for R3G from R3S in mouse liver microsomes (n = 3); A) Time linearity over a 0 – 60 min time period with 0.5 mg/ml final protein concentration B) Protein linearity over a 0.1 - 2.5 mg/ml concentration range using an incubation time of 60 mins.

A)

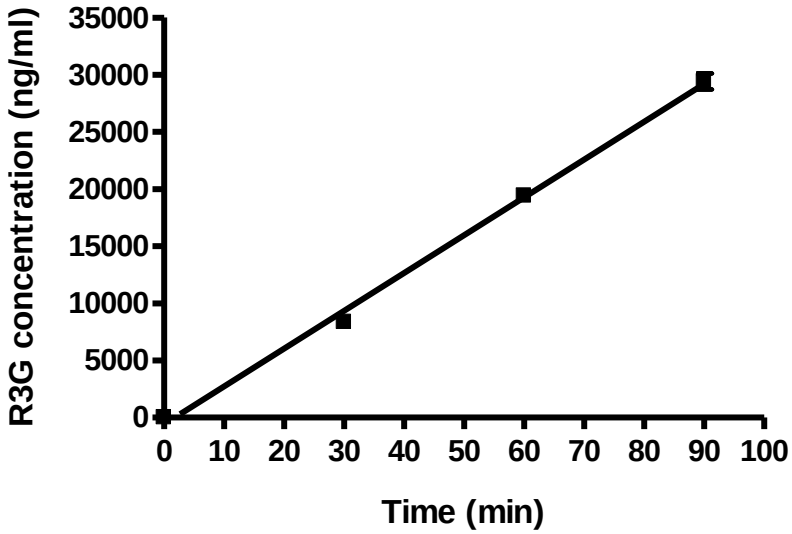

B)

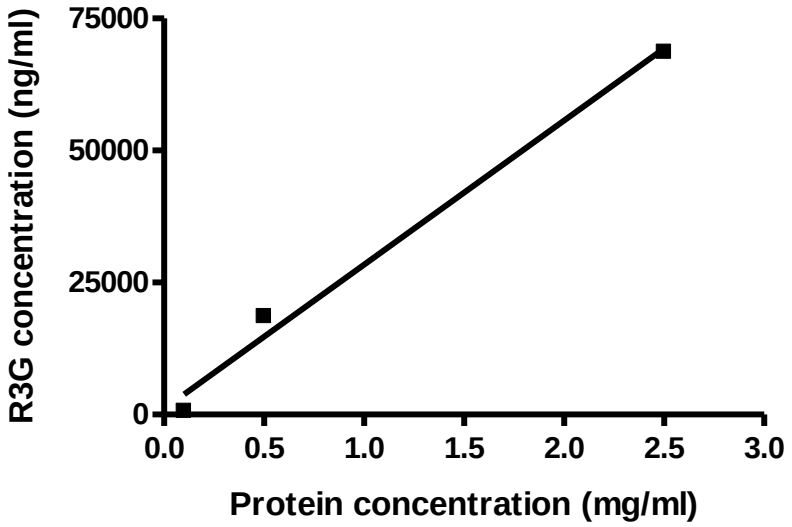

Fig 4.7: Linearity of formation for R3G in human liver microsomes (n =2); A) Time linearity over a 0 – 90 min time period with 0.5 mg/ml final protein concentration B) Protein linearity over a 0.1 - 2.5 mg/ml concentration range using an incubation time of 60 mins.

Table 4.3. Kinetic parameter estimates for the sulfation and glucuronidation of RES and R3S by human and mouse lungs and liver fractions. Data are expressed as estimates ± SD; n = 3. Estimate units are as follows: Vmax: nanomoles per minute per milligram total protein; Km, Ki: micromolar.

Substrate	Conjugation product	Protein source	Vmax (pmol/min/mg)	Km (uM)	Ki (uM)	Goodness of Fit (r^2)	Type of Fit
R3S	R3G	Mouse liver microsome	132.00 ± 5.13	224.30 ± 23.59	NA	0.98	MM
R3S	R3G	Human liver microsome	2081.00 ± 249.9	201.90 ± 36.43	677 ± 157.3	0.98	PSI

(MM: Michaelis Menten, PSI: Partial substrate inhibition)

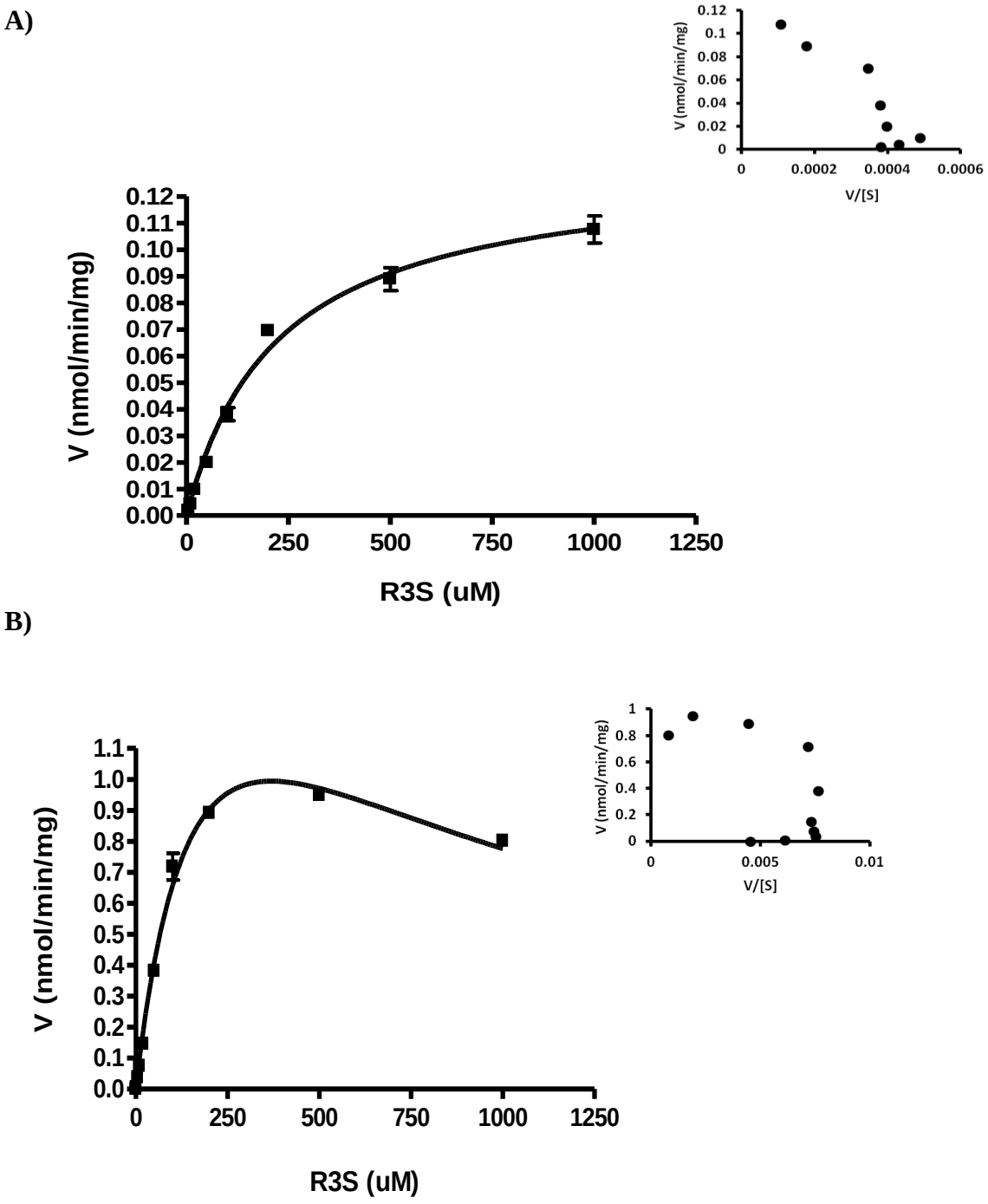

Fig 4.8: Kinetics of A: R3G formation in mouse liver microsomes, B: R3G formation in human liver microsomes. Data reported as mean ± standard deviation, (n = 3). The solid line represents curve fitting with the substrate inhibition equation (equation 3); the dotted line in the inset represents the Eadie-Hofstee plot.

4.3.4. Permeability study:

The results of bidirectional permeability of R3S and R4'S in MDCK cells are presented in table 4.4.

Table 4.4: Bidirectional permeability of R3S and R4'S in MDCK cells.

Compound	**Papp ($\times 10^{-6}$ cm/sec)**		**Efflux Ratio**
	A-to-B	**B-to-A**	
R3S	2.12	1.98	0.93
R4'S	0.68	2.21	3.24

4.4. Discussion and conclusion:

R3G is the major metabolite formed from R3S and R4'S. The present study has characterized the disposition of preformed R3S and R4'S and has provided a better understanding of the influence of sulfated metabolite disposition on RES pharmacokinetics. This study also tested the hypothesis postulated by several researchers that metabolites can act as a depot of RES and can be desulfated to give back RES. In our study we did not find any significant amount of RES in systemic circulation after R3S or R4'S administration. Sulfated metabolites led to the formation of glucuronidated metabolites which is not possible without the intermediate formation of RES.

We have conducted *in vitro* metabolism experiments with both mouse and human liver microsomes with R3S as model substrate for sulfated compound to confirm our *in vivo* findings. Desulfation and subsequent glucuronidation of R3S to R3G was observed in both mouse and human liver microsomes. Our study with STX64 (steroid sulfatase inhibitor) led to very low levels of R3G. Steroid sulfatase, also known as arylsulfatase C, has been shown to have a hydrophobic domain. In BHK-21 cells the steroid sulfatase enzyme has been shown to be mainly located in the endoplasmic reticulum (Stein et al., 1989). It has been suggested that catalytic domain of steroid sulfatase enzyme is located on the lumen side of the endoplasmic reticulum (Ghosh, 2007). Our results with steroid sulfatase inhibitor (STX64) and literature reports support that desulfation of R3S is mainly catalyzed by steroid sulfatase enzyme, and the RES formed upon desulfation is further glucuronidated by UGT enzymes present in the endoplasmic reticulum.

R3S and R3G have been shown to be transported through both the basolateral and bile canalicular side of hepatocyte (Maier-Salamon et al., 2008). Sulfated and glucuronidated metabolites are too hydrophilic to passively diffuse through the plasma membrane and across the cell. The transporters involved in the uptake of R3S in the hepatocyte are not known. It has been reported that for other sulfoconjugates, e.g estrone sulfate, organic anion transporting polypeptides (OATPs) and organic anion transporters (OATs) are involved in their uptake in hepatocyte (Tan et al., 2001; Fahrmayr et al., 2010). It has been earlier shown that BCRP (ABCG2) and MRP2 (ABCC2) are involved in the biliary excretion of R3S (van de Wetering et al., 2009; Juan et al., 2010a). The transport of R3S over the basolateral membrane into the liver sinusoid can take place partly by passive diffusion and partly by MRP4 (ABCC4) and MRP1 (ABCC1) transporters. Although MRP4 (ABCC4) and MRP1 (ABCC1) have not been specifically studied for R3S transport, there are reports which shows both MRP4 and MRP1 to be involved in the transport of sulfo-conjugates such as dehydroepiandrosterone sulfate (Zelcer et al., 2003) and estrone 3-sulfate (Qian et al., 2001) for MRP1. MRP2 (ABCC2) has been shown to play a major and BCRP (ABCG2) a minor role in biliary excretion of R3G (Maier-Salamon et al., 2008; van de Wetering et al., 2009; Juan et al., 2010a). R3G has also been shown to be a high affinity substrate for MRP3 (ABCC3) which transports R3G over the basolateral membrane of hepatocyte (van de Wetering et al., 2009; Juan et al., 2010a). Although the role of MRP1 (ABCC1) has not been shown for transport of R3G, there are reports that MRP1 (ABCC1) can transport steroid glucuronides such as 17β-estradiol-glucuronide (Jedlitschky et al., 1996). Uptake of R3G can occur at the basolateral side of

hepatocyte by organic anion transporter polypeptides (OATPs) as shown for other glucuronides, e.g ezetimibe glucuronide (Oswald et al., 2008; Fahrmayr et al., 2010).

RES has been reported to be glucuronidated at its 3-OH position via UGT1A1, UGT1A7, UGT1A9, UGT1A3, UGT1A6, UGT1A8, UGT1A10 and UGT2B7 (Brill et al., 2006). UGT1A1, 1A7 and 1A9 are the major contributors in the RES glucuronidation at the 3-OH position (Brill et al., 2006). In mouse liver ugt1a1, ugt1a5, ugt1a6 and ugt1a9 are highly expressed (Buckley and Klaassen, 2007). UGT1A1, UGT1A3, UGT1A4, UGT1A6 and UGT1A9 mRNA have been reported to be expressed in human liver (Buckley and Klaassen, 2007). RES sulfation at its 3 -OH position has been reported to be mediated by sulfotransferase (SULT) SULT1A1, SULT1A2, SULT1A3, and SULT1E1, with SULT1A1 to be the major contributor (Miksits et al., 2005). RES sulfation at its 4'-OH position has been reported to be mediated by SULT1A1 and SULT1E1 isoforms, with SULT1E1 to be the major contributor (Miksits et al., 2005). Sut1a1 is the major sult isoform expressed in mouse liver (Alnouti and Klaassen, 2006), whereas SULT1A1 is the major and SULT1E1 is the minor isoform of SULT expressed in human liver (Riches et al., 2009). Therefore based on the expression of UGT isoforms in liver and UGT isoforms responsible for glucuronidation of RES in liver of both mice and humans, UGT1A1 and UGT1A9 are likely to be the major isoforms of UGT responsible for glucuronidation of RES in liver. Similarly SULT1A1 is the major SULT isoform responsible for sulfation of RES in liver of both mice and humans.

Based on the present results and cited literature reports (Tan et al., 2001; Zelcer et al., 2003; Alnouti and Klaassen, 2006; Brill et al., 2006; Buckley and Klaassen, 2007; Ghosh, 2007; Maier-Salamon et al., 2008; Riches et al., 2009; van de Wetering et al., 2009), a proposed pathway for the disposition of R3S is presented in Figure 4.8. R3S when presented to the liver can diffuse into the hepatocyte, as indicated by its Papp B to A of 1.98×10^{-6} cm/sec and undergoes further metabolism in liver. R3S can also be excreted into the bile by MRP2 (ABCC2) and BCRP (ABCG2) (Fig 4.9). R3S gets desulfated rapidly by steroid sulfatase enzymes present in the endoplasmic reticulum (Parenti et al., 1997) to give RES. RES in the endoplasmic reticulum is further metabolized to R3G by UGT isoforms mainly ugt1a1 and 1a9. The glucuronide conjugate of RES i.e. R3G gets transported out to the cyctosolic space and is excreted into the bile by MRP2 (ABCC2), BCRP (ABCG2) or in blood by MRP3 (ABCC3) (Fig 4.9). Desulfation followed by rapid glucuronidation has been reported for other substrates such as estrone sulfate (Tan et al., 2001). RES in the endoplasmic reticulum can also diffuse into the cytoplasm and can be sulfated back to R3S mainly by sult1a1, and then excreted into bile by MRP2 (ABCC2), BCRP (ABCG2). It can also diffuse back into liver sinusoids as indicated by its Papp A to B value of 2.12×10^{-6} cm/sec or undergo desulfation in liver endoplasmic reticulum. The futile cycling of RES/R3S within the hepatocyte can lead to enhanced local presence of RES/R3S in liver. This can be especially important in the light of potential positive biological effects of R3S.

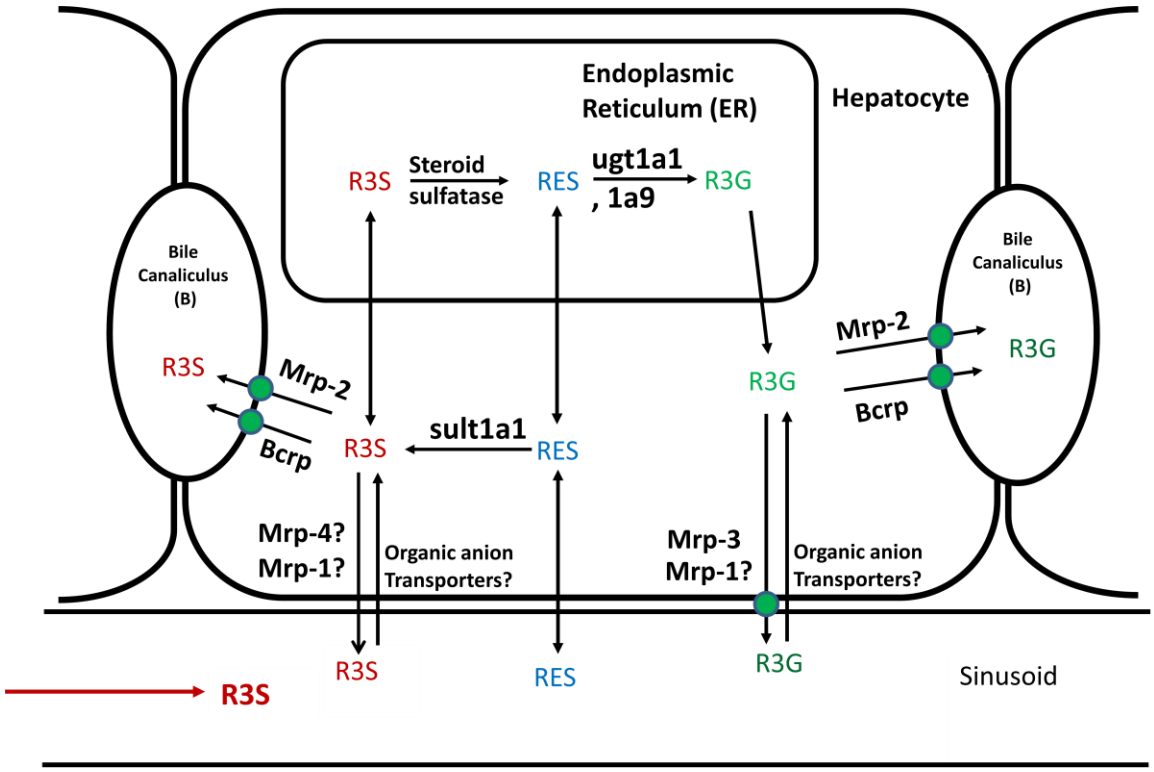

Fig 4.9: Proposed schematic representation of R3S metabolism in hepatocyte. Solid line represents pathways based on results in this manuscript and published literature reports for RES, R3S and R3G. Transporters followed by "?" indicates that the role of these transporters are not known for transport of R3S and R3G, but is suggested by findings of transport of other sulfated and glucuronidated substrates.

Similarly R4'S metabolism can be explained as described in Fig 4.10. R4'S when presented to hepatocyte gets transported as indicated by its P_{app} B to A of 2.21×10^{-6} cm/sec. Similar to R3S, R4'S can be rapidly transported into the endoplasmic reticulum (ER) compartment in the hepatocyte and can get desulfated rapidly to give RES. RES in the ER can be sequentially metabolized to R3G by UGT isoforms, mainly ugt1a1 and 1a9 or can escape in the cytosol where it can be again sulfated to R3S or R4'S mainly by sult1a1. The glucuronide conjugate of RES i.e. R3G can be transported out to the

cytosolic space or is excreted into the bile (Fig 4.10). These phenomena might be so efficient that it may lead to very low concentration of RES in the cytoplasm which are available to diffuse into the sinusoid. RES may therefore be well below our limit of analytical detections leading to RES being not observed in systemic circulation.

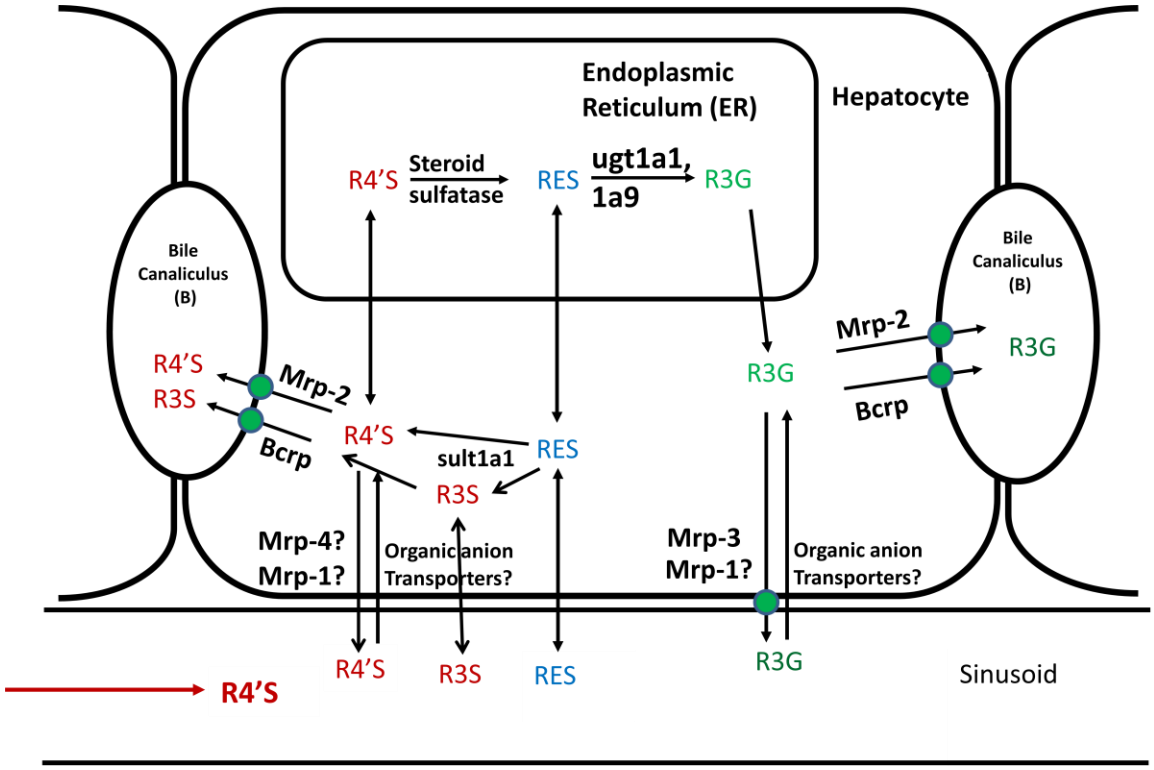

Fig 4.10: Proposed schematic representation of R4'S metabolism in the hepatocyte. The proposed pathways for R4'S metabolism are based on R3S proposed metabolic fate in fig 4.8 and the R4'S *in vivo* results. It has been assumed that since R4'S is also a sulfated metabolite of RES, it therefore may show a similar metabolic fate. Solid line represents pathways based on results of R3S *in vitro* results in this manuscript and published literature reports for RES, R3S and R3G. Transporters followed by "?" indicates that the role of these transporters are not known for transport of R4'S, R3S and R3G, but is suggested by findings on the transport of other sulfated and glucuronidated substrates.

In summary we were able to characterize the pharmacokinetics of R3S and R4'S in the mouse model. Sulfated metabolites are extensively desulfated in the liver and can also undergo futile cycling. They are also observed to be extensively metabolized leading to R3G as the most abundant metabolite being formed and being mainly eliminated in bile. Although no significant RES was observed in the systemic circulation, we observed very clearly that sulfated metabolites are desulfated by steroid sulfatase enzymes present in the hepatocyte. Therefore the hypothesis that sulfated metabolites can get desulfated at tissue level to give parent RES was supported.

CHAPTER 5

PHARMACOKINETICS OF THE GLUCURONIDATED METABOLITE OF RESVERATROL: RESVERATROL 3-GLUCURONIDE (R3G)

5.1. Rationale:

RES is extensively metabolized into its sulfated and glucuronidated metabolites. R3G has been found to be the most significant metabolite in terms of exposure in the mouse. Although glucuronides have generally been assumed to be pharmacologically inactive, there are several studies showing some of them to be pharmacologically active (Osborne et al., 1988; Kroemer and Klotz, 1992; Sperker et al., 1997). Even if glucuronide metabolites themselves are inactive, they can be converted to the parent by reversible metabolism via β-glucuronidases. β-glucuronidases, which are abundantly found in the gut, can deglucuronidate R3G to parent RES and lead to local pharmacological activity in gut e.g., colorectal cancer prevention. Additionally β-glucuronidases have been also reported in macrophages, liver, lung and blood cells (Paigen, 1989; Sperker et al., 1997).

This study was carried out to provide a better understanding of the influence of the glucuronidated metabolite (R3G) disposition on RES pharmacokinetics. The hypothesis that R3G can act as depot of RES and can be deconjugated back to RES was also tested. In this study we investigated the fate of the preformed glucuronidated metabolite, R3G in an *in vivo* mouse model after direct R3G administration by oral and i.a. routes.

5.2. Materials and Methods:

5.2.1. Drug administration and blood sampling: R3G was solubilized in saline. Details about surgery and cannulation have been provided in section 3.2.2. of chapter 3. Carotid artery cannula was used for systemic drug administration and blood sampling. Heparin-saline (20 uL, 50 IU/ml) was used to flush the cannula after systemic administration or blood sampling. R3G was administered at a dose of 3.5 or 26.66 mg/kg i.a. and 26.66 mg/kg orally. The lower dose of 3.5 mg/kg was selected by performing pilot studies which gave R3G exposures (AUCs) in the range comparable to R3G observed upon 15 mg/kg RES (i.a.) administration. The higher dose of 26.66 mg/kg was selected as it was equimolar dose to 15 mg/kg of RES. Blood (20 uL) was serially sampled at 2.5, 5, 10, 15, 45, 90, 180, 300, 420, 600 min and 24 hrs. Blood samples were centrifuged at 14,000 rpm for 2 min the harvested plasma was collected and stored at -80 °C until LCMS/MS analysis. PK analysis was performed as explained in section 3.2.7 of chapter 3.

5.2.2. Statistics: Student's paired t test was used, with $P < 0.05$ set as the significance level. GraphPad Prism for Windows (version 4.03; GraphPad Software Inc., San Diego, CA) was used to perform statistical analysis.

5.3. Results:

5.3.1. Pharmacokinetics of R3G

The pharmacokinetic profiles of R3G and its metabolites after R3G administration at 3.5 mg/kg, 26.67 mg/kg i.a. and 26.67 mg/kg oral doses are shown in Figs 5.1, 5.2 and 5.3 respectively. Resveratrol-3-sulfate (R3S) and resveratrol-4'-glucuronide (R4'G) were observed as major metabolites upon a high dose 26.67 mg/kg of i.a. R3G (Fig 5.2). R3S was not observed in significant concentrations at the lower i.a. R3G dose of 3.5 mg/kg (Fig 5.1). R3S was the major metabolite when R3G was administered orally and R4'G was not observed in significant amount (Fig 5.3). The results of the noncompartmental pharmacokinetic analysis are summarized in Table 5.1. The mouse i.a. studies indicated that R3G exhibits a low clearance and a high volume of distribution in mice. R3G oral administration gives rise to R3S as a major metabolite. R3G is possibly hydrolyzed through the action of bacterial and enteric β-glucuronidase to RES and again subsequently sulfated to R3S.

The apparent oral bioavailability of R3G was found to be high (84.2 % at 26.67 mg/kg). AUC ratios of metabolites to total $AUC_{0\text{-}inf}$ (R3G + R3S + R4'G), for different dose levels and different routes are given in Table 5.2. Peak concentrations (C_{max}) of R4'G occurred between 2.5 to 5 min after the i.a. dose, while that of R3S occurred at 180 min (except for one mouse, 2.5 min) for the higher i.a. dose (Fig 5.2) and between 5 to 15 min after the oral dose (Fig 5.3). Reentry peaks of R3G and R3S in the plasma, likely due to enterohepatic recirculation, were clearly observed at 3 to 5 hours after i.a. administration of 26.66 mg/kg (Fig 5.2) and 3.5 mg/kg (Fig 5.1).

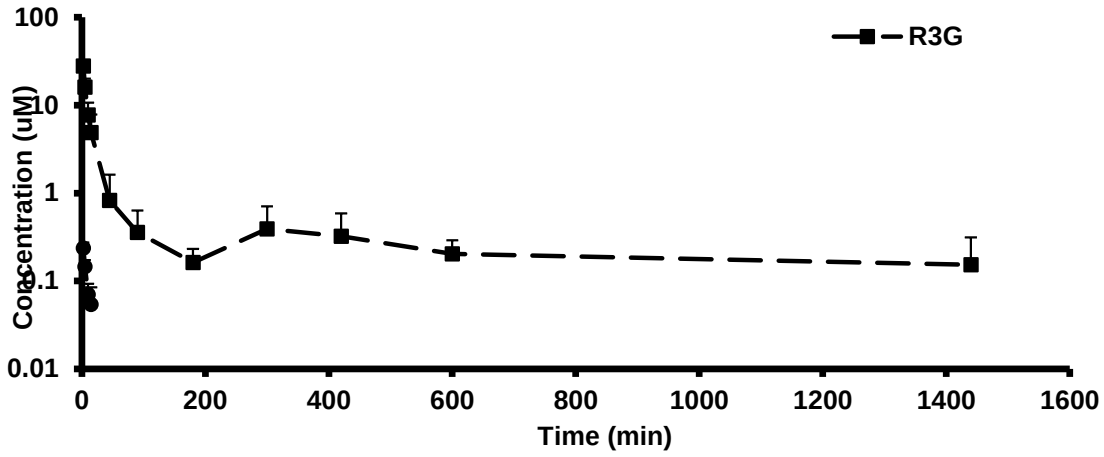

Fig 5.1: Mean plasma concentration-time profiles after administration of R3G (3.5 mg/kg, i.a.). Closed squares represent the mean of R3G plasma concentrations and closed circles represent the mean of R4'G plasma concentration. Data are presented as mean + SD, n = 4.

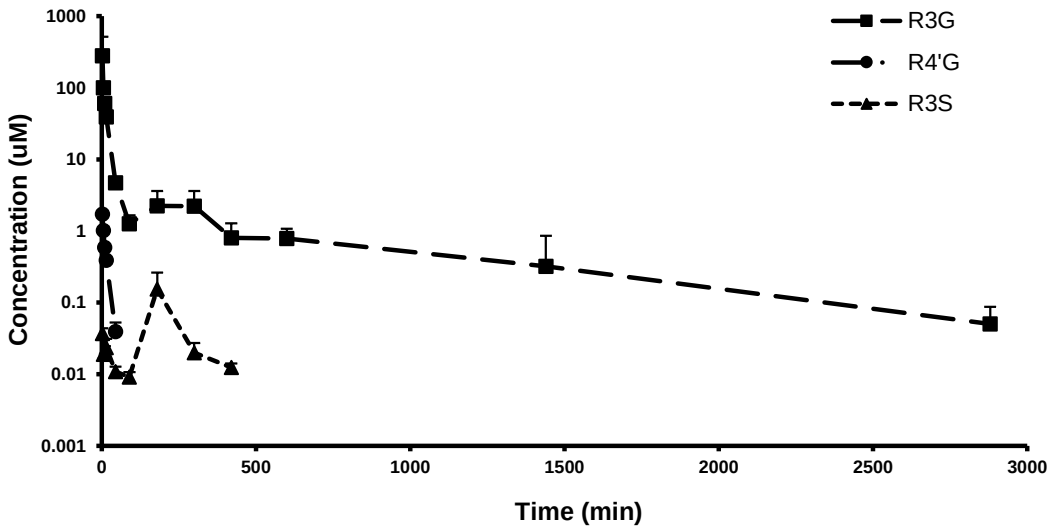

Fig 5.2: Mean plasma concentration-time profiles after administration of R3G (26.66 mg/kg, i.a.). Closed squares represent the mean of R3G plasma concentrations, closed circles represent the mean of R4'G plasma concentrations and closed triangles represent the mean of R3S plasma concentrations. Data are presented as mean + SD, n = 4.

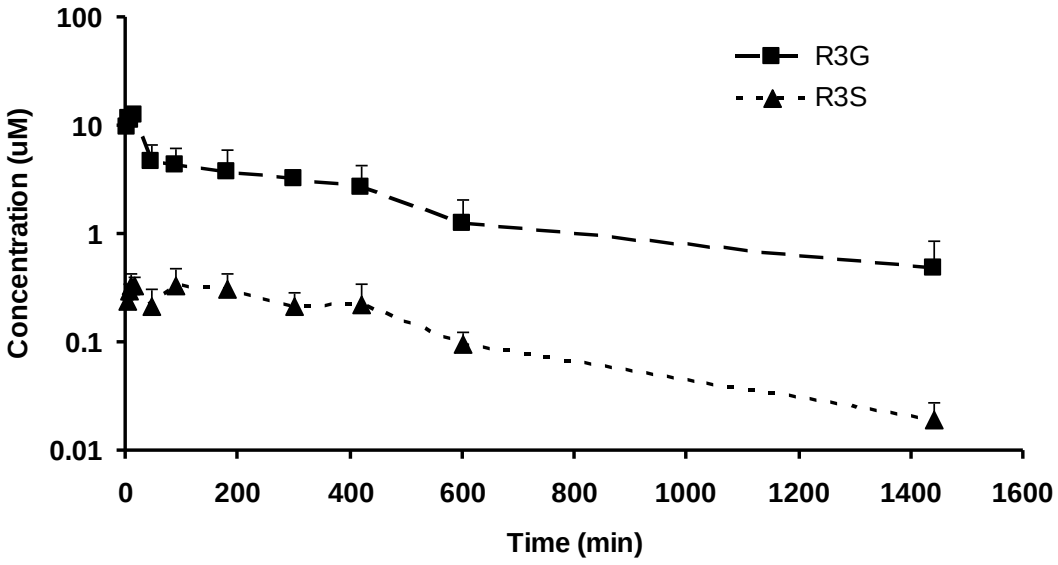

Fig 5.3: Mean plasma concentration-time profiles after administration of R3G (26.66 mg/kg, oral). Closed squares represent the mean of R3G plasma concentrations and closed triangles represent the mean of R3S plasma concentrations. Data are presented as mean + SD, n = 3.

Table 5.1: Pharmacokinetic parameters of R3G

R3G	3.5 mg/kg (i.a.) n = 4	26.66 mg/kg (i.a.) n = 4	26.66 mg/kg (oral) n = 3	Units
AUC_{0-t}	650.66 ± 216.50	3739.56 ± 981.57	2827.62 ± 178.17	min*uM
AUC_{0-inf}	710.10 ± 273.30	3753.29 ± 1010.39	3161.8 ± 174.85	min*uM
Cl	13.78 ± 5.75	18.69 ± 5.60	20.91 ± 1.12	ml/min/kg
Vss	4.55 ± 1.07	4.26 ± 2.54	11.55 ± 4.5	L/kg
$t_{1/2}$	272.48 ± 17.07	371.60 ± 157.85	406.52 ± 165.34	uM
Cmax	27.84 ± 4.70	146.66 ± 44.45	12.31 ± 1.49	uM
Tmax	2.5 ± 0	3.13 ± 1.25	11.66 ± 5.77	min
R3S				
AUC_{0-t}	NA	17.41 ± 11.10	188.73 ± 30.81	min*uM
AUC_{0-inf}	NA	18.93 ± 10.84	198.74 ± 29.06	min*uM
$t_{1/2}$	NA	77.36 ± 28.10	338.09 ± 98.25	min
Cmax	NA	0.13 ± 0.11	0.45 ± 0.05	uM
Tmax	NA	135.63 ± 88.75	93.33 ± 85.05	min
R4'G				
AUC_{0-t}	2.08 ± 1.27	17.81 ± 1.91	NA	min*uM
AUC_{0-inf}	2.51 ± 1.41	18.34 ± 2.02	NA	min*uM
$t_{1/2}$	8.64 ± 5.57	8.96 ± 1.26	NA	min
Cmax	0.24 ± 0.04	1.57 ± 0.31	NA	uM
Tmax	2.5 ± 0	3.13 ± 1.25	NA	min

Note: CL and Vss for oral dose are apparent clearance (Cl/F) and apparent Vss (Vss/F), All results are reported as estimate ± SD

Table 5.2: Ratios of AUC_{0-inf} of parent R3G and individual R3G metabolites (i.e. R3S, R4'G) to the sum of AUC_{0-inf} of R3G and its metabolites after i.a and oral administration of R3G.

	3.5 mg/kg (i.a.) n = 4	26.66 mg/kg (i.a.) n = 4	26.66 mg/kg (oral) n = 3
Metabolites/Total	0.35	0.98	5.91
R3G/Total	99.65	99.02	94.09
R3S/Total	0.00	0.50	5.91
R4'G/Total	0.35	0.48	0.00

*Total refers to [AUC_{0-inf} of R3G + AUC_{0-inf} of R3S + AUC_{0-inf} of R4'G]
R3G refers to AUC_{0-inf} of R3G, R3S refers to AUC_{0-inf} of R3S, R4'G refers to AUC_{0-inf} of R4'G

5.4. Discussion and conclusion:

R3G is the major metabolite formed from RES. The present study has characterized the disposition of preformed R3G and has provided better understanding of the influence of R3G disposition on RES and its metabolites pharmacokinetics. This study also tested the hypothesis postulated by several researchers that metabolites can act as depot of RES and can be deglucuronidated back to RES.

In our study we did not find significant concentrations of RES in systemic circulation when R3G was given either i.a. or orally. However when given orally R3G led to the formation of R3S, which was comparable to the exposure of R3S when RES 15 mg/kg was given intra-arterially (see chapter 3, table 3.1). The exposure of R3S when 26.66 mg/kg R3G was given orally was almost 10 fold higher than R3S exposure when 26.66 mg/kg of R3G was given intra-arterially. This indicates the possibility of R3G being deglucuronidated in the gut to RES by intestinal β-glucuronidases/gut flora and further glucuronidated or sulfated across the enterocyte or hepatocyte to form R3G and R3S before appearing in the systemic circulation. The terminal elimination slopes of R3G and R3S were found not to be statistically different when R3G was administered orally. The parallel decline of parent R3G and metabolite R3S can be due to formation rate limited metabolite kinetics (Houston, 1981) or reversible metabolism (Ebling et al., 1985; Pearson and Wienkers, 2009). However in our previous chapter 4 (see section 4.3.1), we have observed that when R3S was administered R3G was the major metabolite formed. So, the parallel decline of parent R3G and metabolite R3S can be attributed to their reversible metabolism.

RES is glucuronidated at the 3 position primarily by UGT1A isoforms in humans (UGT1A1, UGT1A9, UGT1A7, UGT1A3, UGT1A6, UGT1A8 and UGT1A10) of which UGT1A1, UGT1A7 and UGT1A9 are major contributors (Brill et al., 2006). UGT2B isoforms do not take part in the glucuronidation of RES, except with very low activity by UGT2B7 (Brill et al., 2006). Ugt1a1 is expressed in mouse liver, small and large intestine (Buckley and Klaassen, 2007) whereas Ugt1a7c is expressed mainly in mouse small and large intestine and Ugt1A9 in mouse liver (Buckley and Klaassen, 2007). So, most likely RES is glucuronidated by Ugt1a1 and Ugt1a7c in mouse gut and by Ugt1a1 and 1a9 in mouse liver. UGT1A9 is the major UGT isoform responsible for glucuronidation of RES at 4' position (Aumont et al., 2001; Iwuchukwu and Nagar, 2008), but is poorly expressed in mouse gut (Buckley and Klaassen, 2007). This explains the absence of R4'G in mouse plasma when R3G is administered orally as compared to its systemic administration. RES sulfation at its 3-hydroxy position has been reported to be mediated by SULT1A1, SULT1A2, SULT1A3 and SULT1E1 isoforms (Miksits et al., 2005). Sut1a1 is mainly expressed in mouse liver and large intestine (Alnouti and Klaassen, 2006). Sult1e1 is not expressed in mouse liver and slightly expressed in mouse jejunum (Alnouti and Klaassen, 2006). Therefore moderate sulfation of RES is expected in the mouse small intestine.

Glucuronidated metabolites are too hydrophilic to passively diffuse through the plasma membrane, and into the cell. R3G has been shown to be transported by MRP2 (ABCC2), MRP3 (ABCC3) and BCRP (ABCG2) transporters (Maier-Salamon et al., 2008; van de Wetering et al., 2009; Juan et al., 2010a). Hepatic MRP2 has been shown to be the major

transporter for biliary elimination for R3G in rat liver (Maier-Salamon et al., 2008). R3G has been shown to be a high affinity substrate for the MRP3 transporter (van de Wetering et al., 2009). In an *in vivo* experiment it was found that plasma levels of R3G decreased by more than 10 fold in Mrp3(-/-) mice as compared to wild type mice after RES oral administration (van de Wetering et al., 2009). MRP3 has been shown to have higher affinity for R3G as compared to BCRP (van de Wetering et al., 2009). There is a possibility of uptake of R3G at the apical side of enterocytes and basolateral side of liver by organic anion transporters as shown for other glucuronides (Fahrmayr et al., 2010). BCRP and MRP2 have been shown to be involved in the transport of R3S (van de Wetering et al., 2009; Juan et al., 2010a), with BCRP having high affinity and high capacity for R3S transport (van de Wetering et al., 2009). The transport of R3S over the basolateral membrane can take place partly by MRP4 and MRP1 which have been shown to transport other sulfo-conjugates (Qian et al., 2001; Zelcer et al., 2003).

When R3G was administered i.a., 0.4% and 1% of R3G was metabolized at 3.5 mg/kg and 26.66 mg/kg dose of R3G respectively, indicating minimal deglucuronidation and further metabolism when administered systemically. R3G when given by i.a. route can be taken up by organic anion transporters in the hepatocytes and can get eliminated in the bile by MRP2 and BCRP transporters (Fig 5.4). R3G eliminated by biliary route can again partially enter the systemic circulation by enterohepatic circulation, and a clear indication of that is observed as secondary peak for R3G (Fig 5.1 and 5.2).

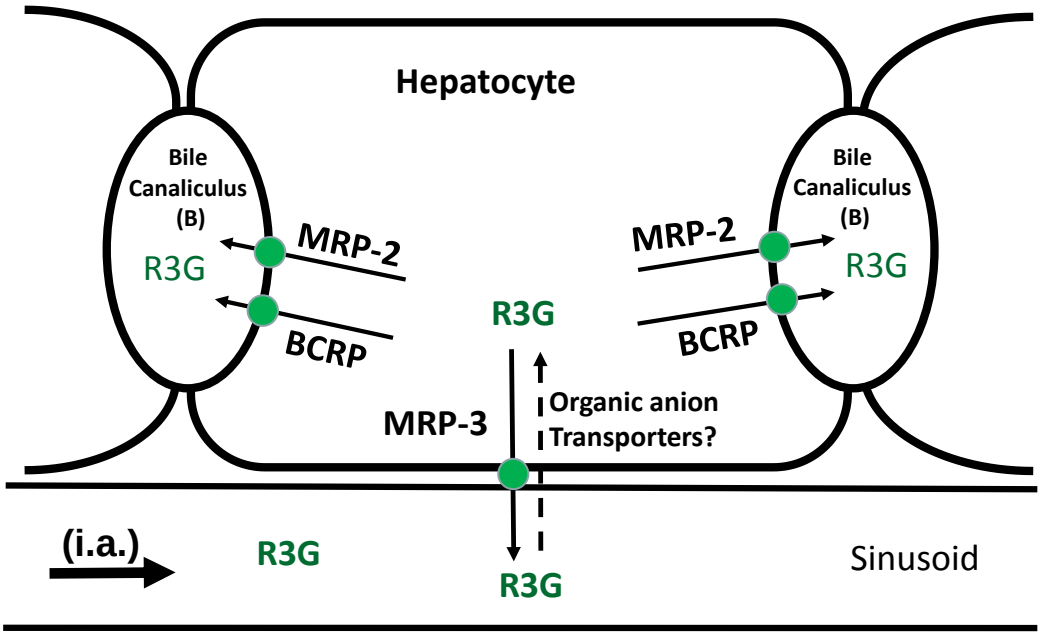

Fig 5.4: Proposed schematic representation of R3G disposition in hepatocyte. Solid line represents pathways based on results in this manuscript and published literature reports for R3G. Dashed line represents pathways based on reports of similar substrates and transporters. Transporters followed by "?" indicates that the role of these transporters are not known for transport of R3G, but is based on findings of transport of other glucronidated substrates.

The presence of efflux transporters MRP2 and BCRP present at the apical side of enterocytes forms a barrier and prevents the absorption of R3G when administered orally (or presented in case of biliary elimination when administered systemically). In an *in vivo* intestinal perfusion experiment in rats, 42% and 12% of absorbed RES was found to be pumped back to the luminal side of intestine as glucuronidated and sulfated metabolites respectively (Juan et al., 2010a). These results elucidated the role of MRP2 and BCRP transporters in efflux of RES conjugates (Juan et al., 2010a).

A pathway for disposition and absorption of R3G has been proposed in Fig 5.5. R3G when administered orally, can get deconjugated in gut by β-glucuronidase/gut flora to form RES, which can then get rapidly absorbed in the enterocyte by passive diffusion (Juan et al., 2010a). RES in the enterocyte can get glucuronidated to form R3G or sulfated to form R3S (Andlauer et al., 2000; De Santi et al., 2000; Kuhnle et al., 2000; Sabolovic et al., 2006). R3G can either be transported to the basolateral side by MRP3 transporters or in the gut lumen by MRP2 or BCRP transporters. R3G excreted in the lumen can further get deconjugated to RES and reabsorbed as RES. This will result in futile cycling of RES/R3G. Futile cycling due to conjugation and deconjugation of estrone sulfate in liver has been previously reported (Tan et al., 2001). R3S formed by SULT enzymes in the enterocyte can get effluxed in the intestinal lumen mainly by BCRP and partly by MRP2 transporter. R3S can also be transported to the basolateral side possibly by MRP1 and MRP4 transporters. These conjugation pathways appear to be so efficient that very low amount of RES is able to escape the enterocyte unconjugated. Even if some RES is able to escape the gut unconjugated, it can be further conjugated in liver. So, we are not able to observe any RES (LLOQ = 10 ng/ml) in the systemic circulation after R3G oral administration, despite RES being formed in gut. This also might help explain the localized therapeutic effect of RES in colon, e.g. chemopreventive activity against colon cancer (Tessitore et al., 2000; Li et al., 2002).

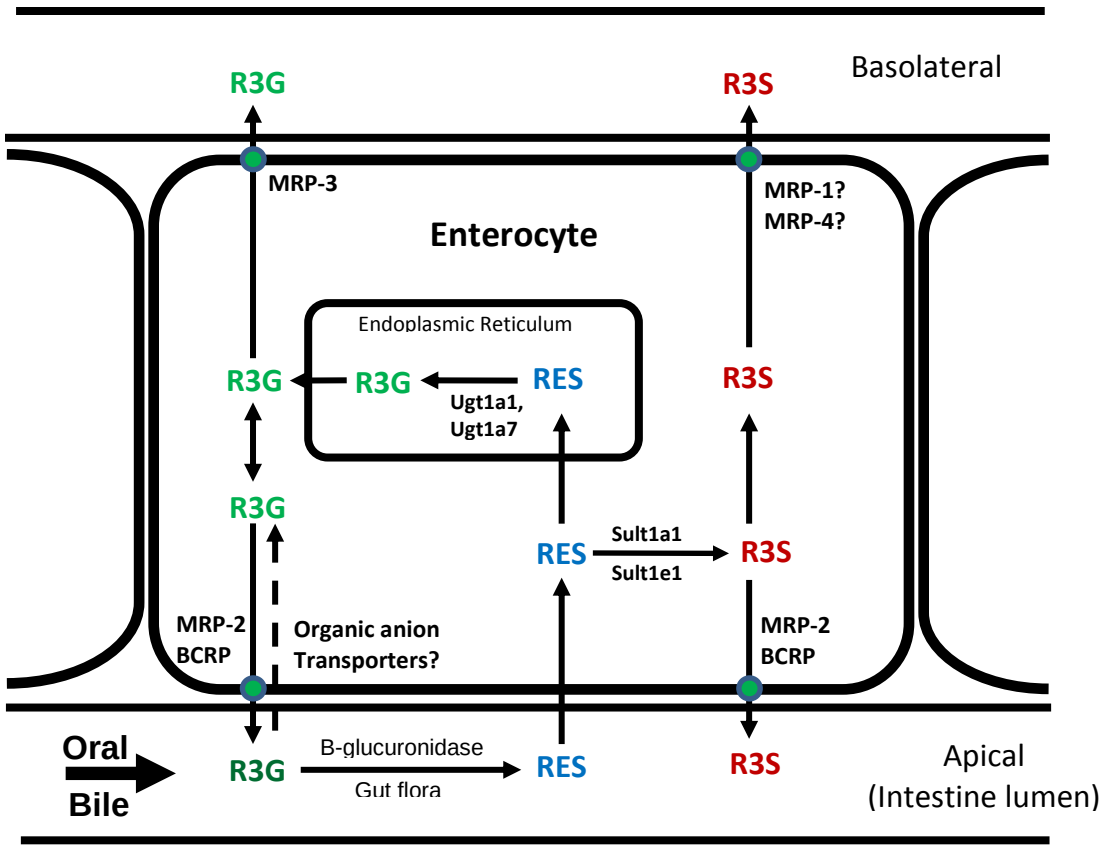

Fig 5.5: Proposed schematic representation of R3G absorption and disposition in enterocyte. Solid line represents pathways based on results in this manuscript and published literature reports. Dashed line represents pathways based on reports of similar substrates and transporters. Transporters followed by "?" indicates that the role of these transporters are not known for transport of R3S and R3G, but is based on findings of transport of other sulfated and glucronidated substrates.

In conclusion, we characterized the systemic and oral pharmacokinetics of R3G. This study is the first report of R3G pharmacokinetics after its i.a. and oral administration. R3G pharmacokinetics was observed to be profoundly influenced by route of administration. A novel mechanistic insight into R3G absorption and disposition was

proposed based on our study and previously reported results which will aid in better understanding of RES pharmacokinetics.

CHAPTER 6
FORMED VERSUS PRE-FORMED METABOLITES.
RESVERATROL: A CASE STUDY

6.1. Rationale

Attention has increasingly focused on the issue of drug metabolites in safety testing (MIST) by both pharmaceutical companies and regulatory agencies (Baillie et al., 2002; Hastings et al., 2003; Smith and Obach, 2005; Prueksaritanont et al., 2006; Frederick and Obach, 2010). Two regulatory guidelines were recently published on this topic (Center for Drug Evaluation and Research (U.S.), 2008; International Conference on Harmonisation, 2009). These guidances recommend metabolite safety evaluation studies to be performed as early as possible during the clinical development program. The recommendation is to synthesize the metabolite and to evaluate it in preclinical toxicity studies.

One major assumption underlying metabolite toxicity evaluation studies is that the kinetic behavior of a preformed metabolite (i.e. a metabolite that is synthesized, purified, and itself dosed) is the same as that of the metabolite formed *in vivo* following administration of parent compound. This has been a topic of debate (Prueksaritanont et al., 2006; Pang et al., 2008; Pang, 2009). It is understood that the pharmacokinetics of a preformed metabolite depends on the ADME properties of the metabolite whereas the kinetics of a metabolite generated *in vivo* depends on the parent as well as the metabolite (Prueksaritanont et al., 2006). Therefore, differences between the kinetic behavior of a preformed metabolite and the same metabolite generated *in vivo* could arise due to intrinsic differences between the disposition of the parent and its metabolite, e.g., their

physicochemical properties or their interactions with transporters. Metabolites are generally more polar than their precursors. A polar preformed metabolite may experience diffusional barriers to its penetration into an eliminating organ, and hence its elimination clearance may be less than that of *in vivo* generated metabolite, whose entry into the eliminating organ is in the form of a more lipophilic parent (Pang, 1985). Additionally it is important to note that the diffusional barrier to penetration in eliminating organ pertains to the biliary excretion of substance and does not refer to renal (filtration) clearance.

As observed by Pang and co-workers (Pang et al., 2008; Pang, 2009), although preformed metabolite administration may not directly reflect the time-course of the *in vivo* formed metabolite, the kinetic data on the preformed metabolite can be extremely useful to develop a robust model for predictions and simulations. The data generated from preformed metabolite administration can be wisely incorporated into a comprehensive pharmacokinetic (PK) model of the parent-metabolite to improve predictions of the behavior of formed metabolite through modeling and simulation.

In the present study, metabolite kinetics of preformed and *in vivo* generated metabolites were compared with two approaches: i) assuming similar PK of preformed versus *in vivo* formed metabolite, ii) assuming dissimilar PK of preformed versus *in vivo* formed metabolite. The first approach assumes that the systemic or elimination clearance of *in vivo* formed and preformed metabolites are similar (Pearson and Wienkers, 2009), whereas the second approach does not make this assumption. The goal of the present

study was to build a comprehensive PK model. This comprehensive PK model was used to predict *in vivo* formation of R3S and R3G after RES administration. Simulation assuming different elimination clearances of preformed and *in vivo* formed metabolites was compared to simulation with the assumption that PK of preformed versus *in vivo* formed metabolites are similar.

The polyphenol resveratrol was used as a model substrate in this study. RES is almost completely metabolized into its sulfated and glucuronidated metabolites in humans as well as rodents (Meng et al., 2004; Hoshino et al., 2010). RES is useful as a model substrate for polyphenols that are heavily conjugated into phase II metabolites. Conjugated metabolites are generally more polar than phase I metabolites. The PK data of RES (i.a., 15 mg/kg or 65.79 umol/kg) and synthesized and purified R3S (i.a., 5 mg/kg or 16.23 umol/kg) and R3G (i.a., 3.5 mg/kg or 8.67 umol/kg) were used from chapters 3, 4 and 5. The relevant data have been consolidated and presented in Table 6.1 again. These doses were selected by performing pilot studies which gave R3S and R3G exposures (AUCs) in the range comparable to R3S and R3G observed upon 15 mg/kg RES (i.a.) administration. These data were utilized to develop PK models. Our models corroborate differences in the PK of preformed versus *in vivo* formed metabolites (Prueksaritanont et al., 2006; Pang et al., 2008; Pang, 2009).

6.2. Materials and methods:

6.2.1. Characterization of metabolite kinetics:

i) Non-compartmental estimation: The apparent fraction of RES converted to R3S and R3G (fm), can be calculated assuming that R3S and R3G are formed directly and only from RES, entry of the metabolite into the eliminating organ is not diffusion limited, and elimination is not perfusion limited, with the following equations :

$$fm_{R3S} = \left[\frac{(AUC_{R3S}^{RES})}{(AUC_{R3S}^{R3S})}\right] x \left[\frac{Dose_{R3S}}{Dose_{RES}}\right] x \left[\frac{Cl_{R3S}^{RES}}{Cl_{R3S}^{R3S}}\right] \qquad \text{[Eq 6.1]}$$

$$fm_{R3G} = \left[\frac{(AUC_{R3G}^{RES})}{(AUC_{R3G}^{R3G})}\right] x \left[\frac{Dose_{R3G}}{Dose_{RES}}\right] x \left[\frac{Cl_{R3G}^{RES}}{Cl_{R3G}^{R3G}}\right] \qquad \text{[Eq 6.2]}$$

If metabolite elimination clearance is assumed to be the same whether preformed or *in vivo* formed, equations 6.1 and 6.2 simplify to equations 6.3 and 6.4 respectively (Pang and Kwan, 1983):

$$fm_{R3S} = \left[\frac{(AUC_{R3S}^{RES})}{(AUC_{R3S}^{R3S})}\right] x \left[\frac{Dose_{R3S}}{Dose_{RES}}\right] \qquad \text{[Eq 6.3]}$$

$$fm_{R3G} = \left[\frac{(AUC_{R3G}^{RES})}{(AUC_{R3G}^{R3G})}\right] x \left[\frac{Dose_{R3G}}{Dose_{RES}}\right] \qquad \text{[Eq 6.4]}$$

where AUC_{R3S}^{RES} is the AUC of R3S when RES is administered i.a., AUC_{R3G}^{RES} is the AUC of R3G when RES is administered i.a., AUC_{R3S}^{R3S} is the AUC of R3S when R3S is administered i.a. and AUC_{R3G}^{R3G} is the AUC of R3G when R3G was administered i.a.

ii) Compartmental analysis: Since there was wide variability in the individual animal data, most likely due to enterohepatic recycling, a naïve averaged data approach was used for modeling (Gabrielsson and Weiner, 2006). This approach has been commonly used (Ogiso et al., 1998). The average concentration of each administration group at each sampling time point was used to perform the PK data analysis using SAAM II software system (version 1.2, SAAM Institute, Seattle, WA, 1997). For each dataset, the simplest compartment model was tested, and complexity was built into the model in subsequent steps. Model selection was based on goodness of fit and comparison of objective functions. Different weighting schemes were tested in SAAM II such as data absolute, data relative, model absolute and model relative. A fractional standard deviation of 0.1 was used, and data- and model- relative as well as absolute variance models were evaluated. Model-absolute variance was selected and used, as it gave parameter estimates with the lowest coefficient of variation (CV). Criteria for goodness of fit of each proposed model to the observed data was based on Akaike's Information Criterion (AIC) as the objective function (Akaike, 1974). The standard error (SE) of the parameter estimation was expressed as % CV (SE/estimate x 100). The PK parameters for RES (model 1), R3G (model 2) and R3S (model 3) were first characterized as independent parent compounds. Linear PK were assumed at the dose levels used, and elimination solely from the central compartment was assumed. Next, a comprehensive PK model (model 4) for the formation of R3S and R3G was built combining models 1, 2 and 3. This model was used to predict the concentration of its two major *in vivo* formed metabolites (R3G and R3S) when RES was administered by an i.a. bolus dose. The volume of distribution of central compartment was calculated as $Vc = Dose/C_0$, where C_0 is the

initial concentration of drug in plasma. Cl, calculated as product of elimination rate constant and volume of central compartment, was calculated and reported (Table 6.2). Formation clearances of R3S and R3G were calculated by multiplying the volume of central compartment of RES to corresponding formation rate constants i.e. $k_{f, R3S}$ and $k_{f, R3G.}$ Fraction metabolized is the fraction of systemically available dose of parent drug that is converted to the metabolite of interest. This was calculated assuming that RES was completely and irreversibly metabolized into R3S and R3G.

6.3. Results:

6.3.1. Estimation of metabolite kinetics assuming similar characteristics of preformed versus *in vivo* formed metabolites:

The fraction of RES being metabolized into R3S(fm_{R3S}) and R3G (fm_{R3G}) using equations 6.3 and 6.4 were found to be 0.168 and 0.17 respectively. The sum of apparent fm values from R3S and R3G was 0.34.

6.3.2. Estimation of metabolite kinetics assuming dissimilar characteristics of preformed versus *in vivo* formed metabolites:

i) PK modeling of RES, preformed R3S and preformed R3G: (Models 1, 2 and 3).

R3S and R3G are the major metabolites based on exposure when RES (15 mg/kg i.a.) was administered (Table 6.1). R4'G and R4'S were minor metabolites and together accounted for only 0.2 % of the total exposure of RES and metabolites combined (Table 6.1). We have therefore ignored these minor metabolites in the model for the sake of simplicity. One, two and three compartment linear models were evaluated to explain the concentration data obtained after i.a. administration of either 15 mg/kg of RES, 5 mg/kg

of R3S or 3.5 mg/kg of R3G. An open three compartment model with elimination from the central compartment (model 1, Fig 6.1) was found to characterize well the concentration-time profiles for RES following its i.a. bolus administration. The predicted and observed RES plasma concentrations from Model 1 are shown in Fig 6.2. An open two compartment model (model 2, Fig 6.3) best described the observed R3S concentration following i.a. bolus administration of 5 mg/kg R3S (Fig 6.4). An open three compartment model with a delay compartment (model 3, Fig 6.5) and elimination from central compartment was used to characterize the concentration-time profile of R3G following i.a. bolus administration of R3G 3.5 mg/kg (Fig 6.6). A delay compartment was included to better describe the data (Davis et al., 2000), as a secondary peak was observed in R3G concentration which might be due to enterohepatic cycling. The delay site is characterized by two parameters that are estimated from the data: the delay time and the number of delay compartments. Mass entering the delay site passes through each of the delay compartments. The delay time was fixed as 180 min based on visual examination of the data and 10 delay compartments were used. Table 6.2 shows the compartmental pharmacokinetic parameter estimates of RES, R3S and R3G. Run tests were performed for Models 1, 2 and 3, and resulted in large p-values ($p = 0.26$, 0.25, and 0.26 respectively), indicative of a lack of run of signs. The mean clearance estimate of RES and preformed R3G and R3S from models 1, 2 and 3 were comparable to the non-compartmental clearance estimates respectively (Tables 6.1 and 6.2).

Table 6.1. Noncompartmental pharmacokinetic analysis upon a single 15 mg/kg (i.a.) RES, 5 mg/kg (i.a.) R3S or 3.5 mg/kg (i.a.) R3G dose. Data are presented as Mean ± SD

ESTIMATE	RES 15 mg/kg i.a. (n = 5)	R3S 5 mg/kg i.a. (n = 4)	R3G 3.5 mg/kg i.a. (n = 4)	Units
AUC_{0-t}	510.01 ± 105.54	243.29 ± 113.10	650.66 ± 216.50	min*uM
AUC_{0-inf}	591.08 ± 167.29	255.84 ± 124.98	710.10 ± 273.30	min*uM
Cl	118.77 ± 33.36	76.29 ± 37.07	13.78 ± 5.75	ml/min/kg
Vss	37.59 ± 23.70	6.37 ± 2.36	4.55 ± 1.07	L/kg
Terminal $t_{1/2}$	190.58 ± 69.65	128.08 ± 26.21	272.48 ± 17.07	min
Cmax	15.27 ± 9.07	14.79 ± 3.15	27.84 ± 4.70	uM
Tmax	2.5 ± 0	2.5 ± 0	2.5 ± 0	min
	R3S	**RES**	**R3S**	
AUC_{0-t}	163.87 ± 42.38	NA	NA	min*uM
AUC_{0-inf}	174.94 ± 45.75	NA	NA	min*uM
Terminal $t_{1/2}$	201.12 ± 158.12	NA	NA	min
	R3G	**R3G**	**RES**	
AUC_{0-t}	857.36 ± 396.17	1.04 ± 0.29	NA	min*uM
AUC_{0-inf}	921.23 ± 457.07	1.59 ± 0.73	NA	min*uM
Terminal $t_{1/2}$	264.75 ± 248.66	10.05 ± 3.98	NA	min
	R4'G	**R4'G**	**R4'G**	
AUC_{0-t}	2.03 ± 1.78	NA	2.08 ± 1.27	min*uM
AUC_{0-inf}	2.61 ± 1.87	NA	2.51 ± 1.41	min*uM
Terminal $t_{1/2}$	14.11 ± 5.98	NA	8.64 ± 5.57	min
	R4'S	**R4'S**	**R4'S**	
AUC_{0-t}	0.83 ± 0.39	NA	NA	min*uM
AUC_{0-inf}	1.07 ± 0.43	NA	NA	min*uM
Terminal $t_{1/2}$	8.85 ± 4.37	NA	NA	min

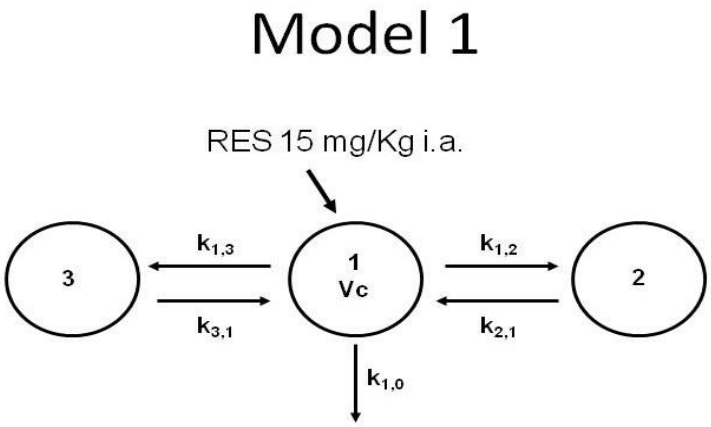

Fig 6.1: Three compartment PK model 1 describing the disposition of RES after administration of RES (15 mg/kg, i.a.). Vc: volume of the central compartment, k: first order rate constants for RES disposition.

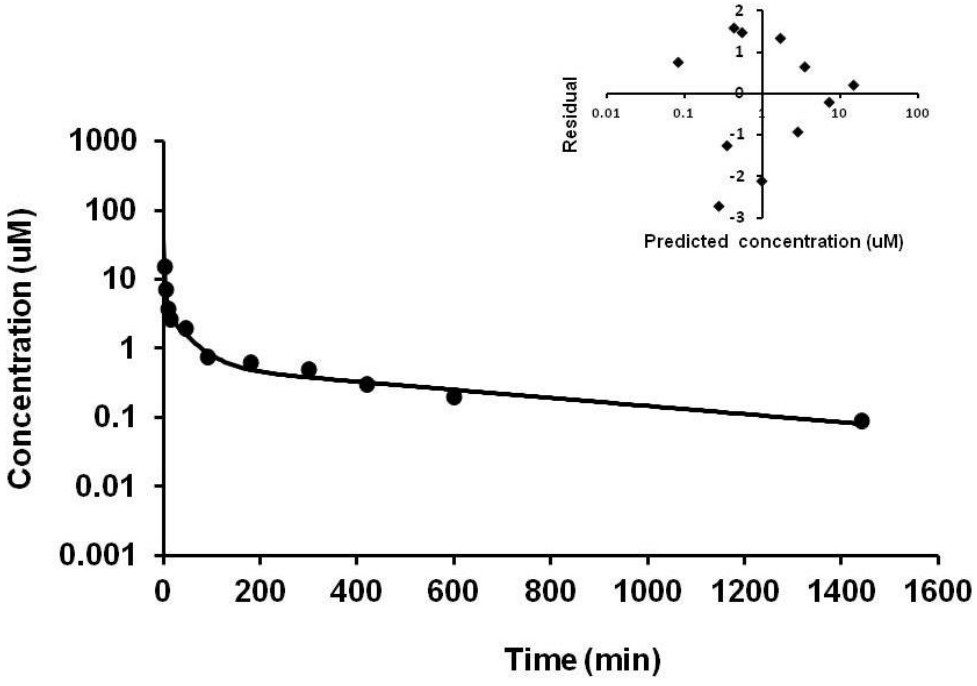

Fig 6.2: Observed average RES concentration (data points) and PK model 1 predicted (solid line) RES concentration time profiles after RES administration, plot of weighted residuals versus predicted RES concentration (inset)

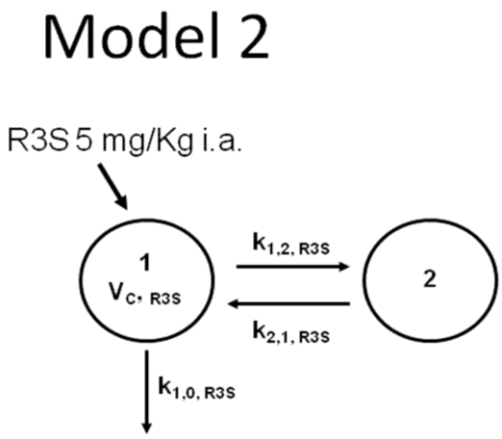

Fig 6.3: Two compartment PK model 2 describing the disposition of R3S after administration of R3S (5 mg/kg, i.a.). $Vc,_{R3S}$: volume of the central compartment, k: first order rate constants for R3S disposition.

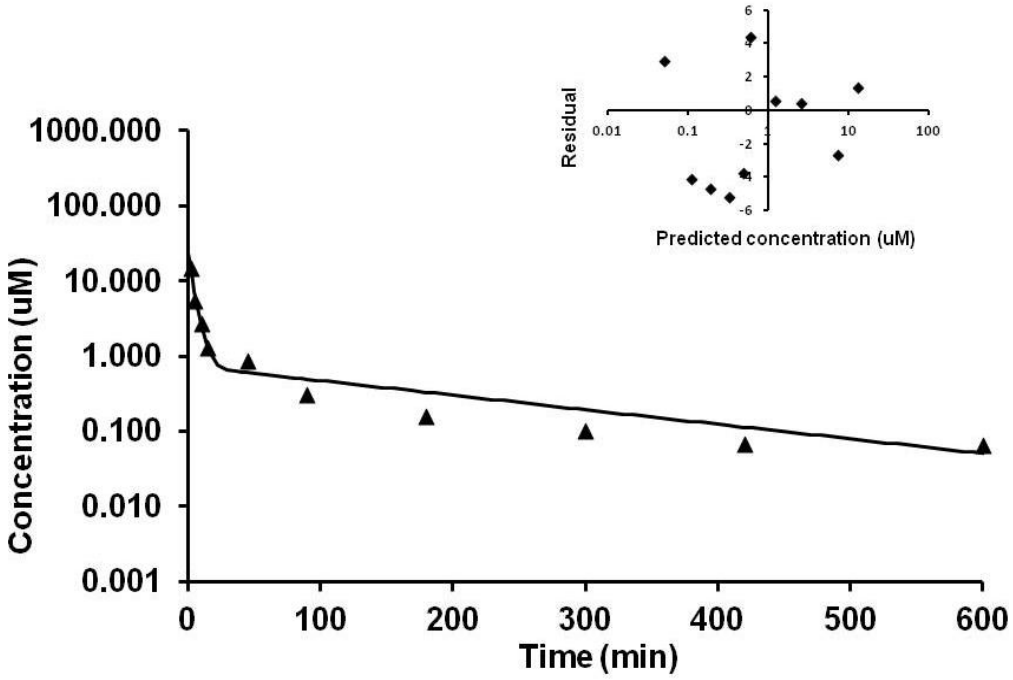

Fig 6.4: Observed average R3S concentration (data points) and PK model 2 predicted (solid line) R3S concentration time profiles after R3S administration, plot of weighted residuals versus predicted R3S concentration (inset).

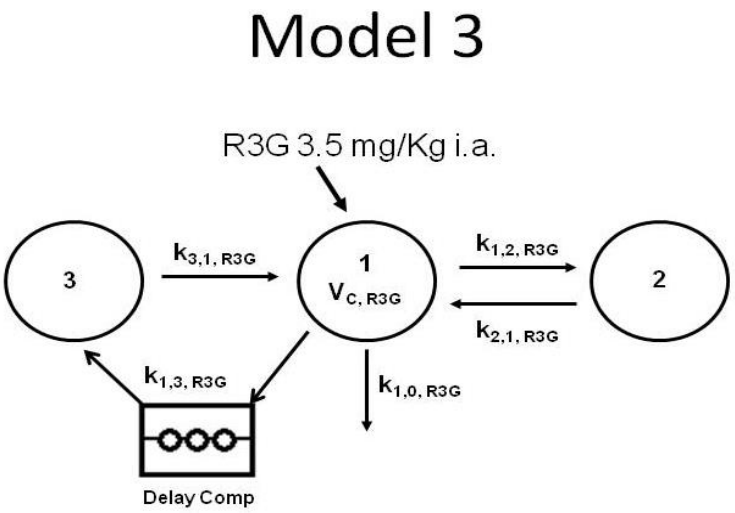

Fig 6.5: Enterohepatic cycling PK model 3 describing the disposition of R3G after administration of R3G (3.5 mg/kg, i.a.). Vc, $_{R3G}$: volume of the central compartment, k: first order rate constants for R3G disposition.

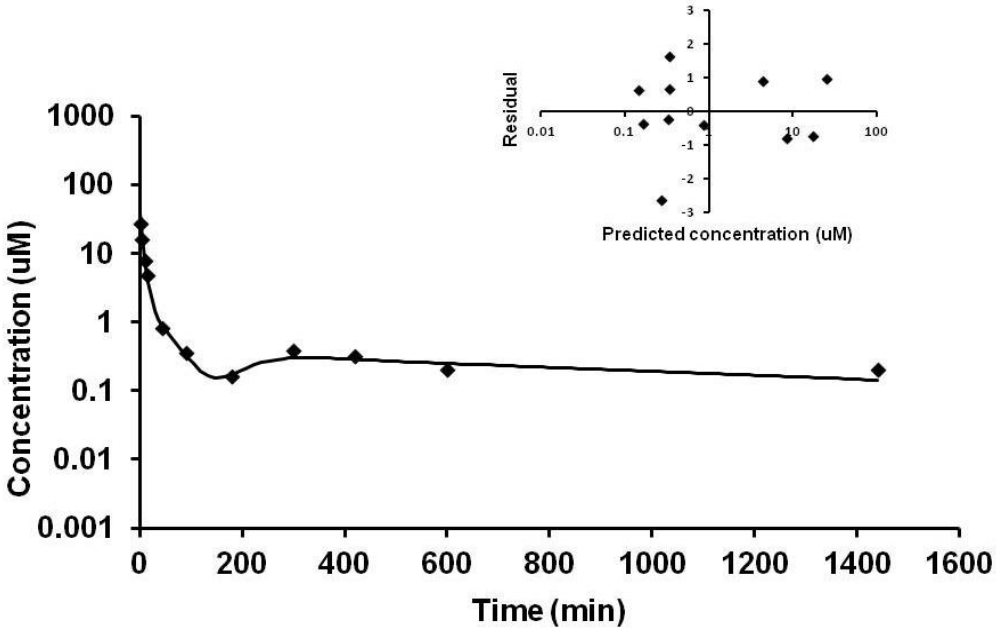

Fig 6.6: Observed average R3G concentration (data points) and PK model 3 predicted (solid line) R3G concentration time profiles after R3G administration, plot of weighted residuals versus predicted R3G concentration (inset).

Table 6.2. Compartmental pharmacokinetic parameters of RES, R3S and R3G administered as parent compound using model 1, 2 and 3, respectively.

Parameters	**RES, Model 1, Estimate (CV%)**	**R3S, Model 2, Estimate (CV%)**	**R3G, Model 3, Estimate (CV%)**
Vc, RES (l/kg)	1.77 (27.29)	NA	NA
Cl, RES (ml/min/kg)	104.54 (3.97)	NA	NA
$k_{1,0}$ (min^{-1})	0.06 (25.66)	NA	NA
$k_{1,2}$ (min^{-1})	0.23 (23.74)	NA	NA
$k_{2,1}$ (min^{-1})	0.06 (14.74)	NA	NA
$k_{1,3}$ (min^{-1})	0.09 (24.73)	NA	NA
$k_{3,1}$ (min^{-1})	0.004 (11.84)	NA	NA
Vc, R3S (l/kg)	NA	0.69 (11.43)	NA
Cl, R3S (ml/min/kg)	NA	63.11 (3.56)	NA
$k_{1,0}$ R3S (min^{-1})	NA	0.09 (9.37)	NA
$k_{1,2}$ R3S (min^{-1})	NA	0.15 (7.17)	NA
$k_{2,1}$ R3S (min^{-1})	NA	0.012 (7.45)	NA
Vc, R3G (l/kg)	NA	NA	0.23 (10.95)
Cl, R3G (ml/min/kg)	NA	NA	10.63 (6.81)
$k_{1,0}$ R3G (min^{-1})	NA	NA	0.05 (11.86)
$k_{1,2}$ R3G (min^{-1})	NA	NA	0.04 (15.53)
$k_{2,1}$ R3G (min^{-1})	NA	NA	0.03 (14.97)
$k_{1,3}$ R3G (min^{-1})	NA	NA	0.07 (9.06)
$k_{3,1}$ R3G (min^{-1})	NA	NA	0.002 (11.27)

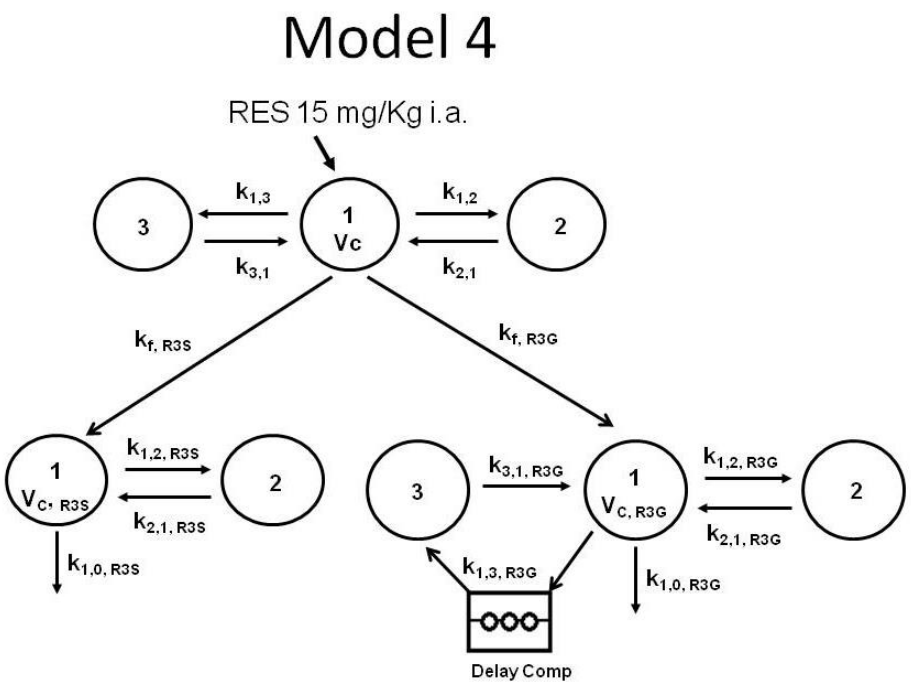

Fig 6.7: PK model 4 describing the disposition of *in vivo* formed metabolite R3S and R3G after RES (15 mg/kg, i.a.) administration. Vc: volumes of central compartments, k: first order disposition rate constants, k_f: first order formation rate constants for RES metabolites.

Note: The notation used throughout is k (from, to). In SAAM II software, the rate constants have a different notation k (to, from).

ii) Simulation of *in vivo* formed metabolites using model 4:

A great deal of time was invested in trying to fit comprehensive models to resveratrol and its *in vivo* formed metabolites simultaneously, but the models did not converge (possibly due to the large number of parameters (n=17) in relation to the data collected). Hence simulations were performed instead of model-fitting. The parameters obtained from model 1, model 2 and model 3 were fixed in model 4 and then the *in vivo* formed R3S and R3G after RES administration (Fig 6.7) predicted under two conditions. In the first condition the elimination clearance of the preformed metabolites was assumed to be equal to that of the *in vivo* formed metabolites. For this all the parameters in model 4 were fixed using parameters from model 1, 2 and 3. Next this was used to predict formation rate constants $k_{f,R3S}$ and $k_{f,R3G}$ (see Fig 6.7). Rate constants k_{fR3S} and $k_{f,R3G}$ were converted to clearance parameters by multiplying with central volume of distribution (Vc). Simulations were performed, but resulted in poor fit of the predicted versus observed plasma concentrations of RES (Fig 6.8A), R3S (6.8B) and R3G (6.8C).

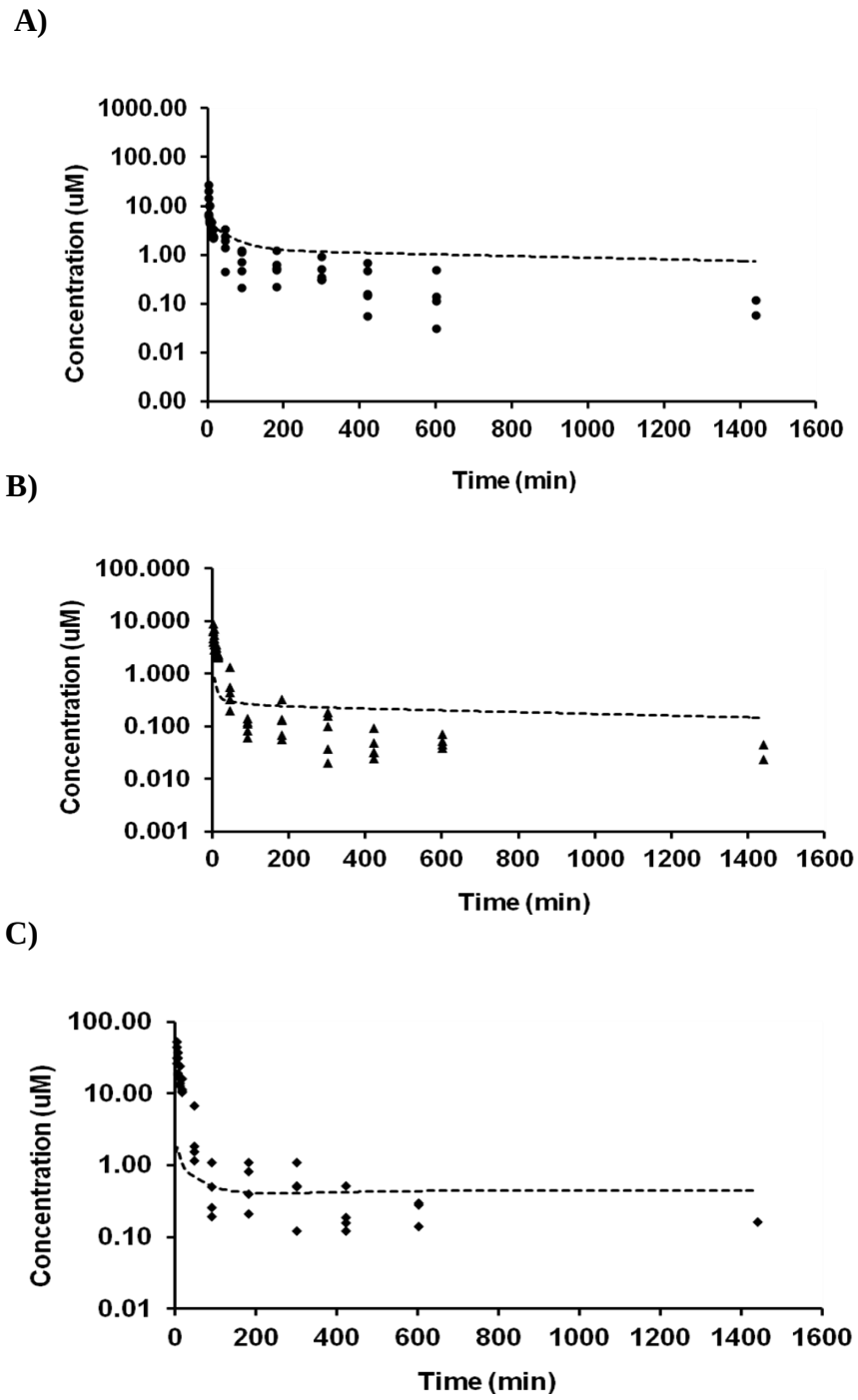

Fig 6.8: Observed and PK model 4 simulated concentration time profiles of RES (A), R3S (B) and R3G (C) after RES administration, assuming elimination clearance of preformed metabolites to be equal to *in vivo* formed metabolites.

In the second condition the elimination clearance of preformed metabolites was assumed to be dissimilar to *in vivo* formed metabolites. For this all the parameters in model 4 were fixed using parameters from models 1, 2 and 3 except for the elimination rate constants of R3S ($k_{1,0,\ R3S}$) and R3G ($k_{1,0,\ R3G}$). The parameters $k_{f,R3S}$ (0.032 min^{-1}), $k_{f,R3G}$ (0.030 min^{-1}), $k_{1,0,\ R3S}$ (0.453 min^{-1}) and $k_{1,0,\ R3G}$ (0.295 min^{-1}) were then obtained from the model (Fig 6.2). Next the simulation was performed by fixing $k_{f,R3S}$, $k_{f,R3G}$, $k_{1,0,\ R3S}$ and $k_{1,0,\ R3G}$ providing a good fit of observed versus model predicted RES, R3S and R3G plasma concentrations after RES 15 mg/kg i.a. administration as shown in Fig 6.9A, 694B and 6.9C respectively. The second condition also provided a more realistic estimate of the fraction of RES metabolized to R3S and R3G to be 52% and 48 % respectively. Parameters were estimated under the assumption that there was no elimination of RES other than R3S and R3G. Elimination clearances of *in vivo* formed R3S (313.08 ml/min/kg) and R3G (67.86 ml/min/kg) (Table 6.3) predicted under the second condition were found to be higher than the elimination clearances of preformed R3S (76.29 ml/min/kg) and R3G (13.78 ml/min/kg; Table 6.1).

A)

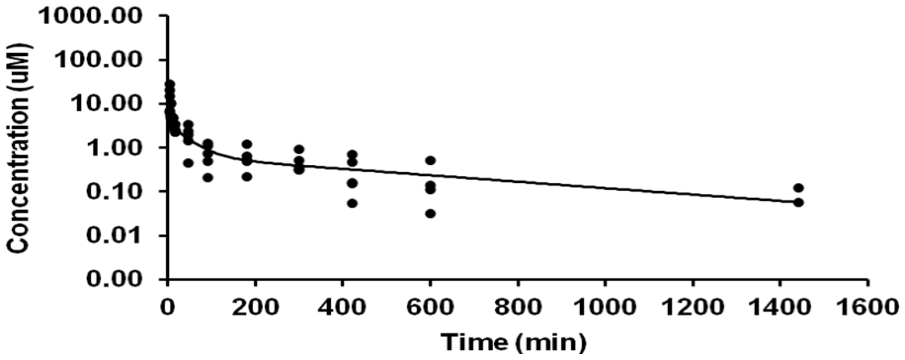

B)

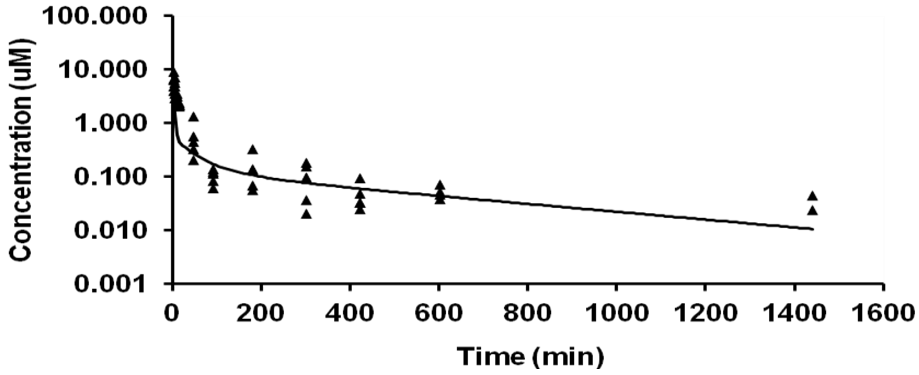

C)

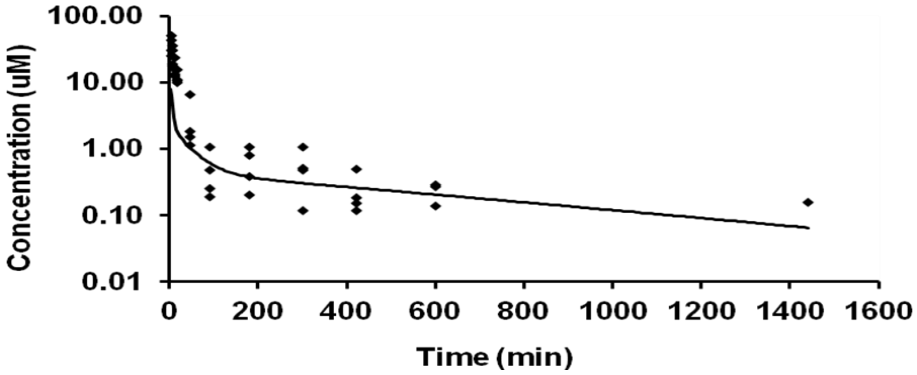

Fig 6.9: Observed and PK model 4 simulated concentration time profiles of RES (A), R3S (B) and R3G (C) after RES administration, assuming elimination clearance of preformed metabolites to be not equal to *in vivo* formed metabolites.

Table 6.3. Comparison of elimination or systemic clearance of *in vivo* formed metabolites and preformed metabolites.

Parameters	**Preformed Metabolite**	***In-vivo* formed metabolite**
Cl,R3S (ml/min/kg)	76.29 ± 37.07[a]	313.08[c]
Cl,R3G (ml/min/kg)	13.78 ± 5.75[a]	67.86[c]
fm_{R3S} (%)	16.87[b]	48.00[d]
fm_{R3G} (%)	17.08[b]	52.00[d]

[a] From Table 1

[b] Fractions calculated using equations 1 and 2.

[c] Values used for simulations in Fig 6.9B and 6.9C

[d] Fractions of RES converted to R3S and R3G, calculated assuming complete metabolism of RES into R3S and R3G for Fig 6.9B and 6.9C.

6.4. Discussion and conclusion:

The utility of the present work lies in development of models to explain the complex kinetics of highly conjugated substrates such as polyphenols. Further, models such as those presented here will be further developed in future studies to evaluate a) kinetics of conjugated metabolites that might be active, and b) potential interactions between polyphenols and co-administered drugs, e.g. enzyme induction or inhibition.

Preformed major metabolites of RES - R3S and R3G - were administered to delineate the metabolite kinetics and to determine the fraction of RES converted to respective metabolites. The present data (Table 6.1) and literature reports clearly indicate much greater conversion of RES to R3S and R3G (Yu et al., 2002; Wenzel and Somoza, 2005) than predicted by equations 1 and 2, which assume similar kinetics of preformed versus *in vivo* formed metabolite. Since these formation clearances are calculated based on preformed metabolite data, the difference in preformed metabolite kinetics as compared to *in vivo* formed metabolite kinetics might be responsible for underprediction of metabolite formation clearances. This prompted the use of a modeling approach to delineate the kinetics of *in vivo* formed metabolites.

The average plasma concentration-time profile of RES after 15mg/kg of RES administration was explained by a 3 compartment model (Fig 6.1). Similar models have been used to explain disposition of drugs undergoing enterohepatic cycling (Hasselström and Säwe, 1993). RES was modeled to be distributed from a central compartment into two peripheral compartments, with elimination from the central compartment. It has been

shown earlier (Colburn, 1982) that enterohepatic circulation increases the apparent volume of distribution. Therefore, a very high volume of distribution of RES can be partially attributed to tissue binding and partially to enterohepatic circulation of RES.

R3S plasma profile was explained by a 2 compartment model with elimination from the central compartment (Fig 6.3). Although enterohepatic cycling of R3S is also a possibility, a two compartment model was found to explain well the plasma profile of R3S after R3S (preformed) administration. An enterohepatic circulation model described the disposition of R3G after R3G (preformed) administration (Fig 6.5). Similar models have been developed for morphine 3-glucuronide (Ouellet and Pollack, 1995), morphine (Dahlström and Paalzow, 1978), phenolphthalein (Colburn et al., 1979) and isoflavones (Moon et al., 2006). These models used either a series of cycling compartments linked by first order rate constants or a single compartment with a lag time to account for the delay observed in the appearance of a secondary peak in plasma. A similar approach was used in the present model by using a delay compartment which was comprised of 10 compartments with a single rate constant ($k_{1,3,\ R3G}$) and a fixed delay time of 3hr. Thus in Fig 6.5, Compartment 1 depicts the blood as well as quickly equilibrating tissues. Compartment 2 depicts more slowly equilibrating tissues and compartment 3 can depict the intestinal compartment. The rate constant $k_{1,3,\ R3G}$ represents several different processes including biliary transport of R3G, transit of R3G through the gastrointestinal lumen, and possible hydrolysis of glucuronides into RES. The rate constant $k_{3,1,\ R3G}$ may denote absorption of re-formed RES and its subsequent glucuronidation into R3G or absorption of R3G from the lower intestine. A lag time of 3 hr is included between biliary

transport and absorption to account for transit from the liver to the site of de-glucuronidation, and subsequent metabolism and reabsorption. The clearance estimates obtained after compartmental analysis of pooled data were found to be comparable to those estimated with individual data by non-compartmental methods (Tables 6.1 and 6.2).

Models 1, 2 and 3 were combined to form a comprehensive model 4 to predict the *in vivo* formed R3S and R3G after RES administration (Fig 6.7). Simulation using the assumption that elimination clearances of preformed and *in vivo* formed metabolites are the same, led to a poor overlap of the observed and predicted *in vivo* formed R3S and R3G (Fig 6.8A, B & C). Simulation using the assumption that elimination clearances of preformed and *in vivo* formed metabolites are different, led to a much improved prediction (Fig 6.9A, B & C). The second approach also gave a more realistic formation ratio of R3S and R3G as 52% and 48% respectively. This value was comparable to the formation ratio of *in vivo* formed R3S (46%) and R3G (54%) predicted by Colom and co-workers (Colom et al., 2011). With the second approach the elimination clearances of R3S and R3G used for the simulation were higher than the preformed metabolites' elimination clearances. It has been suggested that phase II metabolites like glucuronides and sulfates are more hydrophilic and preformed metabolites may experience difficulty penetrating into an eliminating organ, and hence the extent of its elimination may be less than that of *in vivo* generated metabolite, whose entry into the eliminating organ is in the form of a more lipophilic precursor (Pang et al., 1984; Pang, 1985). Therefore the formation and elimination clearances of the formed and preformed metabolites may differ

markedly. Differences in metabolite kinetics of preformed and *in vivo* formed metabolites were clearly visible in the present study.

It has been observed by Pang and coworkers (Pang et al., 2008; Pang, 2009) that although preformed metabolite administration might not be able to provide a complete correlation of the formed metabolite time-course, the accompanying information can be incorporated to build a comprehensive PK model. This can improve the predictions of *in vivo* formed metabolites. In the present work, model 4 was useful for purposes of predicting the disposition of metabolites as well as RES exposure. This and similar models can be further developed and improved to predict events such as interactions with xenobiotics that lead to enzyme induction or inhibition.

As a first study of RES metabolite PK, the present study did not include sample collection of urine, feces, or bile. This is an obvious limitation of the study, as additional data would provide a more detailed picture of RES disposition. Also, plasma data collected here did not aid in discerning elimination from the central versus peripheral compartment (Berezhkovskiy, 2004; Yates and Arundel, 2008). Thus, one criticism of the models presented might be the improper assumption of elimination solely from the central compartment. If peripheral elimination were to play a role in the elimination of RES or its metabolites (e.g. metabolism in tissues kinetically different from the central compartment), the steady-state volume of distribution estimates might be predicted inaccurately with the present models.

In summary, PK models were developed to adequately explain the kinetics of RES and its two major metabolites, R3S and R3G. Preformed and *in vivo* formed R3S and R3G kinetics were compared and a marked difference was observed between the preformed and *in vivo* formed metabolite kinetics. Due to observed kinetic differences between *in vivo* formed metabolites and preformed metabolites, safety and toxicity studies conducted with preformed metabolites are useful only when there is a similarity in the kinetics of preformed and *in vivo* formed metabolites, or when sufficient tissue exposure of preformed metabolites is ensured. However, achieving high tissue exposure can be especially difficult for very hydrophilic metabolites.

Copyright Notice

The work in this study has been published in the following article:

Satish Sharan, Otito F. Iwuchukwu, Daniel J. Canney, Cheryl Zimmerman and Swati Nagar. In-vivo formed versus preformed metabolite kinetics of trans-resveratrol-3-sulfate and trans-resveratrol-3-glucuronide; doi:10.1124/dmd.112.046417; Drug Metabolism and Disposition, 40 (1993-2001) 2012."

January 18, 2013

Satish Sharan
Pharmaceutical Sciences
Temple University
3307 North Broad Street
Philadelphia, PA 19140

Email: satish.sharan@temple.edu

Dear Satish Sharan:

This is to grant you permission to include the following article in your thesis entitled "Pharmacokinetics of Resveratrol, its monoconjugates and its trimethoxy analog TMS" for Temple University:

> Satish Sharan, Otito F. Iwuchukwu, Daniel J. Canney, Cheryl L. Zimmerman, and Swati Nagar, In Vivo-Formed versus Preformed Metabolite Kinetics of *trans*-Resveratrol-3-sulfate and *trans*-Resveratrol-3-glucuronide, *Drug Metab Dispos* October 2012 40:1993-2001

On the first page of each copy of this article, please add the following:

> Reprinted with permission of the American Society for Pharmacology and Experimental Therapeutics. All rights reserved.

In addition, the original copyright line published with the paper must be shown on the copies included with your thesis.

Sincerely yours,

Richard Dodenhoff
Journals Director

American Society for Pharmacology and Experimental Therapeutics

CHAPTER 7

DEVELOPMENT AND VALIDATION OF A LC-MS/MS METHOD FOR THE QUANTIFICATION OF 3, 4', 5 TRIMETHOXY TRANS STILBENE (TMS) IN MOUSE BRAIN AND PLASMA

7.1. Rationale

Due to poor *in vivo* metabolic stability of RES we looked for analogs of RES which have retained the potency of RES and are expected to be more bioavailable. One such analog of RES is 3, 4', 5 trimethoxy-trans-stilbene (TMS), where all three hydroxyl groups of RES are substituted by methoxy groups (Fig 7.1). TMS has been reported to be of similar or higher *in vitro* potency than RES (Matsuda et al., 2004; Belleri et al., 2005; Bader et al., 2008; Pan et al., 2008). Based on its physicochemical properties predicted by ChemDraw (ACDlabs 12.0 software) we additionally hypothesized that TMS might have better brain permeability. Better brain permeability of TMS, if proven, can have implications for several indications in brain where RES has also shown positive biological activities. RES have been shown to have an important role in the protection of nervous system after injury (Zhou et al., 2011), to promote clearance of amyloid-beta peptides in Alzheimer's disease (Marambaud et al., 2005) and demonstrates an antitumor effect in gliomas (Tseng et al., 2004).

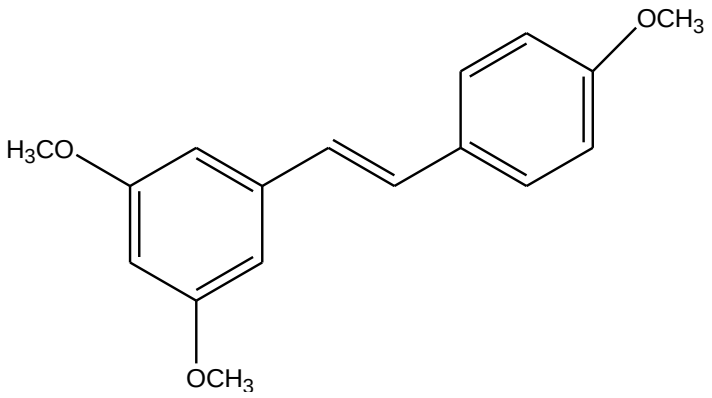

Fig 7.1: Structure of 3, 4', 5 trimethoxy-trans-stilbene (RES analogue; TMS)

The comprehensive *in vivo* study of TMS requires a validated bioanalytical assay with low detection capability. While methods have been reported for the quantitation of TMS in plasma by HPLC (Lin and Ho, 2009) and single MS (Ma et al., 2007), to the best of our knowledge quantitation of TMS in brain has not been conducted to date. Our aim in this study was to develop and validate an LC-MS/MS assay for quantitation of TMS in mouse plasma and brain.

7.2. Assay development:

7.2.1. Preparation of stock solutions, calibration standards (CS) and quality control (QC) samples

7.2.1.1 Plasma

Stock solution of TMS was prepared in DMSO. CS samples were prepared by spiking stock standard working solution into heparinized mouse plasma to give six CS in the concentration range of 10 – 10000 ng/ml. Similar to calibration standards, QC samples were prepared in replicates (n = 3 and 5 for the inter-day and intra-day validation

respectively) at three concentration levels representing the entire range of concentrations (30, 1000 and 10000 ng/ml).

7.2.1.2. Brain

Stock solution of TMS was prepared in DMSO. CS samples were prepared by spiking stock standard working solution into 16.67% (20 gram brain and 100 ml saline) mouse brain homogenate to give five CS in the concentration range of 20 – 10000 ng/ml. Similar to calibration standards, QC samples were prepared in replicates (n = 3 and 5 for the inter-day and intra-day validation respectively) at three concentration levels representing the entire range of concentrations (60, 1000 and 10000 ng/ml).

7.2.2. Sample preparation

7.2.2.1. Plasma

TMS was isolated from plasma with protein precipitation. To 10 uL of plasma sample, 20 uL methanol was added and the resultant solution was vortexed for 1 min and centrifuged at 15,000 rpm for 15 min at room temperature. Supernatant (20 uL) was injected into the liquid chromatography tandem mass spectrometry system.

7.2.2.2. Brain

TMS was isolated from brain homogenate with protein precipitation. To 20 uL of brain homogenate was added 40 uL of methanol, and resulting solution vortexed for 1 min and centrifuged at 15,000 rpm for 15 min at room temperature. Supernatant (20 uL) was injected into the liquid chromatography tandem mass spectrometry system.

7.2.3. LC-MS/MS conditions

The LC-MS/MS assay was carried out on an Agilent series 1100 high-performance liquid chromatography system equipped with a binary pump, autosampler and degasser coupled to an API 4000 triple-quadrupole tandem mass spectrometer (ABSciex) with an ESI source operated in the positive ion mode. Analyst software version 1.4.2 (ABSciex) was used for instrument control, data acquisition and data processing for both chromatography and mass spectrometry. The chromatographic separation system consisted of a guard column (Zorbax SB-C18, 5 um, 4.6 × 12.5 mm; Agilent Technologies), an analytical column (Zorbax SB-C18, 5 um, 4.6 × 250 mm; Agilent Technologies) and a mobile phase consisting of 10mM ammonium acetate (20%) and acetonitrile (80%) containing 0.2% formic acid (pH = 3). The run time was six minutes. Flow rate of the mobile phase was 1.2 mL/min and the flow from the column was split 1:3 into a ABSciex API4000 triple quadrupole mass spectrometer equipped with a Turbo Ionspray source operating at 450°C. The column temperature was maintained at 35°C. The ESI instrument settings were optimized for the analysis and the appropriate multiple reaction monitoring (MRM) transitions and MS/MS parameters were determined for trimethoxy-stilbene (TMS) by direct infusion into the mass spectrometer. Nitrogen was used as the curtain, collision and ion source gas.

7.3. Assay validation

The method was validated according to published recommendations for bioanalytical method validation (Shah et al., 2000). Calibration curves were constructed from the peak

area ratios of TMS versus nominal plasma concentrations with linear least squares regression with a weighting factor of $1/X^2$. Intra-day accuracy and precision were determined by analyzing five replicates of QC samples. Inter-day accuracy and precision were evaluated on five separate days. Precision was expressed as the relative standard deviation of the determined concentrations. Accuracy was calculated using the following equation:

Accuracy = [(mean measured concentration – nominal concentration)/nominal concentration] × 100. Recovery and matrix effect were investigated by analyzing five individual plasma and brain samples at low, medium and high concentrations. These concentrations were: 30, 1000, and 10000 ng/ml for plasma and 60, 1000, and 10000 ng/ml for brain. The recovery was determined by comparing analyte peak area ratio upon extraction from spiked plasma to analyte peak area from post extracted plasma sample. The matrix effects on ionization were evaluated by comparing TMS peak areas of the samples spiked post-extraction with corresponding peak area ratios of the standards prepared in the injection solution.

Efforts were made to incorporate an internal standard into our bioanalytical method. Carbamazepine and fenofibrate were tested to be used as internal standard. Compounds similar in structure to RES, like pterostilbene and trans-stilbene were also tested.

7.4. Results:

ESI operated in positive ion mode was used for the LC-MS/MS analysis to provide optimum sensitivity and selectivity. The optimized tandem mass spectrometry conditions are summarized in Table 7.1. The following precursor-product ion transitions were observed: m/z 271→147 for TMS with a dwell time of 400 ms for ion transition. The retention time was ~ 4.6 min for TMS. TMS was found to have poor ionization and its ionization improved after the addition of 0.2 percent formic acid in mobile phase.

Table 7.1: Optimized ESI-MS/MS operating, MRM and MS/MS parameters for TMS.

Operating parameters	Setting
Collision gas (psi)	6
Curtain gas (psi)	40
Ion source gas 1 (psi)	55
Ion source gas 2 (psi)	55
Ion spray voltage (V)	4500
Temperature (°C)	450
EP (V)	10
Run duration (min)	6
Precursor ion (m/z)	271
Product ion (m/z)	147
Dwell time (ms)	400
DP (V)	66
CE (V)	25
CXP (V)	16

A representative chromatogram of TMS in plasma and brain is presented in Figure 7.1 and 7.2 respectively.

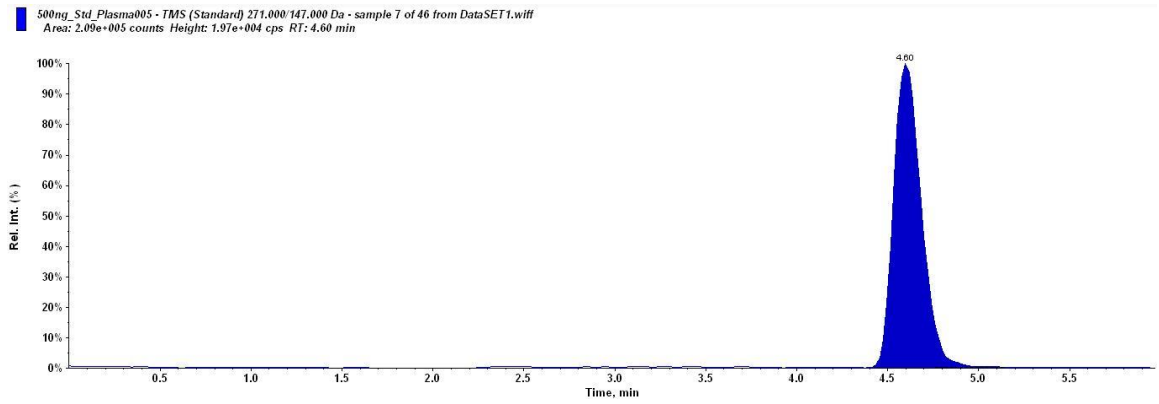

Fig 7.1: Representative chromatogram of TMS in plasma.

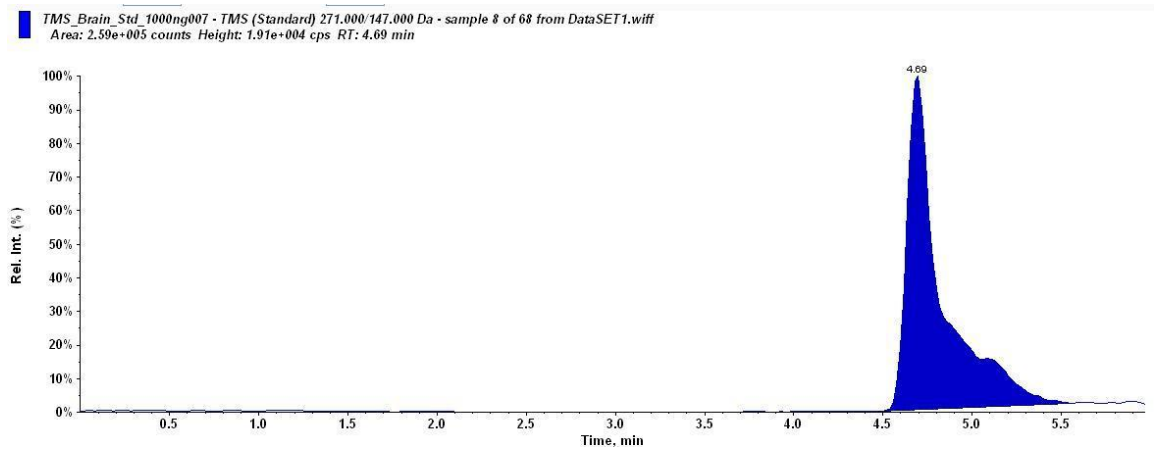

Fig 7.2: Representative chromatogram of TMS in brain homogenate.

Analogs of RES similar in structure to RES e.g. pterostilbene and trans-stilbene were unable to produce reliable signals in the positive ion mode of our analytical method. Carbamazepine and fenofibrate did produce reliable signal during method development with our analytical method. However during validation it was found that carbamazepine and fenofibrate did not track TMS well (Table 7.2). Interestingly it was observed that data analysis without incorporating internal standard provided a more reliable estimate of

the TMS concentration. In the interest of time, it was decided to use an analytical method without an internal standard to quantitate TMS.

Table 7.2: Precision and accuracy for quantitation of TMS in plasma with and without carbamazepine and fenofibrate as internal standard.

TMS quantitation	Nominal Concentration (ng/ml)	Mean observed concentration (ng/ml)	Precision (RSD)	Accuracy (% Bias)
With Carbamazepine (IS)	100000.00	26050.00	32.52	-73.95
	5000.00	24700.00	31.62	394.00
	10.00	4.92	47.20	-50.80
Without Carbamazepine (IS)	100000.00	104633.33	7.00	4.63
	5000.00	5650.00	0.27	13.00
	10.00	10.78	6.02	7.83
With Fenofibrate (IS)	1000.00	1338.25	55.88	33.83
	10.00	7.62	31.72	-23.85
Without Fenofibrate (IS)	1000.00	1077.50	3.16	7.75
	10.00	10.05	1.72	0.47

LOQs were established at the lowest points of the standard curves, i.e. 10 ng/ml for TMS in plasma and 20 ng/ml for TMS in brain homogenate. Representative standard curves of TMS in plasma and brain homogenate are presented in Fig 7.3 and 7.4 respectively.

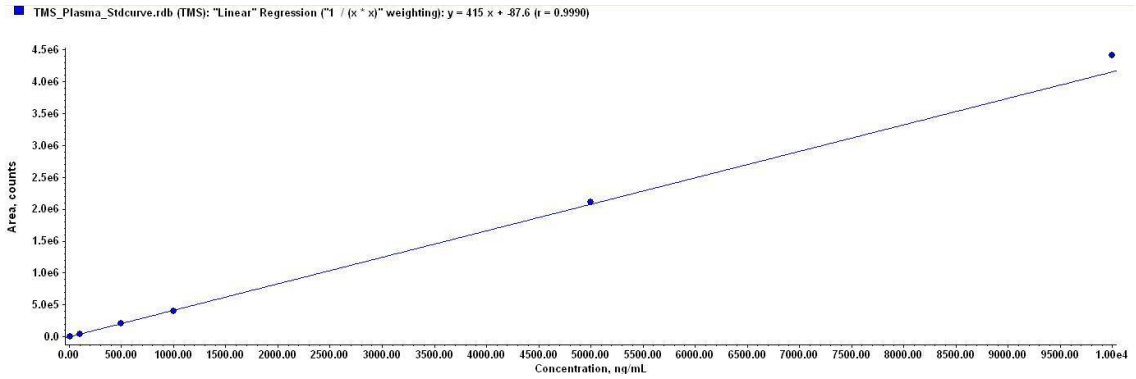

Fig 7.3: Representative calibration curve of TMS in plasma. Substrate concentration range from 10 – 10000 ng/ml, using a weighting factor of $1/X^2$.

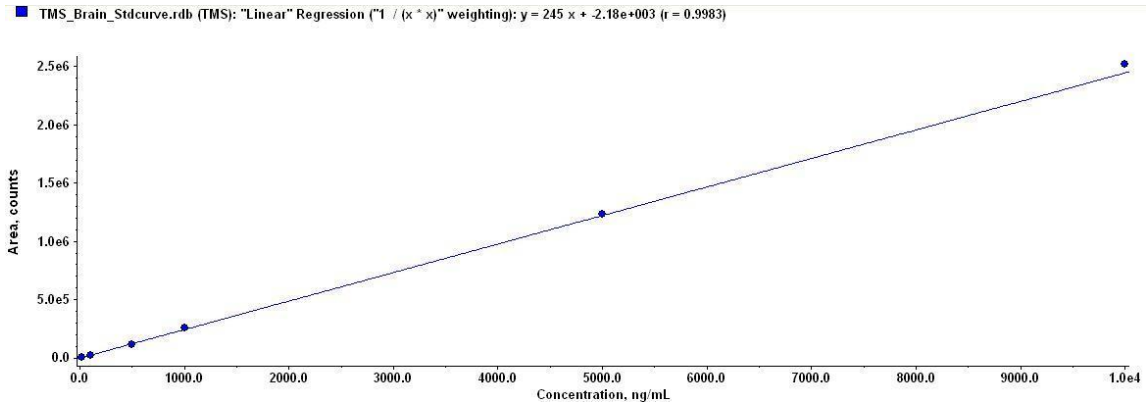

Fig 7.4: Representative calibration curve of TMS in brain homogenate. Substrate concentration range from 20 – 10000 ng/ml, using a weighting factor of $1/X^2$.

The results of intra-day and inter-day accuracy and precision are presented in Table 7.3 and 7.4 respectively. Intra- and inter-day precision for all analytes was less than 15%. The results indicate that the precision and accuracy of this method were adequate for bioanalytical purposes. The recovery and matrix effect of TMS in plasma and brain are presented in Table 7.5. The extraction efficiency of TMS in plasma and brain at different QC concentrations ranged from 70.34 to 83.42 % and 63.70 to 61.69 % respectively. There was no matrix effect observed for plasma samples (97.23 to 101.82 %). For brain samples a matrix effect were observed (81.70 to 73.87 %).

Table 7.3: Inter-day precision and accuracy for TMS in plasma and brain matrix.

Biological Matrix	**Nominal Concentration (ng/ml)**	**Inter-day validation**		
		Mean observed concentration (ng/ml)	**Precision (RSD)**	**Accuracy (% Bias)**
Plasma	10,000	9815.67	5.53	-1.84
	1,000	1002.98	5.47	0.30
	30	30.10	7.40	0.33
Brain	10,000	9210.17	5.65	-7.90
	1,000	951.45	3.70	-4.86
	60	57.30	9.07	-4.50

Table 7.4: Intra-day precision and accuracy for TMS in plasma and brain matrix.

Biological Matrix	Nominal Concentration (ng/ml)	Intra-day validation		
		Mean observed concentration (ng/ml)	Precision (RSD)	Accuracy (% Bias)
Plasma	10,000	10245.00	10.12	2.45
	1,000	919.00	9.77	-8.10
	30	32.72	3.98	9.07
Brain	10,000	8743.33	6.52	-12.57
	1,000	910.50	8.79	-8.95
	60	54.00	5.82	-10.00

Table 7.5: Matrix effect and recovery for TMS in plasma and brain matrix.

TMS	Plasma		Brain	
Concentrations	**Recovery**	**Matrix Effect**	**Recovery**	**Matrix Effect**
Low (30 and 60 ng/ml for plasma and brain respectively)	70.34 ± 5.96	97.23 ± 7.74	63.70 ± 6.34	81.70 ± 4.98
Medium (1,000 ng/ml for both)	70.65 ± 11.99	97.98 ± 14.42	59.52 ± 4.79	74.61 ± 13.40
High (10,000 ng/ml for both)	83.42 ± 8.94	101.82 ± 19.50	61.69 ± 7.05	73.87 ± 14.50

7.5. Discussion and conclusion:

Although there are reports of analytical methods for the quantitation of TMS in plasma (Ma et al., 2007; Lin and Ho, 2009), this is the first analytical method with the use of tandem mass spectrometry to quantitate TMS levels in plasma and brain. This analytical method suffers from the limitation of not having an internal standard. Although the method was devoid of an internal standard, it passed all the validation tests with reasonable accuracy and precision. Efforts were made to find a suitable robust internal standard. But we failed to find a suitable internal standard in a reasonable time frame. It has been shown recently that the internal standard can sometime interfere with the signal of analyte or vice versa via cross-talk or due to competition for ionization (Liang et al., 2003; Sojo et al., 2003). Ideally an isotope labeled TMS would have worked as a good internal standard. But its availability and cost were limitations for our study. Even without an internal standard the analytical method was robust, with accuracy and precision well within 15% limit at all QC concentrations. In brain samples a matrix effect was observed, which can be partly due the fact that brain tissue contains more lipid components than those found in plasma samples and can significantly suppress the ESI response of the analyte (Korfmacher, 2009).

In conclusion the method validation results demonstrate that the analytical method is robust and is consistent with good accuracy and reproducibility despite the absence of the internal standard.

CHAPTER 8

PHARMACOKINETICS AND BRAIN PERMEABILITY OF 3, 4', 5 TRIMETHOXY TRANS STILBENE (TMS) IN A MOUSE MODEL

8.1. Rationale

Due to the low systemic bioavailability of RES there is a need to test analogues of RES which have better plasma profile and which are at least equally potent to RES. Trimethoxy stilbene (TMS) is one of the analogs of RES where hydroxyl groups of RES are substituted by methoxy groups and has been reported to be of similar or more potency than RES (Matsuda et al., 2004; Belleri et al., 2005; Bader et al., 2008; Pan et al., 2008). It has also the advantage of its hydroxyl groups being protected by methoxy groups which might lead to decreased metabolism and enhanced exposure compared to RES. Its physicochemical properties are also favorable to cross the blood brain barrier (BBB). It satisfies the Lipinski's rule of five (Lipinski et al., 2001). Lipinski's rule of five predicts that molecules with less than 5 hydrogen bond donors, 10 hydrogen bond acceptors, a molecular weight less than 500 and a calculated log P of less than 5 are more likely to have good permeability. It has been observed that the molecules with a molecular weight below 400 are more favorable to cross BBB (Gleeson, 2008). TMS has a molecular weight of 270.32 which makes it a favorable candidate to cross the BBB. It has only three hydrogen bond acceptors and no hydrogen bond donors. Its logP value is 3.85 compared to 3.06 of RES (ACDlabs 12.0 software). It has been shown that with an increase in lipophilicity (up to a certain limit) there is increase in the permeation through BBB (Lanevskij et al., 2009). The polar surface area (tPSA) value of TMS is 27.69

(ACDlabs 12.0 software). Polar surface area is defined as the sum of surfaces of polar atoms in a molecule. PSA shows good correlation with passive molecular transport through membranes and therefore allows the prediction of passive transport properties of drugs (Ertl et al., 2000). It has been reported that a lower tPSA leads to enhanced BBB penetration (Gleeson, 2008).

RES at lower doses (40 mg/kg/day) exerts significant antitumor effects on subcutaneous (s.c.) glioma tumors, evidenced by slower tumor growth rate, longer survival time and higher survival rate in a rat model. It has been shown that RES at a higher dose (100 mg/kg/day) prolongs the survival time without improving the survival rate in rats bearing intracranial glioma tumors (Tseng et al., 2004). The enhanced survival of animals with intracranially implanted glioma tumors at higher dose compared to s.c. implanted tumor may be due to decreased permeability of RES in brain due to the restrictions at BBB or efflux by transporters at the BBB. For these reasons there is a need to test the better analogues of RES which are more potent, have better physicochemical properties for permeation through BBB and have a better exposure in body compared to RES.

TMS is one of the potent analogues of RES (Bader et al., 2008; Pan et al., 2008; Wang et al., 2010) with better exposure compared to RES (Lin and Ho, 2011; Sharan et al., 2012) and better physicochemical properties. TMS, if proved to have good brain permeability, can be explored as a therapeutic agent for treatment of glioma, as well as for various indications, e.g. Alzheimer's disease (Albani et al., 2010) where RES has shown positive biological activity.

The objective of this study is to characterize the pharmacokinetics of TMS and to measure the brain permeability of TMS in a mouse model.

8.2. Materials and methods:

8.2.1. Solubilization of TMS: 100 mg of TMS was suspended in 20 ml of 0.3 M 2-hydroxypropyl-β-cyclodextrin (HP-β-CD) solution prepared with isotonic saline. The resultant suspension was sonicated for 1 hour and then shaken on horizontal rotary shaker for 1 day. Finally the supension was filtered through a 0.22 um syringe-driven filter. The solution was then diluted and analyzed on LC/MS/MS for TMS content with calibration standards made in DMSO (Lin et al., 2000).

8.2.2. Drug administration and blood sampling for PK study: A carotid artery cannula was used for systemic drug administration and blood sampling. The details of surgical procedure have been mentioned in chapter 3 (section 3.2.2). Heparin-saline (20 uL, 50 IU/ml) was used to flush the cannula after systemic administration or blood sampling. TMS was administered at a dose of 5 mg/kg (i.a). Blood (20 uL) was serially sampled at 2.5, 5, 10, 15, 45, 90, 180, 300, 420 and 600 min. Blood samples were centrifuged at 14,000 rpm for 2 min, the harvested plasma was collected and stored at -80 °C until LC-MS/MS analysis

8.2.3. Study design for achieving steady state TMS concentration in blood and brain: A steady state plasma concentration of around 100 fold higher than the lowest level of quantitation of the analytical method was desired. This targeted concentration

would be approximately 1 ug/ml. Even after assuming the brain penetration to be 1/10th that of plasma, we assumed that we would be able to detect and quantitate brain TMS levels on MS/MS. A comprehensive PK study was performed to delineate the PK parameters for selection of the appropriate TMS dose regimen for achieving steady state in plasma. First, a single dose pharmacokinetic study was conducted by administering 5 mg/kg of TMS by i.a. route to 4 animals. A 2 compartment model was fitted to the average plasma profile of mice (n = 4) administered with 5 mg/kg TMS (i.a.). The resultant PK parameter estimates were used in an i.a. bolus/i.v. infusion model for simulation to design the dosage regimen for achieving steady state of TMS in plasma. A dose of 5 mg/kg i.a. bolus loading dose and 5 mg/kg i.v. infusion dose (6.25 uL/min infusion rate of 0.5 mg/ml TMS for 25 g mouse) was selected based on simulations with SAAMII software using compartmental PK parameters (Table 8.2) obtained from the 5 mg/kg (i.a.) TMS study. To ensure that TMS achieved the predicted plasma concentration during the study time (40 min), blood was withdrawn from carotid artery cannula at 5, 10, 20, 25, 30, 35 and 40 min. Blood samples were centrifuged at 14,000 rpm for 2 min, the harvested plasma was collected and stored at -80 °C until LC-MS/MS analysis. Forty minutes after the start of infusion, animals were slightly anesthetized by isoflurane and euthanized using cervical dislocation. Blood was collected by cardiac puncture. After draining the blood from animals, they were decapitated and brain was excised. Brain was washed with saline and stored at – 80° C until analysis.

8.2.4. Plasma and brain protein binding assay: Plasma protein binding assay was performed at TMS concentrations of 1, 5 and 20 uM as explained in section 3.2.4 of this thesis. For the brain protein binding assay equilibrium dialysis was performed using a 96-well equilibrium dialysis apparatus with molecular weight cutoff of 5000 (Harvard Apparatus, Holliston, MA) placed in a 37° C incubator with a 10% CO_2 atmospheric environment. Mouse brain tissue was diluted with 5 volumes of Dulbecco's phosphate-buffered saline (DPBS, pH 7.4, 0.2 g brain and 1 ml of buffer) and homogenized via ultrasonic probe. TMS was added to brain homogenate to achieve a final concentration of 1, 5 and 20 uM, and 200 µL aliquots (n = 3) were added to the 96-well dialysis plate and dialyzed against an equal volume of DPBS buffer. The plate was then placed in the rotator inside the incubator and allowed to dialyze for 22 h. Following 22 h of dialysis, 25 µL of buffer and brain homogenate were removed from each side of dialysis plate and mixed with 25 µL of the opposite matrix in a 96-deep well plate. Samples were then stored at -20 °C until analysis. Samples were analyzed as reported in chapter 7 except that the standard and QCs were prepared in plasma diluted with an equal volume of buffer (Maurer et al., 2005; Kalvass et al., 2007; Kochansky et al., 2008). The fraction unbound (fu) value in diluted brain tissue was calculated as:

$$fu_{meas} = 1 - [(PC - PF)/PC] \qquad \text{Equation 8.1}$$

where, fm_{meas} = fraction unbound using diluted brain tissue

PC = test compound concentration in protein-containing compartment

PF = test compound concentration in protein-free compartment

Since the brain was diluted during homogenization, equation 8.2 was used to calculate the brain undiluted fu value (Kalvass et al., 2007):

$fu_{brain} = (1/D)/[(1/fu_{meas}) – 1) + 1/D]$ Equation 8.2

where, fu_{brain} = fraction unbound in brain

D = dilution factor of brain tissue

Initial attempts were also made to detect and characterize the metabolites of TMS. This has been attached in the appendix.

8.3. Results:

8.3.1. Pharmacokinetics of TMS: PK study was performed in four mice (Fig 8.1) and non-compartmental analysis was carried out with Kinetica 5.0 (build 5.0.11, kinetic west palm beach, Florida USA) software. Results are tabulated in Table 8.1. The plasma concentration of TMS showed a biexponential decline indicating a rapid distribution phase followed by an elimination phase. TMS showed a moderate clearance and high volume of distribution. The average TMS plasma concentration was fitted to a two compartment model with first order elimination (Fig 8.2). From this we obtained PK estimates, i.e. volume of the central compartment and inter-compartment micro rate constants to use in an i.a. bolus/i.v. infusion model for simulation in order to design the dosage regimen for achieving a steady state concentration of TMS in plasma. A dose of 5 mg/kg i.a. bolus and 5 mg/kg i.v. infusion was selected based on simulations by SAAMII software using compartmental PK parameters of TMS. The observed TMS concentration in i.a./i.v. infusion study was comparable to the simulated plasma concentration (Fig 8.3) and achieved steady state around 30 – 40 minutes. The clearance estimates obtained after compartmental analysis of pooled data were found to be comparable with those obtained from individual data by the noncompartmental approach (Tables 8.1 and 8.2).

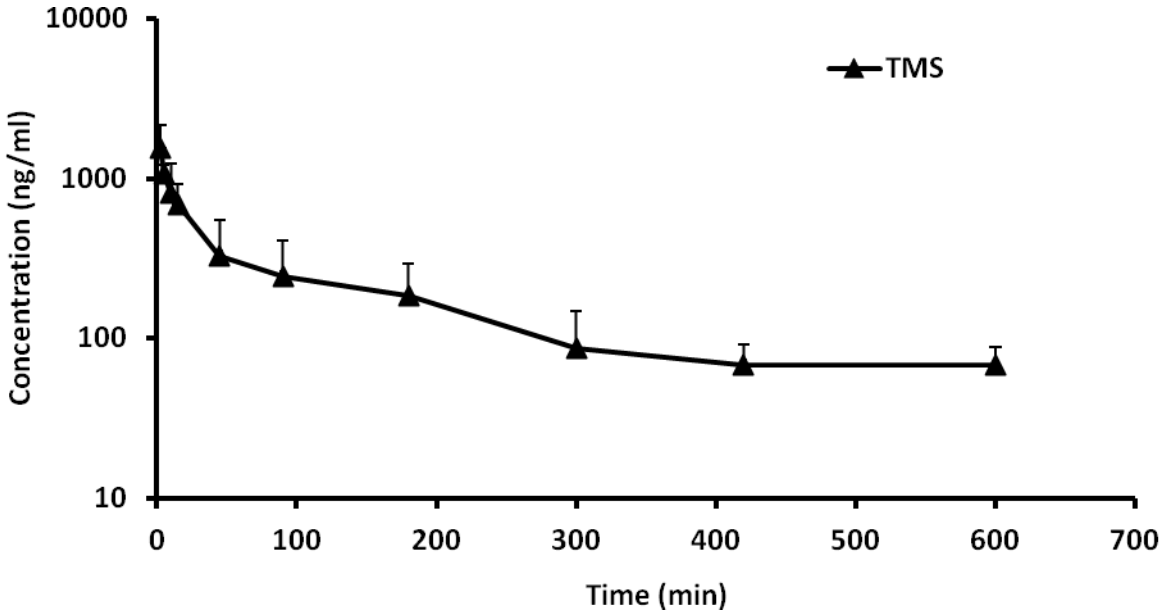

Fig 8.1: Pharmacokinetic profile of TMS in C57BL/6 mice after i.a. administration of TMS at the dose of 5 mg/kg. Closed triangles represent mean values while error represent SD (n = 4).

Table 8.1: Plasma pharmacokinetic paramaters calculated by noncompartmental analysis after administration of 5 mg/kg of TMS (i.a.). Data are expressed as Mean ± SD, (n = 4).

	5 mg/kg (i.a.)	**Units**
AUC_{0-t}	97.24 ± 30.21	**(min)*(ug/ml)**
AUC_{0-inf}	118.22 ± 25.34	**(min)*(ug/ml)**
Cl	43.65 ± 8.47	**ml/min/kg**
Vss	14.21 ± 5.48	**L/kg**
$t_{1/2}$	215.76 ± 78.29	**min**
Cmax	1.56 ± 0.60	**ug/ml**
MRT	318.08 ± 101.43	**min**

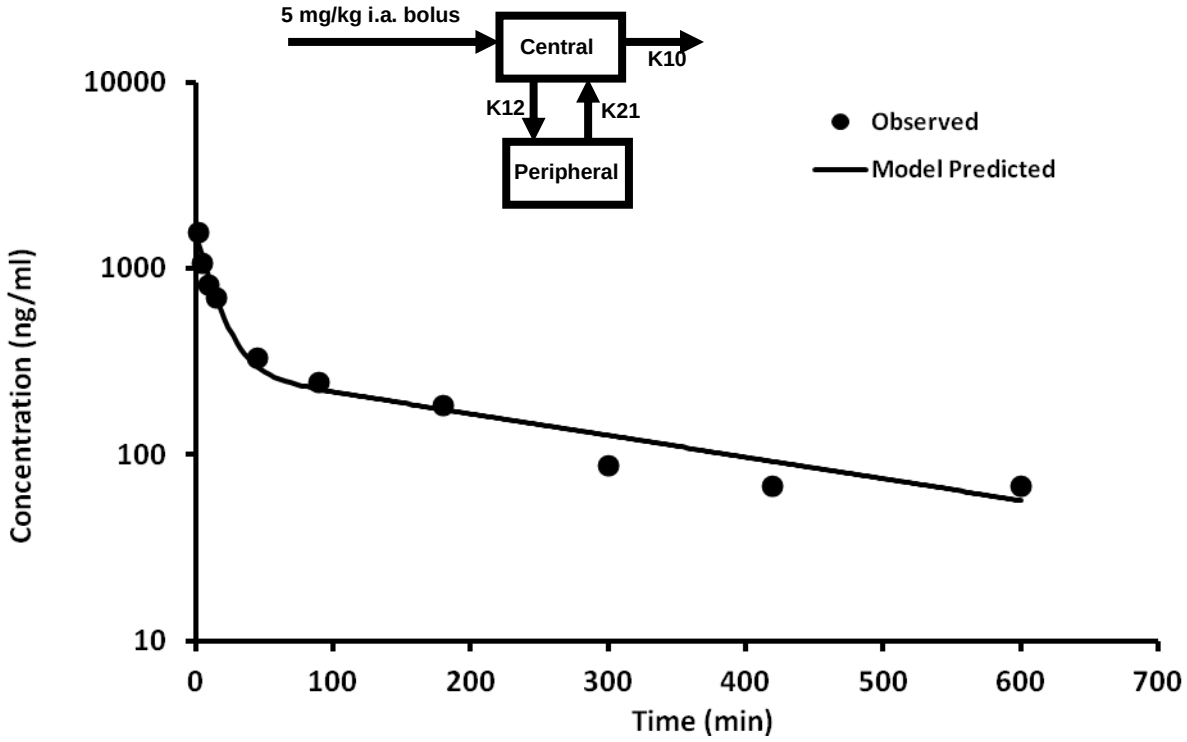

Fig 8.2: Observed average (n =4) TMS concentration (data points) and two compartment model predicted (solid line) TMS concentration-time profiles after TMS (5mg/kg i.a. bolus) administration.

Table 8.2: Plasma pharmacokinetic parameters calculated for average plasma concentration (n = 4) by compartmental analysis after administration of a 5 mg/kg dose of TMS by i.a. route.

Parameter	Value	SD	CV (%)
Vc (L/kg)	3.162	0.298	9.42
k10 (min^{-1})	0.013	0.001	10.32
k21 (min^{-1})	0.016	0.003	16.14
k12 (min^{-1})	0.049	0.010	20.77
Cl (ml/min/kg)	40.64	1.65	4.06

8.3.2. Brain permeability of TMS: Brain permeability of TMS was calculated by two approaches. In the first approach the brain permeability of TMS at steady state was determined by comparing brain concentration of TMS with plasma concentration of TMS obtained by arterial sampling at 40 min (Table 8.3). In second approach TMS brain permeability was calculated by comparing brain concentration of TMS with plasma concentration of TMS in blood obtained by cardiac puncture (Table 8.3). The total brain to total plasma concentration ratio of TMS at steady state by arterial sampling approach and cardiac puncture approach was found to be 4.82 ± 1.66 and 12.73 ± 1.74 respectively.

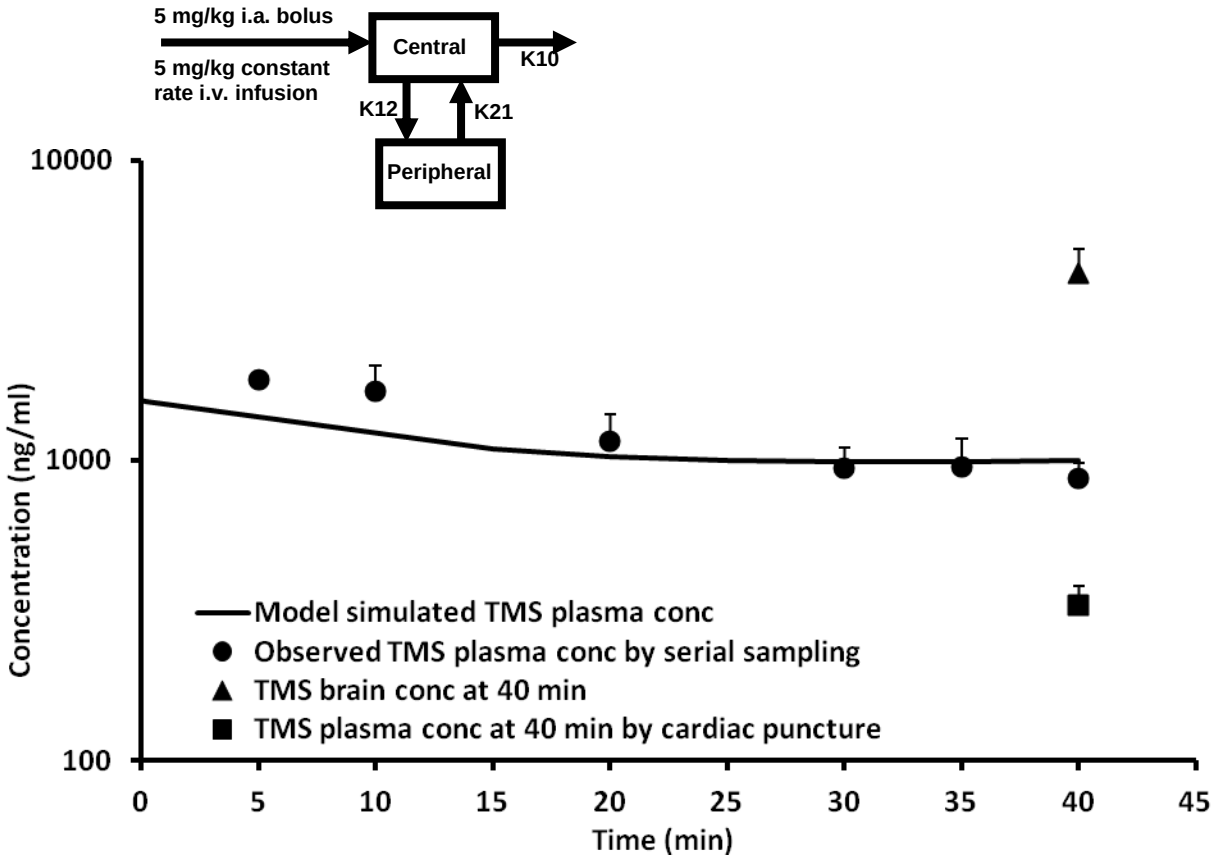

Fig 8.3: Pharmacokinetic profile of TMS in plasma and brain in a steady state infusion study. The solid line represents predicted TMS plasma concentrations after administration of 5 mg/kg i.a. bolus/5 mg/kg i.v. infusion. Solid circles represent observed mean TMS plasma concentration by serial sampling approach, solid triangle represents mean total concentration of TMS in brain at 40 min and solid square represent average total plasma concentration of TMS in blood obtained by cardiac puncture at 40 min. Symbols represents mean values while error represent SD (n = 4).

Table 8.3: Plasma and brain concentration of TMS at 40 min. Values are reported as means ± SD (n = 4).

Steady-state concentration	TMS (ng/ml)
Brain	4194.00 ± 853.37
Plasma (serial sampling)	870.75 ± 109.75
Plasma (cardiac puncture)	329.50 ± 46.59
Brain/Plasma ratio (serial sampling)	4.82 ± 1.66
Brain/Plasma ratio (cardiac puncture)	12.73 ± 1.74

8.3.3. Plasma and brain protein binding assay: There was no quantifiable TMS concentration on the buffer side of the wells of equilibrium dialysis plate for either the plasma or brain protein binding assay. Even at higher TMS concentration of 20 uM TMS was not observed on the buffer side. Due to limited aqueous solubility and possible non-specific binding to equilibrium dialysis membrane and plate, calculation of plasma and brain protein binding of TMS was not possible. It has been earlier reported that TMS was not detectable in aqueous filtrate in the absence of cyclodextrin (< 10 ng/ml) (Lin and Ho, 2011). Another widely used method for measuring protein binding of drug is the ultrafiltration method. This method has been shown to have even higher non specific binding (Zhirkov YuA and Piotrovskii, 1984) and so was not pursued.

8.4. Discussion and conclusion: RES has shown limited activity in intracranial glioma tumor compared to subcutaneous glioma tumor, possibly due to its limited brain permeability (Tseng et al., 2004). For a drug to be effective in indications related to the brain, apart from having good potency it should also possess good brain penetration. TMS is a naturally occurring analog of RES (Blair et al., 1969; MacRae and Towers, 1985). It has shown anti-invasive and anti-angiogenic activities (Belleri et al., 2005; Yang et al., 2009; Alex et al., 2010; Weng et al., 2010). Based on TMS physicochemical properties we hypothesized that it might have good brain permeability. To the best of our knowledge, this is the first study about brain permeability of TMS. In this study we additionally observed the effect of blood collection by two approaches and their impact on the calculation of brain to plasma ratio.

Recently detailed pharmacokinetics of TMS has been published (Lin and Ho, 2011). The systemic clearance of TMS observed in the present study (43.65 ± 8.47 ml/min/kg; Table 8.1) was comparable to that reported in rats (35.5 ± 5.3 ml/min/kg) by Lin and Ho (Lin and Ho, 2011). Its clearance was found to be less than half of RES (Sharan et al., 2012). The better PK profile of TMS has been attributed to methoxylation of the hydroxyl groups, which hinders conjugation as compared to extensive phase II conjugation of RES (Meng et al., 2004; Walle et al., 2004; Sharan et al., 2012).

Brain to plasma ratio, a measure of partitioning of the drug between the brain tissue and the blood compartment is commonly used for substrate exposure in brain (Hattori et al., 2004; Zheng et al., 2006; Ogino et al., 2008; Padowski and Pollack, 2012; Sane et al., 2012; Wang et al., 2012b). In these studies the total plasma drug concentration which is equal to bound plus unbound drug concentrations in blood samples and in the entire brain are measured and used to calculate the brain/plasma ratio. Brain to plasma ratio has been calculated either as the ratio of areas under the concentration-time curve (AUC) in brain versus plasma or at steady state. For practical reasons, the C_{brain}/C_{plasma} ratio under nonequilibrium conditions often is also used as a surrogate for the true substrate partitioning. In our study we calculated brain to plasma ratio at steady state. It has been suggested that using free drug concentration in the brain is a better strategy (Smith et al., 2010). Data from equilibrium dialysis between brain homogenate and buffer can be used to calculate free drug concentration in the brain (Smith et al., 2010). However due to non availability of the fraction unbound in brain data we were not able to calculate the free fraction of TMS in brain. This is an obvious limitation of this study.

We additionally observed that different methods of blood sample collection (serial sampling versus cardiac puncture) resulted in differences in the observed drug concentration in plasma and therefore different brain to plasma ratios. Site-dependent differences in drug levels have been previously discussed by Chiou (Chiou, 1989). There are reports showing that different blood sampling techniques can lead to differences in the observed plasma drug concentrations (Angus et al., 2008). It was observed that when CO_2 was used for the euthanasia as compared to cardiac puncture or serial sampling,

higher blood concentrations of drugs were found in blood for basic drugs due to possible acidification of the blood by CO_2 (Angus et al., 2008). This is not applicable to our study as we have used cervical dislocation for euthanasia. One other possible explanation can be that sampling by cardiac puncture technique sometime leads to hemolysis and can possibly dilute the plasma concentration. The exact cause for lower TMS concentration in cardiac puncture approach as compared to serial sampling is not clear. In our opinion blood drawn by serial sampling provided a better and reliable estimate because it correlated well with the model simulated plasma concentration based on our single dose PK study and has been used for calculation of brain to plasma ratio (Fig 8.3).

We observed that TMS concentration in mouse brain was 4.82 ± 1.66 fold higher than plasma at steady state. We understand that in the absence of free brain concentration data, there is a possibility of overpredicting brain to plasma ratio due to nonspecific binding to lipids and proteins in the brain. However there are reports of correlation between brain/plasma ratios and *in vivo* efficacy in neuropathic pain models (Zheng et al., 2006). Due to significantly higher brain concentrations of TMS, its favorable PK and its previously reported anti-cancer and anti-angiogenic activities, TMS can be considered a promising candidate for further evaluation for treatment of brain tumors.

In conclusion, we confirmed our hypothesis based on *in-silico* predictions that TMS will have better brain permeability. It should be further explored for indications related to the brain where RES has also shown positive biological activity. We also observed differences in the plasma concentration and over prediction of TMS brain to plasma ratio based on plasma TMS levels obtained by the cardiac puncture technique.

CHAPTER 9

CONCLUSIONS

The summary of our studies with the overall goal to better understand the complicated pharmacokinetics of RES, its conjugated metabolites and its trimethoxy analog TMS, has been presented below.

To be able to characterize the metabolites kinetics a validated bioanalytical method to directly quantify the metabolites was needed. A bioanalytical method on LC-MS/MS for direct quantitation of RES and its monoconjugates was developed and validated. This work has been published in combination with a report of the synthesis of the metabolites - *"Analytical method development for synthesized conjugated metabolites of trans-resveratrol, and application to pharmacokinetic studies, Journal of Pharmaceutical and Biomedical Analysis, 63 (1-8) 2012."*

The lung as a clearance organ for RES was evaluated by administering RES by both intravenous (i.v., before the lung) and intra-arterial (i.a., after the lung) and sampling by i.a. route to delineate the contribution of lung in the metabolism of RES. We found a significant increase in the AUC exposure of R3G after i.v. administration as compared to i.a. administration of RES. These findings were further corroborated by performing *in vitro* studies with mouse and human lung fractions. We found extensive glucuronidation and sulfation in mouse lung fractions. The *in vitro* experiments using human lung fractions showed mainly sulfation of RES. In conclusion, we found the lung to be a major

organ contributing to the metabolism of RES, with large inter-species differences in pulmonary RES conjugation. *This work has been submitted for peer review to Drug Metabolism and Disposition.*

The ability of conjugated metabolites of RES to be deconjugated to 'recycle' and provide RES systemically was evaluated. For this *in vivo* pharmacokinetic study were carried out where synthesized and purified RES sulfated and glucuronidated metabolites were administered to mice. Interestingly, we did not find significant RES in the systemic circulation after resveratrol-3-sulfate (R3S), resveratrol-4'-sulfate (R4'S) and resveratrol-3-glucuronide (R3G) administration to C57BL mice. Sulfated metabolites led to the formation of resveratrol-3-glucuronide (R3G), which is not possible without the intermediate formation of RES. *In vitro* studies were conducted using mouse and human liver microsomes. It was observed that R3S was rapidly desulfated in liver microsomes, presumably by steroid sulfatase enzymes. RES produced by desulfation in liver microsomes was rapidly glucuronidated to resveratrol-3-glucuronide (R3G). R3G is reported to be efficiently excreted into the bile by the ABC transporter Mrp-2. This efficient desulfation followed by glucuronidation and biliary elimination might explain the absence of RES in systemic circulation. When R3G was given orally it led to the formation of R3S. This indicates the possibility of R3G being deglucuronidated in the gut to give RES by the intestinal β-glucuronidases. It can be expected that RES formed from deconjugation in the gut can be sulfated or glucuronidated again to give R3G and R3S due to high extraction of RES during its passage across gut wall and liver. This might lead to levels of RES below our level of quantitation in the systemic circulation. *This*

work has been written up and is ready for submission for peer review to Drug Metabolism and Disposition.

The assumption that kinetics of preformed and *in vivo* formed metabolites are different, especially for more polar phase II metabolites, was evaluated. The metabolite kinetics of preformed and *in vivo* generated metabolites were compared by using modeling and simulation with two approaches: i) assuming similar PK of preformed versus *in vivo* formed metabolite, ii) assuming dissimilar PK of preformed versus *in vivo* formed metabolite. Simulations using the assumption that elimination clearances of preformed and *in vivo* formed metabolites are the same, led to a poor overlap of the observed and predicted *in vivo* formed R3S and R3G. Simulations using the assumption that elimination clearances of preformed and *in vivo* formed metabolites are different, led to improved predictions. The second approach also gave a more realistic formation ratio of R3S and R3G as 0.52 and 0.48 respectively. Differences in metabolite kinetics of preformed and *in vivo* formed metabolites were clearly visible in our study. This work has been published - *"In vivo-Formed versus Preformed Metabolite Kinetics of trans-Resveratrol-3-sulfate and trans-Resveratrol-3-glucuronide, Drug Metabolism and Disposition, 40 (1993-2001) 2012."*

The brain permeability of TMS was evaluated. For this we first needed a validated bioanalytical method for quantification of TMS in plasma and brain. We successfully developed a robust bioanalytical method to quantitate TMS in plasma and brain matrix. Our hypothesis, based on favorable TMS physicochemical properties (low molecular

weight, 270.32 and low polar surface area, tPSA 27.69), that it might have better brain permeability was found to be true. *This work has been written up and is ready for submission for peer review.*

In summary, the kinetics of metabolites of RES i.e. R3S, R4'S and R3G were studied for the first time by administering the preformed metabolites. This study not only increases the understanding of the PK of this polyphenol and its metabolites but might also be applicable to other polyphenols. Pulmonary metabolism of RES was also a novel finding of our study. Preformed and *in vivo* formed R3S and R3G kinetics were compared and a marked difference was observed between the preformed and *in vivo* formed metabolite kinetics. TMS, a trimethoxy analog of RES, was found to have good brain permeability.

Future Directions:

Traditionally, variability in the pharmacokinetics of drugs has been thought to be the outcome of how drugs are metabolized by our body. However, recent advances in the field of transporters have made it clear that behavior of drugs in the body includes an intricate interplay between drug metabolizing enzymes and drug transporters (Wacher et al., 1998; Schuetz and Schinkel, 1999; Tachibana et al., 2009). The need for better understanding of drug metabolizing enzyme-tranporter interplay is being increasingly realized to better understand and predict drug-drug interactions (DDIs) (Pang et al., 2009; Zhang et al., 2009). Since RES and its metabolites disposition has been intricately involved with transporters as well as metabolizing enzymes, they can be used as model

substrates to probe and advance our knowledge in the field of interplay of enzymes and transporters and their impact on processing of drugs and metabolites.

Based on our studies it is clear that RES and its sulfated metabolites are ultimately metabolized into R3G which is mostly eliminated by biliary excretion into the gut, where it gets deconjugated to give RES locally. So, tissue levels of RES and its metabolites should be investigated in the colon and rectum because of its relevance to colorectal cancer prevention.

TMS was shown to have better brain permeability and should be screened *in vitro* against various glioma cell lines, e.g. U87, and further *in vivo* pharmacodynamic studies can be performed if TMS is shown to be active *in vitro*.

BIBLIOGRAPHY

Aggarwal BB, Bhardwaj A, Aggarwal RS, Seeram NP, Shishodia S, and Takada Y (2004) Role of resveratrol in prevention and therapy of cancer: preclinical and clinical studies. *Anticancer Res* **24:**2783-2840.

Akaike H (1974) A new look at the statistical model identification. *Automatic Control, IEEE Transactions on* **19:**716-723.

Albani D, Polito L, Signorini A, and Forloni G (2010) Neuroprotective properties of resveratrol in different neurodegenerative disorders. *Biofactors* **36:**370-376.

Alex D, Leong EC, Zhang ZJ, Yan GT, Cheng SH, Leong CW, Li ZH, Lam KH, Chan SW, and Lee SM (2010) Resveratrol derivative, trans-3,5,4'-trimethoxystilbene, exerts antiangiogenic and vascular-disrupting effects in zebrafish through the downregulation of VEGFR2 and cell-cycle modulation. *J Cell Biochem* **109:**339-346.

Almeida L, Vaz-da-Silva M, Falcão A, Soares E, Costa R, Loureiro AI, Fernandes-Lopes C, Rocha JF, Nunes T, Wright L, and Soares-da-Silva P (2009) Pharmacokinetic and safety profile of trans-resveratrol in a rising multiple-dose study in healthy volunteers. *Mol Nutr Food Res* **53 Suppl 1:**S7-15.

Alnouti Y and Klaassen CD (2006) Tissue distribution and ontogeny of sulfotransferase enzymes in mice. *Toxicol Sci* **93:**242-255.

Andlauer W, Kolb J, Siebert K, and Fürst P (2000) Assessment of resveratrol bioavailability in the perfused small intestine of the rat. *Drugs Exp Clin Res* **26:**47-55.

Angus DW, Baker JA, Mason R, and Martin IJ (2008) The potential influence of CO2, as an agent for euthanasia, on the pharmacokinetics of basic compounds in rodents. *Drug Metab Dispos* **36:**375-379.

Araki E, Ishikawa M, Iigo M, Koide T, Itabashi M, and Hoshi A (1993) Relationship between development of diarrhea and the concentration of SN-38, an active metabolite of CPT-11, in the intestine and the blood plasma of athymic mice following intraperitoneal administration of CPT-11. *Jpn J Cancer Res* **84:**697-702.

Aumont V, Krisa S, Battaglia E, Netter P, Richard T, Mérillon JM, Magdalou J, and Sabolovic N (2001) Regioselective and stereospecific glucuronidation of trans- and cis-resveratrol in human. *Arch Biochem Biophys* **393:**281-289.

Aziz MH, Kumar R, and Ahmad N (2003) Cancer chemoprevention by resveratrol: *in vitro* and *in vivo* studies and the underlying mechanisms (review). *Int J Oncol* **23:**17-28.

Bader Y, Madlener S, Strasser S, Maier S, Saiko P, Stark N, Popescu R, Huber D, Gollinger M, Erker T, Handler N, Szakmary A, Jäger W, Kopp B, Tentes I,

Fritzer-Szekeres M, Krupitza G, and Szekeres T (2008) Stilbene analogues affect cell cycle progression and apoptosis independently of each other in an MCF-7 array of clones with distinct genetic and chemoresistant backgrounds. *Oncol Rep* **19:**801-810.

Baillie TA, Cayen MN, Fouda H, Gerson RJ, Green JD, Grossman SJ, Klunk LJ, LeBlanc B, Perkins DG, and Shipley LA (2002) Drug metabolites in safety testing. *Toxicol Appl Pharmacol* **182:**188-196.

Banerjee S, Bueso-Ramos C, and Aggarwal BB (2002) Suppression of 7,12-dimethylbenz(a)anthracene-induced mammary carcinogenesis in rats by resveratrol: role of nuclear factor-kappaB, cyclooxygenase 2, and matrix metalloprotease 9. *Cancer Res* **62:**4945-4954.

Baur JA and Sinclair DA (2006) Therapeutic potential of resveratrol: the *in vivo* evidence. *Nat Rev Drug Discov* **5:**493-506.

Belleri M, Ribatti D, Nicoli S, Cotelli F, Forti L, Vannini V, Stivala LA, and Presta M (2005) Antiangiogenic and vascular-targeting activity of the microtubule-destabilizing trans-resveratrol derivative 3,5,4'-trimethoxystilbene. *Mol Pharmacol* **67:**1451-1459.

Berezhkovskiy LM (2004) Volume of distribution at steady state for a linear pharmacokinetic system with peripheral elimination. *J Pharm Sci* **93:**1628-1640.

Birrell MA, McCluskie K, Wong S, Donnelly LE, Barnes PJ, and Belvisi MG (2005) Resveratrol, an extract of red wine, inhibits lipopolysaccharide induced airway neutrophilia and inflammatory mediators through an NF-kappaB-independent mechanism. *FASEB J* **19:**840-841.

Blair GE, Cassady JM, Robbers JE, Tyler VE, and Raffauf RF (1969) Isolation of 3,4′,5-trimethoxy-trans-stilbene, otobaene and hydroxyotobain from Virola cuspidata. **8:**497-500.

Boocock DJ, Faust GE, Patel KR, Schinas AM, Brown VA, Ducharme MP, Booth TD, Crowell JA, Perloff M, Gescher AJ, Steward WP, and Brenner DE (2007) Phase I dose escalation pharmacokinetic study in healthy volunteers of resveratrol, a potential cancer chemopreventive agent. *Cancer Epidemiol Biomarkers Prev* **16:**1246-1252.

Bosquillon C (2010) Drug transporters in the lung--do they play a role in the biopharmaceutics of inhaled drugs? *J Pharm Sci* **99:**2240-2255.

Brill SS, Furimsky AM, Ho MN, Furniss MJ, Li Y, Green AG, Bradford WW, Green CE, Kapetanovic IM, and Iyer LV (2006) Glucuronidation of trans-resveratrol by human liver and intestinal microsomes and UGT isoforms. *J Pharm Pharmacol* **58:**469-479.

Brown VA, Patel KR, Viskaduraki M, Crowell JA, Perloff M, Booth TD, Vasilinin G, Sen A, Schinas AM, Piccirilli G, Brown K, Steward WP, Gescher AJ, and Brenner DE (2010) Repeat dose study of the cancer chemopreventive agent resveratrol in healthy volunteers: safety, pharmacokinetics, and effect on the insulin-like growth factor axis. *Cancer Res* **70:**9003-9011.

Bråkenhielm E, Cao R, and Cao Y (2001) Suppression of angiogenesis, tumor growth, and wound healing by resveratrol, a natural compound in red wine and grapes. *FASEB J* **15:**1798-1800.

Buckley DB and Klaassen CD (2007) Tissue- and gender-specific mRNA expression of UDP-glucuronosyltransferases (UGTs) in mice. *Drug Metab Dispos* **35:**121-127.

Buiarelli F, Coccioli F, Jasionowska R, Merolle M, and Terracciano A (2007) Analysis of some stilbenes in Italian wines by liquid chromatography/tandem mass spectrometry. *Rapid Commun Mass Spectrom* **21:**2955-2964.

Calamini B, Ratia K, Malkowski MG, Cuendet M, Pezzuto JM, Santarsiero BD, and Mesecar AD (2010) Pleiotropic mechanisms facilitated by resveratrol and its metabolites. *Biochem J* **429:**273-282.

Cao Z and Li Y (2004) Potent induction of cellular antioxidants and phase 2 enzymes by resveratrol in cardiomyocytes: protection against oxidative and electrophilic injury. *Eur J Pharmacol* **489:**39-48.

Carbó N, Costelli P, Baccino FM, López-Soriano FJ, and Argilés JM (1999) Resveratrol, a natural product present in wine, decreases tumour growth in a rat tumour model. *Biochem Biophys Res Commun* **254:**739-743.

Cassidy MK and Houston JB (1980) *In vivo* assessment of extrahepatic conjugative metabolism in first pass effects using the model compound phenol. *J Pharm Pharmacol* **32:**57-59.

Cassidy MK and Houston JB (1984) *In vivo* capacity of hepatic and extrahepatic enzymes to conjugate phenol. *Drug Metab Dispos* **12:**619-624.

Center for Drug Evaluation and Research (U.S.) (2008) Guidance for industry safety testing of drug metabolites, pp 1 online resource (11 p.) chart., U.S. Dept. of Health and Human Services, Food and Drug Administration, Center for Drug Evaluation and Research,, Rockville, MD.

Chan WK and Delucchi AB (2000) Resveratrol, a red wine constituent, is a mechanism-based inactivator of cytochrome P450 3A4. *Life Sci* **67:**3103-3112.

Chang TK, Lee WB, and Ko HH (2000) Trans-resveratrol modulates the catalytic activity and mRNA expression of the procarcinogen-activating human cytochrome P450 1B1. *Can J Physiol Pharmacol* **78:**874-881.

Chiou WL (1989) The phenomenon and rationale of marked dependence of drug concentration on blood sampling site. Implications in pharmacokinetics, pharmacodynamics, toxicology and therapeutics (Part I). *Clin Pharmacokinet* **17:**175-199.

Ciolino HP, Daschner PJ, and Yeh GC (1998) Resveratrol inhibits transcription of CYP1A1 *in vitro* by preventing activation of the aryl hydrocarbon receptor. *Cancer Res* **58:**5707-5712.

Colburn WA (1982) Pharmacokinetic and biopharmaceutic parameters during enterohepatic circulation of drugs. *Journal of pharmaceutical sciences* **71:**131-133.

Colburn WA, Hirom PC, Parker RJ, and Milburn P (1979) A pharmacokinetic model for enterohepatic recirculation in the rat: phenolphthalein, a model drug. *Drug Metab Dispos* **7:**100-102.

Collins JM and Dedrick RL (1982) Contribution of lungs to total body clearance: linear and nonlinear effects. *J Pharm Sci* **71:**66-70.

Colom H, Alfaras I, Maijó M, Juan ME, and Planas JM (2011) Population pharmacokinetic modeling of trans-resveratrol and its glucuronide and sulfate conjugates after oral and intravenous administration in rats. *Pharm Res* **28:**1606-1621.

Csiszar A, Smith K, Labinskyy N, Orosz Z, Rivera A, and Ungvari Z (2006) Resveratrol attenuates TNF-alpha-induced activation of coronary arterial endothelial cells: role of NF-kappaB inhibition. *Am J Physiol Heart Circ Physiol* **291:**H1694-1699.

Culpitt SV, Rogers DF, Fenwick PS, Shah P, De Matos C, Russell RE, Barnes PJ, and Donnelly LE (2003) Inhibition by red wine extract, resveratrol, of cytokine release by alveolar macrophages in COPD. *Thorax* **58:**942-946.

Dahlström BE and Paalzow LK (1978) Pharmacokinetic interpretation of the enterohepatic recirculation and first-pass elimination of morphine in the rat. *J Pharmacokinet Biopharm* **6:**505-519.

Davies B and Morris T (1993) Physiological parameters in laboratory animals and humans. *Pharm Res* **10:**1093-1095.

Davis TM, Daly F, Walsh JP, Ilett KF, Beilby JP, Dusci LJ, and Barrett PH (2000) Pharmacokinetics and pharmacodynamics of gliclazide in Caucasians and Australian Aborigines with type 2 diabetes. *Br J Clin Pharmacol* **49:**223-230.

de la Lastra CA and Villegas I (2007) Resveratrol as an antioxidant and pro-oxidant agent: mechanisms and clinical implications. *Biochem Soc Trans* **35:**1156-1160.

De Santi C, Pietrabissa A, Spisni R, Mosca F, and Pacifici GM (2000) Sulphation of resveratrol, a natural product present in grapes and wine, in the human liver and duodenum. *Xenobiotica* **30:**609-617.

Deeley RG and Cole SP (2006) Substrate recognition and transport by multidrug resistance protein 1 (ABCC1). *FEBS Lett* **580:**1103-1111.

Demrow HS, Slane PR, and Folts JD (1995) Administration of wine and grape juice inhibits *in vivo* platelet activity and thrombosis in stenosed canine coronary arteries. *Circulation* **91:**1182-1188.

Ebling WF, Szefler SJ, and Jusko WJ (1985) Methylprednisolone disposition in rabbits. Analysis, prodrug conversion, reversible metabolism, and comparison with man. *Drug Metab Dispos* **13:**296-304.

Eisenhofer G, Coughtrie MW, and Goldstein DS (1999) Dopamine sulphate: an enigma resolved. *Clin Exp Pharmacol Physiol Suppl* **26:**S41-53.

Elmali N, Esenkaya I, Harma A, Ertem K, Turkoz Y, and Mizrak B (2005) Effect of resveratrol in experimental osteoarthritis in rabbits. *Inflamm Res* **54:**158-162.

Ertl P, Rohde B, and Selzer P (2000) Fast calculation of molecular polar surface area as a sum of fragment-based contributions and its application to the prediction of drug transport properties. *J Med Chem* **43:**3714-3717.

Fahrmayr C, Fromm MF, and König J (2010) Hepatic OATP and OCT uptake transporters: their role for drug-drug interactions and pharmacogenetic aspects. *Drug Metab Rev* **42:**380-401.

Fonseca-Kelly Z, Nassrallah M, Uribe J, Khan RS, Dine K, Dutt M, and Shindler KS (2012) Resveratrol neuroprotection in a chronic mouse model of multiple sclerosis. *Front Neurol* **3:**84.

Frankel EN, Kanner J, German JB, Parks E, and Kinsella JE (1993) Inhibition of oxidation of human low-density lipoprotein by phenolic substances in red wine. *Lancet* **341:**454-457.

Frederick CB and Obach RS (2010) Metabolites in safety testing: "MIST" for the clinical pharmacologist. *Clin Pharmacol Ther* **87:**345-350.

Fuhrman B, Lavy A, and Aviram M (1995) Consumption of red wine with meals reduces the susceptibility of human plasma and low-density lipoprotein to lipid peroxidation. *Am J Clin Nutr* **61:**549-554.

Gabrielsson J and Weiner D (2006) *Pharmacokinetic and pharmacodynamic data analysis: Concepts and Applications*.

Ghosh D (2007) Human sulfatases: a structural perspective to catalysis. *Cell Mol Life Sci* **64:**2013-2022.

Gleeson M (2008) Generation of a set of simple, interpretable ADMET rules of thumb. *J Med Chem* **51:**817-834.

Goldberg DM, Hahn SE, and Parkes JG (1995) Beyond alcohol: beverage consumption and cardiovascular mortality. *Clin Chim Acta* **237:**155-187.

Goldberg DM, Yan J, and Soleas GJ (2003) Absorption of three wine-related polyphenols in three different matrices by healthy subjects. *Clin Biochem* **36:**79-87.

Hasselström J and Säwe J (1993) Morphine pharmacokinetics and metabolism in humans. Enterohepatic cycling and relative contribution of metabolites to active opioid concentrations. *Clin Pharmacokinet* **24:**344-354.

Hastings KL, El-Hage J, Jacobs A, Leighton J, Morse D, and Osterberg RE (2003) Drug metabolites in safety testing. *Toxicol Appl Pharmacol* **190:**91-92;author reply 93-94.

Hattori K, Kido Y, Yamamoto H, Ishida J, Kamijo K, Murano K, Ohkubo M, Kinoshita T, Iwashita A, Mihara K, Yamazaki S, Matsuoka N, Teramura Y, and Miyake H (2004) Rational approaches to discovery of orally active and brain-penetrable quinazolinone inhibitors of poly(ADP-ribose)polymerase. *J Med Chem* **47:**4151-4154.

Hebbar V, Shen G, Hu R, Kim BR, Chen C, Korytko PJ, Crowell JA, Levine BS, and Kong AN (2005) Toxicogenomics of resveratrol in rat liver. *Life Sci* **76:**2299-2314.

Herman RJ, Van Pham JD, and Szakacs CB (1989) Disposition of lorazepam in human beings: enterohepatic recirculation and first-pass effect. *Clin Pharmacol Ther* **46:**18-25.

Hoshino J, Park EJ, Kondratyuk TP, Marler L, Pezzuto JM, van Breemen RB, Mo S, Li Y, and Cushman M (2010) Selective synthesis and biological evaluation of sulfate-conjugated resveratrol metabolites. *J Med Chem* **53:**5033-5043.

Houston JB (1981) Drug metabolite kinetics. *Pharmacology & Therapeutics* **15:**521-552.

Hutzler JM and Tracy TS (2002) Atypical kinetic profiles in drug metabolism reactions. *Drug Metab Dispos* **30:**355-362.

International Conference on Harmonisation (2009) Non-clinical safety studies for the conduct of human clinical trials for pharmaceuticals.

Iwuchukwu OF and Nagar S (2008) Resveratrol (trans-resveratrol, 3,5,4'-trihydroxy-trans-stilbene) glucuronidation exhibits atypical enzyme kinetics in various protein sources. *Drug Metab Dispos* **36:**322-330.

Iwuchukwu OF, Sharan S, Canney DJ, and Nagar S (2012) Analytical method development for synthesized conjugated metabolites of trans-resveratrol, and application to pharmacokinetic studies. *J Pharm Biomed Anal* **63:**1-8.

Jang M, Cai L, Udeani G, Slowing K, Thomas C, Beecher C, Fong H, Farnsworth N, Kinghorn A, Mehta R, Moon R, and Pezzuto J (1997a) Cancer chemopreventive activity of resveratrol, a natural product derived from grapes. *Science* **275:**218-220.

Jang M, Cai L, Udeani GO, Slowing KV, Thomas CF, Beecher CW, Fong HH, Farnsworth NR, Kinghorn AD, Mehta RG, Moon RC, and Pezzuto JM (1997b) Cancer chemopreventive activity of resveratrol, a natural product derived from grapes. *Science* **275:**218-220.

Jedlitschky G, Leier I, Buchholz U, Barnouin K, Kurz G, and Keppler D (1996) Transport of glutathione, glucuronate, and sulfate conjugates by the MRP gene-encoded conjugate export pump. *Cancer Res* **56:**988-994.

Juan ME, González-Pons E, and Planas JM (2010a) Multidrug resistance proteins restrain the intestinal absorption of trans-resveratrol in rats. *J Nutr* **140:**489-495.

Juan ME, Maijó M, and Planas JM (2010b) Quantification of trans-resveratrol and its metabolites in rat plasma and tissues by HPLC. *J Pharm Biomed Anal* **51:**391-398.

Kalvass JC, Maurer TS, and Pollack GM (2007) Use of plasma and brain unbound fractions to assess the extent of brain distribution of 34 drugs: comparison of unbound concentration ratios to *in vivo* p-glycoprotein efflux ratios. *Drug Metab Dispos* **35:**660-666.

Kang SS, Cuendet M, Endringer DC, Croy VL, Pezzuto JM, and Lipton MA (2009) Synthesis and biological evaluation of a library of resveratrol analogues as inhibitors of COX-1, COX-2 and NF-kappaB. *Bioorg Med Chem* **17:**1044-1054.

Kapetanovic IM, Muzzio M, Huang Z, Thompson TN, and McCormick DL (2011) Pharmacokinetics, oral bioavailability, and metabolic profile of resveratrol and its dimethylether analog, pterostilbene, in rats. *Cancer Chemother Pharmacol* **68:**593-601.

Kelder J, Grootenhuis PD, Bayada DM, Delbressine LP, and Ploemen JP (1999) Polar molecular surface as a dominating determinant for oral absorption and brain penetration of drugs. *Pharm Res* **16:**1514-1519.

Kennelly EJ, Gerhäuser C, Song LL, Graham JG, Beecher CWW, Pezzuto JM, and Kinghorn AD (1997) Induction of Quinone Reductase by Withanolides Isolated from Physalis philadelphica (Tomatillos). *Journal of Agricultural and Food Chemistry* **45:**3771-3777.

Kensler T, Guyton K, Egner P, McCarthy T, Lesko S, and Akman S (1995) Role of reactive intermediates in tumor promotion and progression. *Prog Clin Biol Res* **391:**103-116.

Khanduja KL, Bhardwaj A, and Kaushik G (2004) Resveratrol inhibits N-nitrosodiethylamine-induced ornithine decarboxylase and cyclooxygenase in mice. *J Nutr Sci Vitaminol (Tokyo)* **50:**61-65.

Kimura Y and Okuda H (2001) Resveratrol isolated from Polygonum cuspidatum root prevents tumor growth and metastasis to lung and tumor-induced neovascularization in Lewis lung carcinoma-bearing mice. *J Nutr* **131:**1844-1849.

Kochansky CJ, McMasters DR, Lu P, Koeplinger KA, Kerr HH, Shou M, and Korzekwa KR (2008) Impact of pH on plasma protein binding in equilibrium dialysis. *Mol Pharm* **5:**438-448.

Korfmacher WA (2009) Using Mass Spectrometry for Drug Metabolism Studies, pp 1 online resource (454 p.), CRC Press, Hoboken.

Korzekwa KR, Nagar S, Tucker J, Weiskircher EA, Bhoopathy S, and Hidalgo IJ (2012) Models to predict unbound intracellular drug concentrations in the presence of transporters. *Drug Metab Dispos* **40:**865-876.

Kroemer HK and Klotz U (1992) Glucuronidation of drugs. A re-evaluation of the pharmacological significance of the conjugates and modulating factors. *Clin Pharmacokinet* **23:**292-310.

Kuhnle G, Spencer JP, Chowrimootoo G, Schroeter H, Debnam ES, Srai SK, Rice-Evans C, and Hahn U (2000) Resveratrol is absorbed in the small intestine as resveratrol glucuronide. *Biochem Biophys Res Commun* **272:**212-217.

Lanevskij K, Japertas P, Didziapetris R, and Petrauskas A (2009) Ionization-specific prediction of blood-brain permeability. *J Pharm Sci* **98:**122-134.

Leslie EM, Ito K, Upadhyaya P, Hecht SS, Deeley RG, and Cole SP (2001) Transport of the beta -O-glucuronide conjugate of the tobacco-specific carcinogen 4-(methylnitrosamino)-1-(3-pyridyl)-1-butanol (NNAL) by the multidrug resistance protein 1 (MRP1). Requirement for glutathione or a non-sulfur-containing analog. *J Biol Chem* **276:**27846-27854.

Li L, Luo XJ, Liu YZ, Zhang YS, Yuan Q, Tan N, Xiang DX, and Peng J (2010) The role of the DDAH-ADMA pathway in the protective effect of resveratrol analog BTM-0512 on gastric mucosal injury. *Can J Physiol Pharmacol* **88:**562-567.

Li ZG, Hong T, Shimada Y, Komoto I, Kawabe A, Ding Y, Kaganoi J, Hashimoto Y, and Imamura M (2002) Suppression of N-nitrosomethylbenzylamine (NMBA)-

induced esophageal tumorigenesis in F344 rats by resveratrol. *Carcinogenesis* **23:**1531-1536.

Liang HR, Foltz RL, Meng M, and Bennett P (2003) Ionization enhancement in atmospheric pressure chemical ionization and suppression in electrospray ionization between target drugs and stable-isotope-labeled internal standards in quantitative liquid chromatography/tandem mass spectrometry. *Rapid Commun Mass Spectrom* **17:**2815-2821.

Lin H-S and Ho PC (2009) A rapid HPLC method for the quantification of 3,5,4'-trimethoxy-trans-stilbene (TMS) in rat plasma and its application in pharmacokinetic study. *Journal of Pharmaceutical and Biomedical Analysis* **49:**387-392.

Lin HS, Chan SY, Low KS, Shoon ML, and Ho PC (2000) Kinetic study of a 2-hydroxypropyl-beta-cyclodextrin-based formulation of all-trans-retinoic acid in Sprague-Dawley rats after oral or intravenous administration. *J Pharm Sci* **89:**260-267.

Lin HS and Ho PC (2011) Preclinical pharmacokinetic evaluation of resveratrol trimethyl ether in sprague-dawley rats: the impacts of aqueous solubility, dose escalation, food and repeated dosing on oral bioavailability. *J Pharm Sci*.

Lipinski CA (2004) Lead- and drug-like compounds: the rule-of-five revolution. *Drug Discovery Today: Technologies* **1:**337-341.

Lipinski CA, Lombardo F, Dominy BW, and Feeney PJ (2001) Experimental and computational approaches to estimate solubility and permeability in drug discovery and development settings. *Adv Drug Deliv Rev* **46:**3-26.

Lyons MM, Yu C, Toma RB, Cho SY, Reiboldt W, Lee J, and van Breemen RB (2003) Resveratrol in raw and baked blueberries and bilberries. *J Agric Food Chem* **51:**5867-5870.

López-Miranda V, Soto-Montenegro ML, Vera G, Herradón E, Desco M, and Abalo R (2012) [Resveratrol: a neuroprotective polyphenol in the Mediterranean diet]. *Rev Neurol* **54:**349-356.

Ma MK and McLeod HL (2003) Lessons learned from the irinotecan metabolic pathway. *Curr Med Chem* **10:**41-49.

Ma N, Liu W-Y, Li H-D, Jiang X-Y, Zhang B-K, Zhu R-H, Wang F, Liu W, Liu X, and Xiang D-X (2007) Determination of 3,5,4′-Trimethoxystilbene in Rat Plasma by LC with ESI-MS. *Chromatographia* **66:**251-255.

MacRae WD and Towers GHN (1985) Non-alkaloidal constituents of Virola elongata bark. **24:**561-566.

Magyar K, Halmosi R, Palfi A, Feher G, Czopf L, Fulop A, Battyany I, Sumegi B, Toth K, and Szabados E (2012) Cardioprotection by resveratrol: A human clinical trial in patients with stable coronary artery disease. *Clin Hemorheol Microcirc* **50:**179-187.

Maher JM, Slitt AL, Cherrington NJ, Cheng X, and Klaassen CD (2005) Tissue distribution and hepatic and renal ontogeny of the multidrug resistance-associated protein (Mrp) family in mice. *Drug Metab Dispos* **33:**947-955.

Maier-Salamon A, Hagenauer B, Reznicek G, Szekeres T, Thalhammer T, and Jäger W (2008) Metabolism and disposition of resveratrol in the isolated perfused rat liver: Role of Mrp2 in the biliary excretion of glucuronides. *Journal of Pharmaceutical Sciences* **97:**1615-1628.

Marambaud P, Zhao H, and Davies P (2005) Resveratrol promotes clearance of Alzheimer's disease amyloid-beta peptides. *J Biol Chem* **280:**37377-37382.

Marier J, Vachon P, Gritsas A, Zhang J, Moreau J, and Ducharme M (2002) Metabolism and disposition of resveratrol in rats: extent of absorption, glucuronidation, and enterohepatic recirculation evidenced by a linked-rat model. *J Pharmacol Exp Ther* **302:**369-373.

Matsuda H, Tewtrakul S, Morikawa T, and Yoshikawa M (2004) Anti-allergic activity of stilbenes from Korean rhubarb (Rheum undulatum L.): structure requirements for

inhibition of antigen-induced degranulation and their effects on the release of TNF-alpha and IL-4 in RBL-2H3 cells. *Bioorg Med Chem* **12:**4871-4876.

Maurer TS, Debartolo DB, Tess DA, and Scott DO (2005) Relationship between exposure and nonspecific binding of thirty-three central nervous system drugs in mice. *Drug Metab Dispos* **33:**175-181.

Meng X, Maliakal P, Lu H, Lee MJ, and Yang CS (2004) Urinary and plasma levels of resveratrol and quercetin in humans, mice, and rats after ingestion of pure compounds and grape juice. *J Agric Food Chem* **52:**935-942.

Michael M, Brittain M, Nagai J, Feld R, Hedley D, Oza A, Siu L, and Moore MJ (2004) Phase II study of activated charcoal to prevent irinotecan-induced diarrhea. *J Clin Oncol* **22:**4410-4417.

Miksits M, Maier-Salamon A, Aust S, Thalhammer T, Reznicek G, Kunert O, Haslinger E, Szekeres T, and Jaeger W (2005) Sulfation of resveratrol in human liver: evidence of a major role for the sulfotransferases SULT1A1 and SULT1E1. *Xenobiotica* **35:**1101-1119.

Milewich L, Garcia RL, and Gerrity LW (1984) Steroid sulfatase and 17 beta-hydroxysteroid oxidoreductase activities in mouse tissues. *J Steroid Biochem* **21:**529-538.

Milewich L, Garcia RL, and Johnson AR (1983) Steroid sulfatase activity in human lung tissue and in endothelial pulmonary cells in culture. *J Clin Endocrinol Metab* **57:**8-14.

Milne JC, Lambert PD, Schenk S, Carney DP, Smith JJ, Gagne DJ, Jin L, Boss O, Perni RB, Vu CB, Bemis JE, Xie R, Disch JS, Ng PY, Nunes JJ, Lynch AV, Yang H, Galonek H, Israelian K, Choy W, Iffland A, Lavu S, Medvedik O, Sinclair DA, Olefsky JM, Jirousek MR, Elliott PJ, and Westphal CH (2007) Small molecule activators of SIRT1 as therapeutics for the treatment of type 2 diabetes. *Nature* **450:**712-716.

Mistry M and Houston JB (1985) Quantitation of extrahepatic metabolism. Pulmonary and intestinal conjugation of naphthol. *Drug Metab Dispos* **13:**740-745.

Mollerup S, Ovrebø S, and Haugen A (2001) Lung carcinogenesis: resveratrol modulates the expression of genes involved in the metabolism of PAH in human bronchial epithelial cells. *Int J Cancer* **92:**18-25.

Moon YJ, Sagawa K, Frederick K, Zhang S, and Morris ME (2006) Pharmacokinetics and bioavailability of the isoflavone biochanin A in rats. *AAPS J* **8:**E433-442.

Mulder GJ, Weitering JG, Scholtens E, Dawson JR, and Pang KS (1984) Extrahepatic sulfation and glucuronidation in the rat *in vivo*. Determination of the hepatic

extraction ratio of harmol and the extrahepatic contribution to harmol conjugation. *Biochem Pharmacol* **33:**3081-3087.

Murias M, Handler N, Erker T, Pleban K, Ecker G, Saiko P, Szekeres T, and Jäger W (2004) Resveratrol analogues as selective cyclooxygenase-2 inhibitors: synthesis and structure-activity relationship. *Bioorg Med Chem* **12:**5571-5578.

Nakamura A, Nakajima M, Yamanaka H, Fujiwara R, and Yokoi T (2008) Expression of UGT1A and UGT2B mRNA in human normal tissues and various cell lines. *Drug Metab Dispos* **36:**1461-1464.

Norinder U and Haeberlein M (2002) Computational approaches to the prediction of the blood-brain distribution. *Adv Drug Deliv Rev* **54:**291-313.

Novakovic A, Gojkovic-Bukarica L, Peric M, Nezic D, Djukanovic B, Markovic-Lipkovski J, and Heinle H (2006) The mechanism of endothelium-independent relaxation induced by the wine polyphenol resveratrol in human internal mammary artery. *J Pharmacol Sci* **101:**85-90.

Nowell S, Green B, Tang YM, Wiese R, and Kadlubar FF (2005) Examination of human tissue cytosols for expression of sulfotransferase isoform 1A2 (SULT1A2) using a SULT1A2-specific antibody. *Mol Pharmacol* **67:**394-399.

Ogino Y, Ohtake N, Nagae Y, Matsuda K, Ishikawa M, Moriya M, Kanesaka M, Mitobe Y, Ito J, Kanno T, Ishihara A, Iwaasa H, Ohe T, Kanatani A, and Fukami T (2008) Syntheses and structure-activity relationships of novel, potent, and selective trans-2-[3-oxospiro[isobenzofuran-1(3H),1'-cyclohexan]-4'-yl]benzimidazole NPY Y5 receptor antagonists. *Bioorg Med Chem Lett* **18:**4997-5001.

Ogiso T, Iwaki M, Tanino T, Ikeda K, Paku T, Horibe Y, and Suzuki H (1998) Pharmacokinetics of aniracetam and its metabolites in rats. *J Pharm Sci* **87:**594-598.

Oguri T, Takahashi T, Miyazaki M, Isobe T, Kohno N, Mackenzie PI, and Fujiwara Y (2004) UGT1A10 is responsible for SN-38 glucuronidation and its expression in human lung cancers. *Anticancer Res* **24:**2893-2896.

Osborne R, Joel S, Trew D, and Slevin M (1988) Analgesic activity of morphine-6-glucuronide. *Lancet* **1:**828.

Oswald S, König J, Lütjohann D, Giessmann T, Kroemer HK, Rimmbach C, Rosskopf D, Fromm MF, and Siegmund W (2008) Disposition of ezetimibe is influenced by polymorphisms of the hepatic uptake carrier OATP1B1. *Pharmacogenet Genomics* **18:**559-568.

Ouellet DM and Pollack GM (1995) Biliary excretion and enterohepatic recirculation of morphine-3-glucuronide in rats. *Drug Metab Dispos* **23:**478-484.

Pace-Asciak CR, Hahn S, Diamandis EP, Soleas G, and Goldberg DM (1995) The red wine phenolics trans-resveratrol and quercetin block human platelet aggregation and eicosanoid synthesis: implications for protection against coronary heart disease. *Clin Chim Acta* **235:**207-219.

Padowski JM and Pollack GM (2012) Influence of enterohepatic recycling on the time course of brain-to-blood partitioning of valproic acid in rats. *Drug Metab Dispos* **40:**1846-1853.

Paigen K (1989) Mammalian beta-glucuronidase: genetics, molecular biology, and cell biology. *Prog Nucleic Acid Res Mol Biol* **37:**155-205.

Pan M, Gao J, Lai C, Wang Y, Chen W, Lo C, Wang M, Dushenkov S, and Ho C (2008) Antitumor activity of 3,5,4'-trimethoxystilbene in COLO 205 cells and xenografts in SCID mice. *Mol Carcinog* **47:**184-196.

Pang KS (1985) A review of metabolite kinetics. *J Pharmacokinet Biopharm* **13:**633-662.

Pang KS (2009) Safety testing of metabolites: Expectations and outcomes. *Chem Biol Interact* **179:**45-59.

Pang KS, Cherry WF, Terrell JA, and Ulm EH (1984) Disposition of enalapril and its diacid metabolite, enalaprilat, in a perfused rat liver preparation. Presence of a diffusional barrier for enalaprilat into hepatocytes. *Drug Metab Dispos* **12:**309-313.

Pang KS and Kwan KC (1983) A commentary: methods and assumptions in the kinetic estimation of metabolite formation. *Drug Metab Dispos* **11:**79-84.

Pang KS, Maeng HJ, and Fan J (2009) Interplay of transporters and enzymes in drug and metabolite processing. *Mol Pharm* **6:**1734-1755.

Pang KS, Morris ME, and Sun H (2008) Formed and preformed metabolites: facts and comparisons. *J Pharm Pharmacol* **60:**1247-1275.

Parenti G, Meroni G, and Ballabio A (1997) The sulfatase gene family. *Curr Opin Genet Dev* **7:**386-391.

Patwardhan RV, Johnson RF, Hoyumpa A, Sheehan JJ, Desmond PV, Wilkinson GR, Branch RA, and Schenker S (1981) Normal metabolism of morphine in cirrhosis. *Gastroenterology* **81:**1006-1011.

Pearson PG and Wienkers LC (2009) *Handbook of drug metabolism*. Informa Healthcare USA, New York.

Piver B, Berthou F, Dreano Y, and Lucas D (2001) Inhibition of CYP3A, CYP1A and CYP2E1 activities by resveratrol and other non volatile red wine components. *Toxicol Lett* **125:**83-91.

Prueksaritanont T, Lin JH, and Baillie TA (2006) Complicating factors in safety testing of drug metabolites: kinetic differences between generated and preformed metabolites. *Toxicol Appl Pharmacol* **217:**143-152.

Qian YM, Song WC, Cui H, Cole SP, and Deeley RG (2001) Glutathione stimulates sulfated estrogen transport by multidrug resistance protein 1. *J Biol Chem* **276:**6404-6411.

Qian YP, Cai YJ, Fan GJ, Wei QY, Yang J, Zheng LF, Li XZ, Fang JG, and Zhou B (2009) Antioxidant-based lead discovery for cancer chemoprevention: the case of resveratrol. *J Med Chem* **52:**1963-1974.

Rayalam S, Yang JY, Ambati S, Della-Fera MA, and Baile CA (2008) Resveratrol induces apoptosis and inhibits adipogenesis in 3T3-L1 adipocytes. *Phytother Res* **22:**1367-1371.

Renaud S and de Lorgeril M (1992) Wine, alcohol, platelets, and the French paradox for coronary heart disease. *Lancet* **339:**1523-1526.

Renaud S and Gueguen R (1998) The French paradox and wine drinking. *Novartis Found Symp* **216:**208-217; discussion 217-222, 152-208.

Riches Z, Stanley EL, Bloomer JC, and Coughtrie MW (2009) Quantitative evaluation of the expression and activity of five major sulfotransferases (SULTs) in human tissues: the SULT "pie". *Drug Metab Dispos* **37:**2255-2261.

Rivera H, Shibayama M, Tsutsumi V, Perez-Alvarez V, and Muriel P (2008) Resveratrol and trimethylated resveratrol protect from acute liver damage induced by CCl4 in the rat. *J Appl Toxicol* **28:**147-155.

Roberts MS, Magnusson BM, Burczynski FJ, and Weiss M (2002) Enterohepatic circulation: physiological, pharmacokinetic and clinical implications. *Clin Pharmacokinet* **41:**751-790.

Sabolovic N, Humbert AC, Radominska-Pandya A, and Magdalou J (2006) Resveratrol is efficiently glucuronidated by UDP-glucuronosyltransferases in the human gastrointestinal tract and in Caco-2 cells. *Biopharm Drug Dispos* **27:**181-189.

Sanders TH, McMichael RW, and Hendrix KW (2000) Occurrence of resveratrol in edible peanuts. *J Agric Food Chem* **48:**1243-1246.

Sane R, Agarwal S, and Elmquist WF (2012) Brain Distribution and Bioavailability of Elacridar after Different Routes of Administration in the Mouse. *Drug Metabolism and Disposition* **40:**1612-1619.

Scheffer GL, Pijnenborg AC, Smit EF, Müller M, Postma DS, Timens W, van der Valk P, de Vries EG, and Scheper RJ (2002) Multidrug resistance related molecules in human and murine lung. *J Clin Pathol* **55:**332-339.

Schuetz EG and Schinkel AH (1999) Drug disposition as determined by the interplay between drug-transporting and drug-metabolizing systems. *J Biochem Mol Toxicol* **13:**219-222.

Segel I (1993) *Enzyme Kinetics: Behavior and Analysis of Rapid Equilibrium and Steady-State Enzyme Systems*.

Shah VP, Midha KK, Findlay JW, Hill HM, Hulse JD, McGilveray IJ, McKay G, Miller KJ, Patnaik RN, Powell ML, Tonelli A, Viswanathan CT, and Yacobi A (2000) Bioanalytical method validation--a revisit with a decade of progress. *Pharm Res* **17:**1551-1557.

Sharan S, Iwuchukwu OF, Canney DJ, Zimmerman CL, and Nagar S (2012) *In vivo*-Formed versus Preformed Metabolite Kinetics of trans-Resveratrol-3-sulfate and trans-Resveratrol-3-glucuronide. *Drug Metab Dispos* **40:**1993-2001.

Simoni D, Roberti M, Invidiata FP, Aiello E, Aiello S, Marchetti P, Baruchello R, Eleopra M, Di Cristina A, Grimaudo S, Gebbia N, Crosta L, Dieli F, and Tolomeo M (2006) Stilbene-based anticancer agents: resveratrol analogues active toward HL60 leukemic cells with a non-specific phase mechanism. *Bioorg Med Chem Lett* **16:**3245-3248.

Smith DA, Di L, and Kerns EH (2010) The effect of plasma protein binding on *in vivo* efficacy: misconceptions in drug discovery. *Nat Rev Drug Discov* **9:**929-939.

Smith DA and Obach RS (2005) Seeing through the mist: abundance versus percentage. Commentary on metabolites in safety testing. *Drug Metab Dispos* **33:**1409-1417.

Sojo LE, Lum G, and Chee P (2003) Internal standard signal suppression by co-eluting analyte in isotope dilution LC-ESI-MS. *Analyst* **128:**51-54.

Somers GI, Lindsay N, Lowdon BM, Jones AE, Freathy C, Ho S, Woodrooffe AJ, Bayliss MK, and Manchee GR (2007) A comparison of the expression and metabolizing activities of phase I and II enzymes in freshly isolated human lung parenchymal cells and cryopreserved human hepatocytes. *Drug Metab Dispos* **35:**1797-1805.

Song LL, Kosmeder JW, Lee SK, Gerhäuser C, Lantvit D, Moon RC, Moriarty RM, and Pezzuto JM (1999) Cancer chemopreventive activity mediated by 4'-

bromoflavone, a potent inducer of phase II detoxification enzymes. *Cancer Res* **59:**578-585.

Sperker B, Backman JT, and Kroemer HK (1997) The role of beta-glucuronidase in drug disposition and drug targeting in humans. *Clin Pharmacokinet* **33:**18-31.

Stein C, Hille A, Seidel J, Rijnbout S, Waheed A, Schmidt B, Geuze H, and von Figura K (1989) Cloning and expression of human steroid-sulfatase. Membrane topology, glycosylation, and subcellular distribution in BHK-21 cells. *J Biol Chem* **264:**13865-13872.

Tachibana T, Kato M, Watanabe T, Mitsui T, and Sugiyama Y (2009) Method for predicting the risk of drug-drug interactions involving inhibition of intestinal CYP3A4 and P-glycoprotein. *Xenobiotica* **39:**430-443.

Takasuna K, Hagiwara T, Hirohashi M, Kato M, Nomura M, Nagai E, Yokoi T, and Kamataki T (1996) Involvement of beta-glucuronidase in intestinal microflora in the intestinal toxicity of the antitumor camptothecin derivative irinotecan hydrochloride (CPT-11) in rats. *Cancer Res* **56:**3752-3757.

Talalay P, Fahey JW, Holtzclaw WD, Prestera T, and Zhang Y (1995) Chemoprotection against cancer by phase 2 enzyme induction. *Toxicol Lett* **82-83:**173-179.

Tan E, Lu T, and Pang KS (2001) Futile cycling of estrone sulfate and estrone in the recirculating perfused rat liver preparation. *J Pharmacol Exp Ther* **297:**423-436.

Tessitore L, Davit A, Sarotto I, and Caderni G (2000) Resveratrol depresses the growth of colorectal aberrant crypt foci by affecting bax and p21(CIP) expression. *Carcinogenesis* **21:**1619-1622.

Toyoda Y, Hagiya Y, Adachi T, Hoshijima K, Kuo MT, and Ishikawa T (2008) MRP class of human ATP binding cassette (ABC) transporters: historical background and new research directions. *Xenobiotica* **38:**833-862.

Tracy TS and Hummel MA (2004) Modeling kinetic data from *in vitro* drug metabolism enzyme experiments. *Drug Metab Rev* **36:**231-242.

Tseng S, Lin S, Chen J, Su Y, Huang H, Chen C, Lin P, and Chen Y (2004) Resveratrol suppresses the angiogenesis and tumor growth of gliomas in rats. *Clin Cancer Res* **10:**2190-2202.

Turgeon D, Carrier JS, Lévesque E, Hum DW, and Bélanger A (2001) Relative enzymatic activity, protein stability, and tissue distribution of human steroid-metabolizing UGT2B subfamily members. *Endocrinology* **142:**778-787.

Valenzano DR, Terzibasi E, Genade T, Cattaneo A, Domenici L, and Cellerino A (2006) Resveratrol prolongs lifespan and retards the onset of age-related markers in a short-lived vertebrate. *Curr Biol* **16:**296-300.

van de Wetering K, Burkon A, Feddema W, Bot A, de Jonge H, Somoza V, and Borst P (2009) Intestinal breast cancer resistance protein (BCRP)/Bcrp1 and multidrug resistance protein 3 (MRP3)/Mrp3 are involved in the pharmacokinetics of resveratrol. *Mol Pharmacol* **75:**876-885.

Vitrac X, Desmoulière A, Brouillaud B, Krisa S, Deffieux G, Barthe N, Rosenbaum J, and Mérillon JM (2003) Distribution of [14C]-trans-resveratrol, a cancer chemopreventive polyphenol, in mouse tissues after oral administration. *Life Sci* **72:**2219-2233.

Wacher VJ, Silverman JA, Zhang Y, and Benet LZ (1998) Role of P-glycoprotein and cytochrome P450 3A in limiting oral absorption of peptides and peptidomimetics. *J Pharm Sci* **87:**1322-1330.

Walle T, Hsieh F, DeLegge MH, Oatis JE, and Walle UK (2004) High absorption but very low bioavailability of oral resveratrol in humans. *Drug Metab Dispos* **32:**1377-1382.

Wang D, Hang T, Wu C, and Liu W (2005a) Identification of the major metabolites of resveratrol in rat urine by HPLC-MS/MS. *J Chromatogr B Analyt Technol Biomed Life Sci* **829:**97-106.

Wang J, Gao JS, Chen JW, Li F, and Tian J (2012a) Effect of resveratrol on cartilage protection and apoptosis inhibition in experimental osteoarthritis of rabbit. *Rheumatol Int* **32:**1541-1548.

Wang Q, Strab R, Kardos P, Ferguson C, Li J, Owen A, and Hidalgo IJ (2008) Application and limitation of inhibitors in drug-transporter interactions studies. *Int J Pharm* **356:**12-18.

Wang T, Agarwal S, and Elmquist WF (2012b) Brain distribution of cediranib is limited by active efflux at the blood-brain barrier. *J Pharmacol Exp Ther* **341:**386-395.

Wang TT, Schoene NW, Kim YS, Mizuno CS, and Rimando AM (2010) Differential effects of resveratrol and its naturally occurring methylether analogs on cell cycle and apoptosis in human androgen-responsive LNCaP cancer cells. *Mol Nutr Food Res* **54:**335-344.

Wang Z, Zou J, Cao K, Hsieh TC, Huang Y, and Wu JM (2005b) Dealcoholized red wine containing known amounts of resveratrol suppresses atherosclerosis in hypercholesterolemic rabbits without affecting plasma lipid levels. *Int J Mol Med* **16:**533-540.

Weng CJ, Wu CF, Huang HW, Wu CH, Ho CT, and Yen GC (2010) Evaluation of anti-invasion effect of resveratrol and related methoxy analogues on human hepatocarcinoma cells. *J Agric Food Chem* **58:**2886-2894.

Wenzel E, Soldo T, Erbersdobler H, and Somoza V (2005) Bioactivity and metabolism of trans-resveratrol orally administered to Wistar rats. *Mol Nutr Food Res* **49:**482-494.

Wenzel E and Somoza V (2005) Metabolism and bioavailability of trans-resveratrol. *Mol Nutr Food Res* **49:**472-481.

Wu JM, Wang ZR, Hsieh TC, Bruder JL, Zou JG, and Huang YZ (2001) Mechanism of cardioprotection by resveratrol, a phenolic antioxidant present in red wine (Review). *Int J Mol Med* **8:**3-17.

Yamaoka K, Nakagawa T, and Uno T (1978) Statistical moments in pharmacokinetics. *J Pharmacokinet Biopharm* **6:**547-558.

Yang YT, Weng CJ, Ho CT, and Yen GC (2009) Resveratrol analog-3,5,4'-trimethoxy-trans-stilbene inhibits invasion of human lung adenocarcinoma cells by suppressing the MAPK pathway and decreasing matrix metalloproteinase-2 expression. *Mol Nutr Food Res* **53:**407-416.

Yates JW and Arundel PA (2008) On the volume of distribution at steady state and its relationship with two-compartmental models. *J Pharm Sci* **97:**111-122.

Yu C, Shin YG, Chow A, Li Y, Kosmeder JW, Lee YS, Hirschelman WH, Pezzuto JM, Mehta RG, and van Breemen RB (2002) Human, rat, and mouse metabolism of resveratrol. *Pharm Res* **19:**1907-1914.

Yu C, Shin YG, Kosmeder JW, Pezzuto JM, and van Breemen RB (2003) Liquid chromatography/tandem mass spectrometric determination of inhibition of human cytochrome P450 isozymes by resveratrol and resveratrol-3-sulfate. *Rapid Commun Mass Spectrom* **17:**307-313.

Yuan Q, Peng J, Liu SY, Wang CJ, Xiang DX, Xiong XM, Hu CP, and Li YJ (2010) Inhibitory effect of resveratrol derivative BTM-0512 on high glucose-induced cell senescence involves dimethylaminohydrolase/asymmetric dimethylarginine pathway. *Clin Exp Pharmacol Physiol* **37:**630-635.

Zelcer N, Reid G, Wielinga P, Kuil A, van der Heijden I, Schuetz JD, and Borst P (2003) Steroid and bile acid conjugates are substrates of human multidrug-resistance protein (MRP) 4 (ATP-binding cassette C4). *Biochem J* **371:**361-367.

Zhang L, Huang M, Blair IA, and Penning TM (2012a) Detoxication of benzo[a]pyrene-7,8-dione by sulfotransferases (SULTs) in human lung cells. *J Biol Chem* **287:**29909-29920.

Zhang L, Zhang Y, and Huang SM (2009) Scientific and regulatory perspectives on metabolizing enzyme-transporter interplay and its role in drug interactions: challenges in predicting drug interactions. *Mol Pharm* **6:**1766-1774.

Zhang W, Wang X, and Chen T (2011) Resveratrol induces mitochondria-mediated AIF and to a lesser extent caspase-9-dependent apoptosis in human lung adenocarcinoma ASTC-a-1 cells. *Mol Cell Biochem* **354:**29-37.

Zhang W, Wang X, and Chen T (2012b) Resveratrol induces apoptosis via a Bak-mediated intrinsic pathway in human lung adenocarcinoma cells. *Cell Signal* **24:**1037-1046.

Zheng GZ, Bhatia P, Kolasa T, Patel M, El Kouhen OF, Chang R, Uchic ME, Miller L, Baker S, Lehto SG, Honore P, Wetter JM, Marsh KC, Moreland RB, Brioni JD, and Stewart AO (2006) Correlation between brain/plasma ratios and efficacy in neuropathic pain models of selective metabotropic glutamate receptor 1 antagonists. *Bioorg Med Chem Lett* **16:**4936-4940.

Zheng Z, Fang JL, and Lazarus P (2002) Glucuronidation: an important mechanism for detoxification of benzo[a]pyrene metabolites in aerodigestive tract tissues. *Drug Metab Dispos* **30:**397-403.

Zhirkov YuA and Piotrovskii VK (1984) On the usefulness of ultrafiltration in drug-protein binding studies. *J Pharm Pharmacol* **36:**844-845.

Zhou H, Chen Q, Kong DL, Guo J, Wang Q, and Yu SY (2011) Effect of resveratrol on gliotransmitter levels and p38 activities in cultured astrocytes. *Neurochem Res* **36:**17-26.

APPENDIX

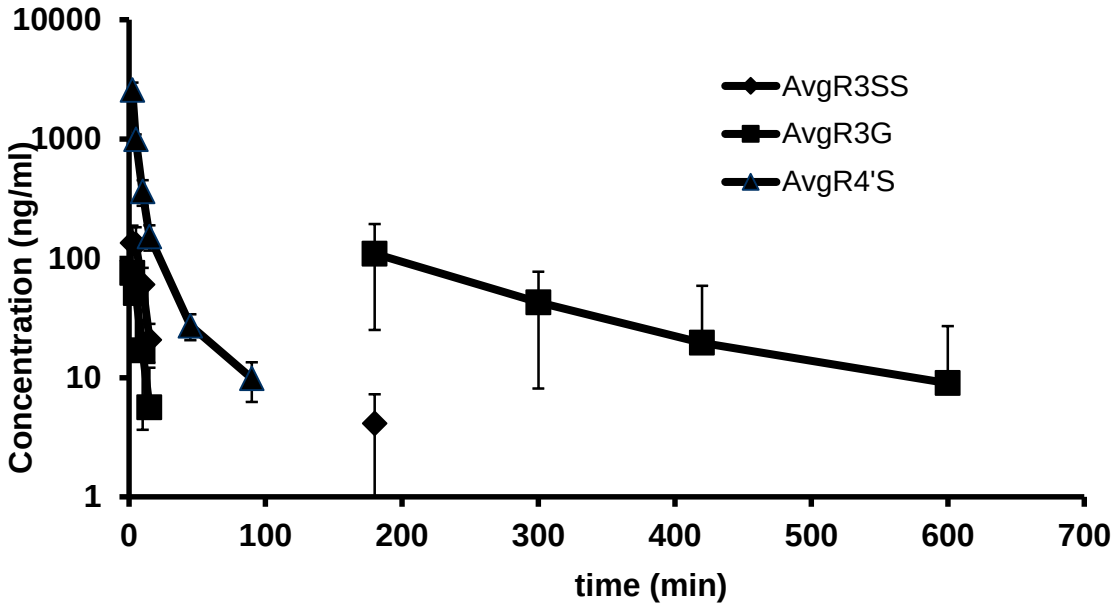

Fig A: Mean plasma concentration profiles after administration of 5 mg/kg of R4'S (i.a., n = 4). Data is presented as mean ± SD.

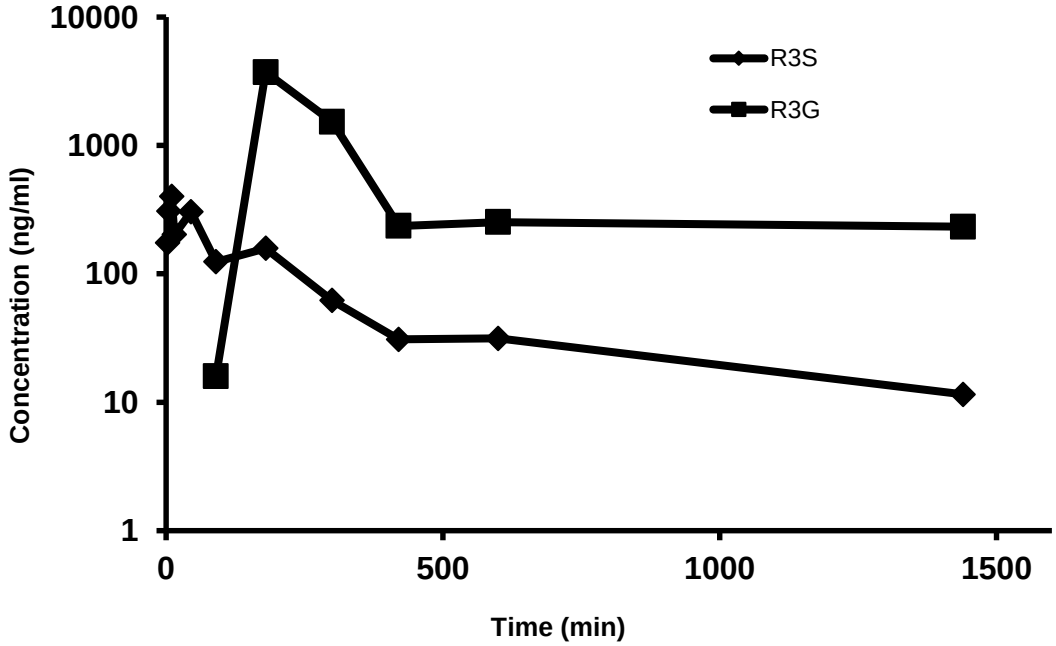

Fig B: Plasma concentration profile after administration of 40 mg/kg of R3S (oral, n =1)

Drug administration, sample collection and urine sample preparation for metabolite identification study: For examination of *in vivo* TMS metabolism, a single oral dose of 20 mg/kg of TMS or saline was administered to two groups of 5 healthy C57BL/6 male mice. Urine samples were collected in metabolism cages (5 mice per cage) for 24 h after administration of vehicle (control group, n = 5) or TMS (test group, n = 5). These samples were stored at -80°C until analysis. To 50 uL of control and TMS treated group urine samples, 100uL of methanol was added to precipitate proteins. After centrifugation at 15000 rpm for 15 min, the supernatant was transferred into vials for LC/MS/MS analysis.

LC/MS/MS method for metabolite identification of TMS in urine: The LC-MS/MS assay was carried out on an Agilent series 1100 high-performance liquid chromatography system equipped with a binary pump, autosampler and degasser coupled to an API 4000 triple-quadrupole tandem mass spectrometer from ABSciex with ESI source operated in both negative and positive ion mode. Analyst software version 1.4.2 (ABSciex) was used for instrument control, data acquisition and data processing for both chromatography and mass spectrometry. The chromatographic separation system consisted of a guard column (Zorbax SB-C18, 5 um, 4.6 × 12.5 mm; Agilent Technologies), an analytical column (Zorbax SB-C18, 5 um, 4.6 × 250 mm; Agilent Technologies) and a mobile phase of A 10mM ammonium acetate and B acetonitrile containing 0.2% formic acid (pH = 3). The elution started with 90% A at 0 min to 2 min and then to 60% at 7 min, 40% at min 12, 10% at min 25 and 90% at min 27. Flow rate of the mobile phase was 1ml/min and the flow from the column was split 1:3 into an ABSciex API4000 triple quadrupole mass

spectrometer equipped with a Turbo ionspray source operating at 450°C. The column temperature was maintained at 35°C. Nitrogen was used as the curtain, collision and ion source gas.

Preliminary metabolite identification in mouse urine: We used knowledge based metabolite identification strategy for structural characterization and identification of TMS metabolites. It has been found that demethylation (M-14) was the major biotransformation pathway for nobiletin (a polymethoxyflavones) (Li et al., 2006). Therefore, we postulated that demethylation can be the major biotransformation pathway for TMS. With our previous study with RES we knew that RES is a good substrate for phase II biotransformation, such as glucuronidation (M+176) and sulfation (M+80). So, we postulated that TMS after demethylation can be further glucuronidated or sulfated. In addition it has been also reported that RES can be metabolized to form dihydro and hydroxylated metabolites, such as dihydroresveratrol sulfates, glucuronides and piceatannol. We first used neutral loss scan (NL) mode to search all possible phase II conjugated metabolites from mouse urine samples collected after administration of TMS (20 mg/Kg oral). Identification of phase II metabolites made our work easy to identify the phase I metabolites, as it was easy to postulate the probable phase I metabolites which might have given rise to phase II metabolites. Below is the scheme of TMS metabolism we hypothesize based on the prior knowledge of polymethoxy flavones (Li et al., 2006), RES (Baur and Sinclair, 2006) and pterostilbene (Shao et al., 2010) metabolism.

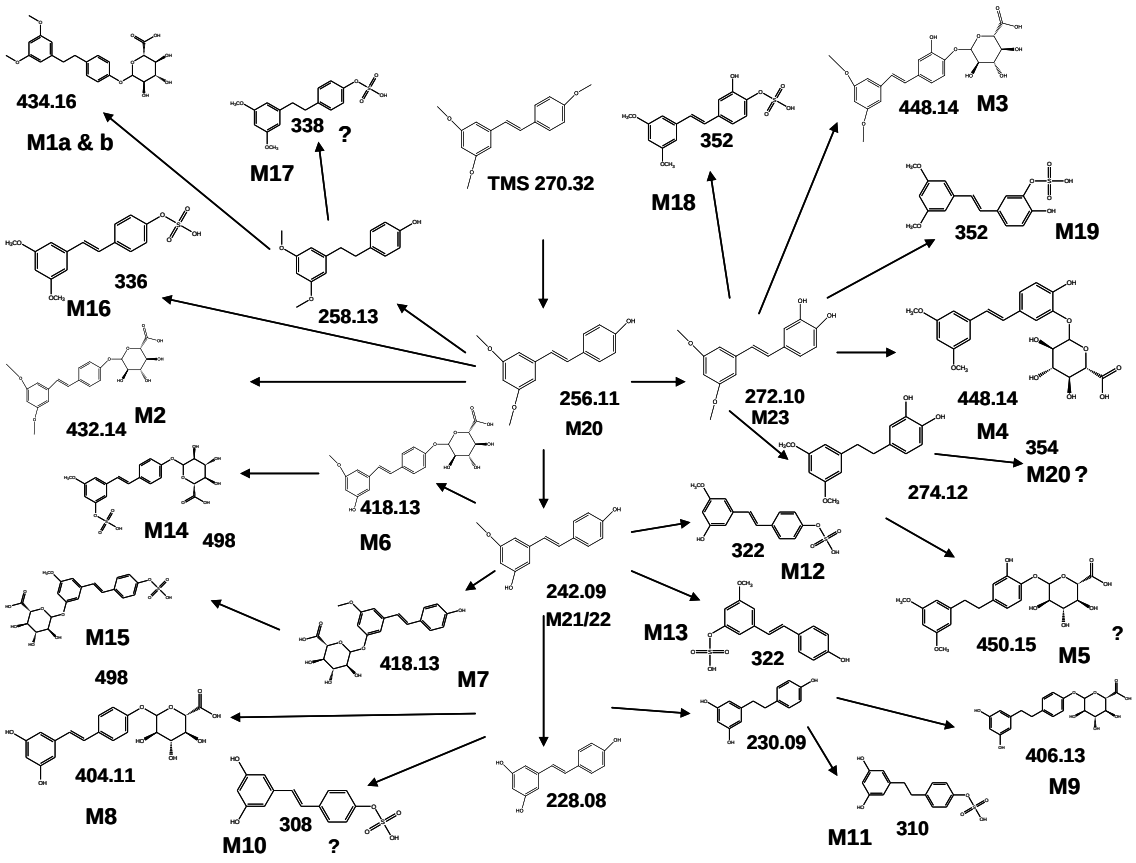

Fig C: Proposed metabolites of TMS

Product ion analysis for M2 with a m/z of 431, in negative ion mode at collision energy of 30 gave a major product ion peak of 255 (-14 + 176), which depicts demethylation and glucuronidation of TMS (Fig 8.5). A peak at m/z 431 was also observed as a single peak in a neutral loss scan of 176.

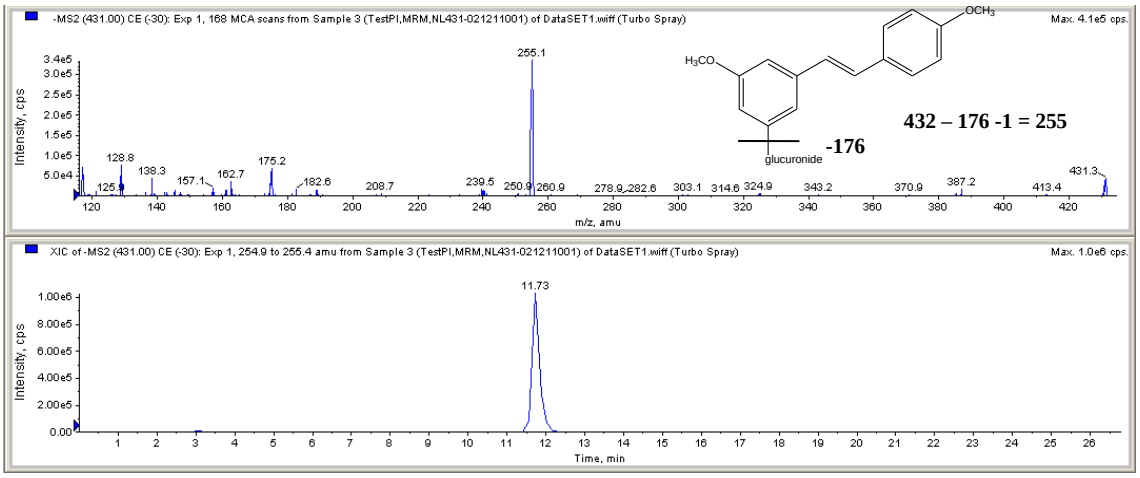

Fig D: ESI of M2 in negative ion mode at collision energy of 30. The CID porduct ion spectrum of M2 afforded TMS (-14 + 176). A peak at m/z 431 was also observed as a single peak in a neutral loss scan of 176.

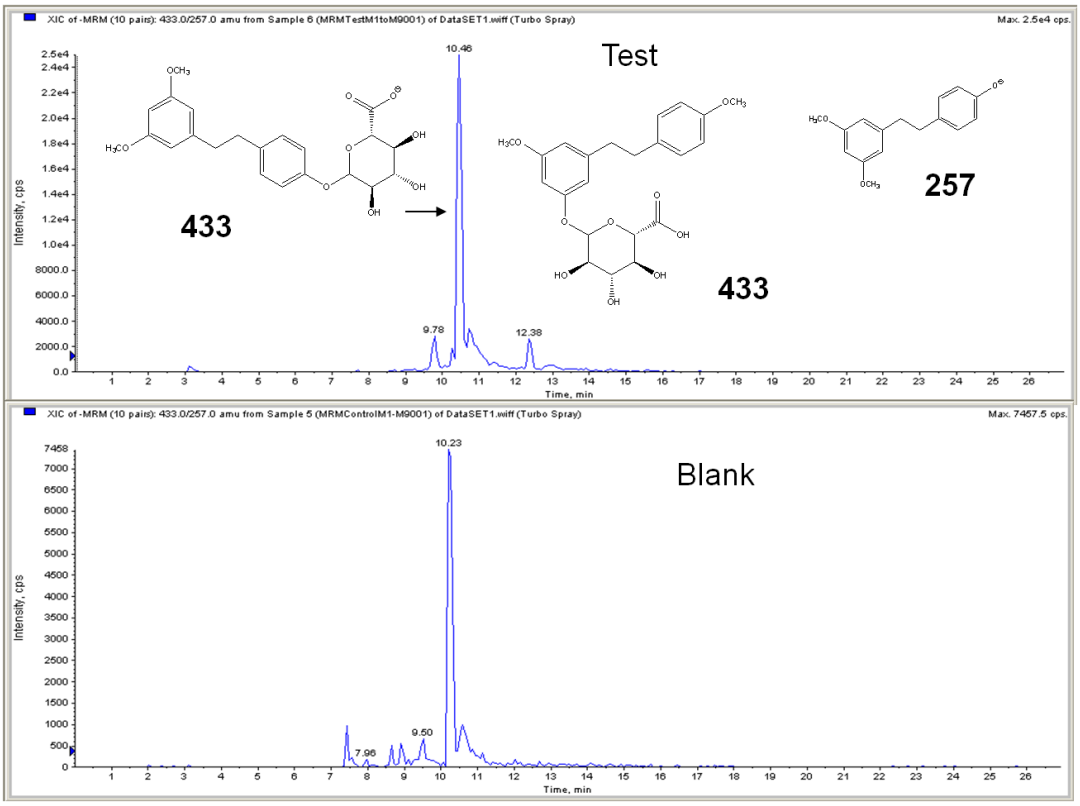

Fig E: MRM of 434 (433 – 257) Test and Blank urine.

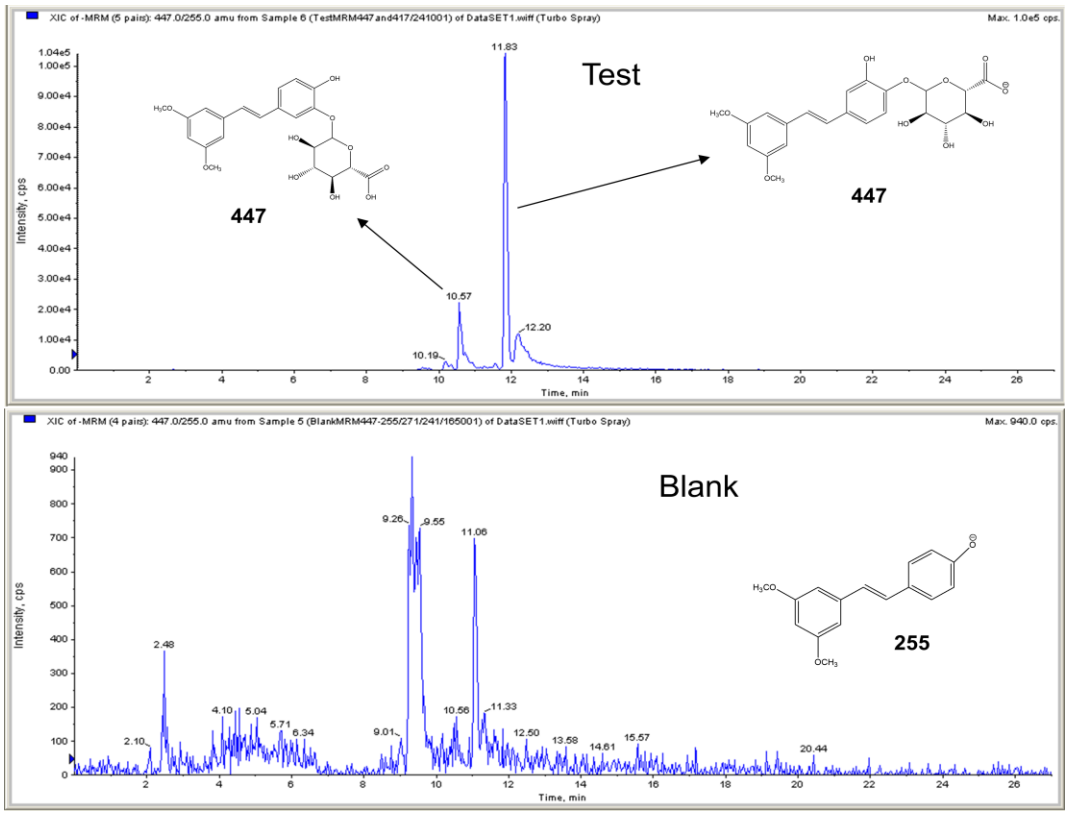

Fig F: MRM 448 (447 – 255) Test and Blank urine.

Hepatic Desulfation Assay: Desulfation of R3S was determined in pooled human liver microsomes. Conditions of protein and time linearity were not optimized. The incubation mixture consisted of the substrate R3S (final concentration range of 0.01 uM to 1 mM of R3S) solubilized in water, alamethicin (10 ug/ml), $MgCl_2$ (5 mM final concentration), and potassium phosphate buffer (10 mM, pH 6.5, 37°C). The reaction mixture was preincubated for 3 min in a shaking water bath at 37°C. The reaction was started by adding 0.5 uL of HLM (final concentration 0.5 mg/ml) and incubated in a shaking water bath for 60 min at 37°C. Appropriate negative control experiments were performed under the same conditions but without the HLM. All reactions were performed in triplicate. For all incubations, 5 uL of ascorbic acid (15%) and 60 uL of ice cold methanol containing

APAP (IS) were added to 20 uL of reaction mixture at the end of 60 min to stop the reaction. The kinetic profile of R3S desulfation followed partial substrate inhibition kinetics. The Vmax was found to be 2.26 ± 0.29 nmol/min/mg, Km to be 195.3 ± 41.96 uM and Ki to be 1959 ± 848.9 uM.

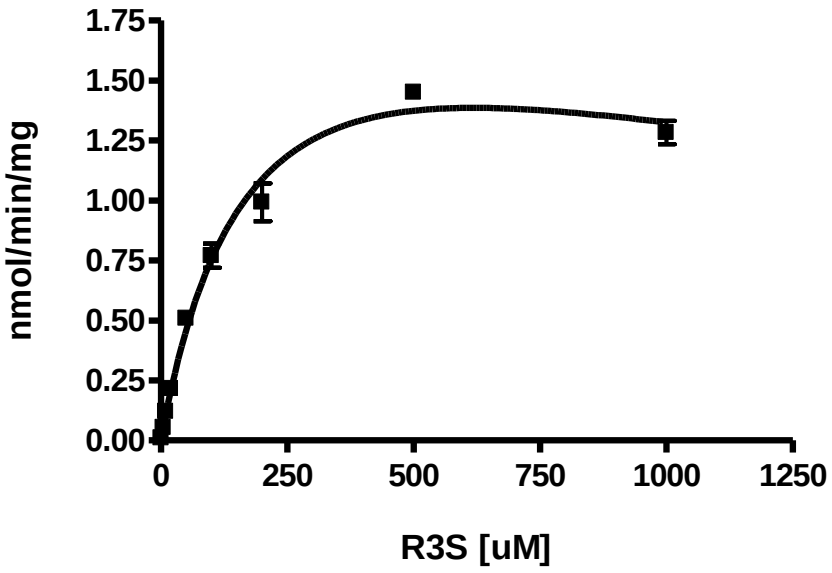

Fig G: Kinetics of RES formation from R3S in human lung microsomes. Data reported as mean ± standard deviation, (n = 3). The solid line represents curve fitting with the partial substrate inhibition equation (Eq 3.4).

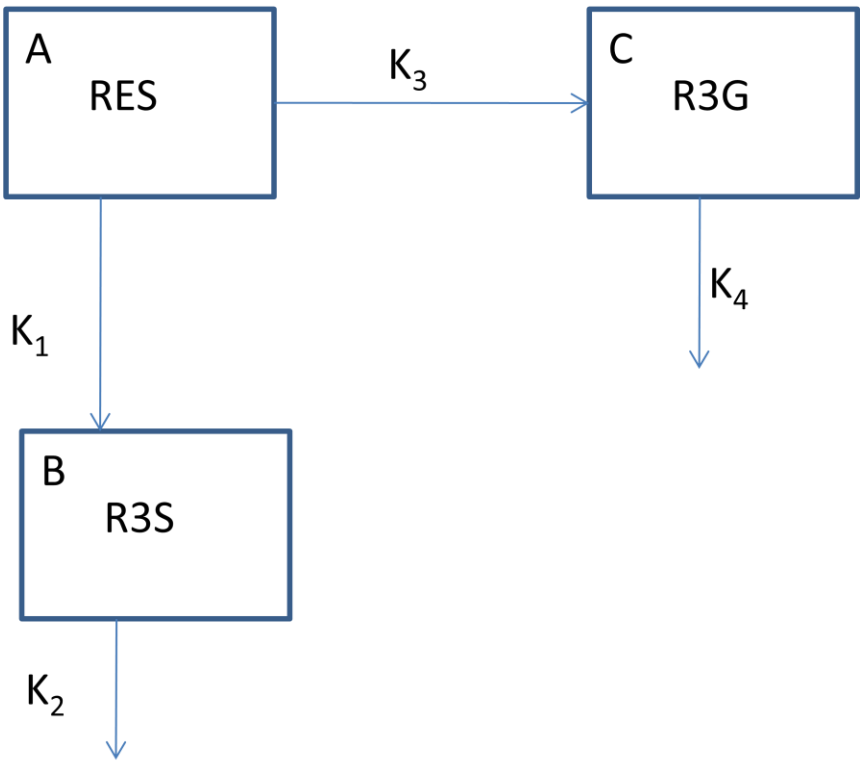

Fig H: Simplified model of RES metabolism, assuming RES is completely and irreversibly metabolized into R3S and R3G.

1) **When Res 15 mg/kg is dosed IA:**

Rate of change of Res (dA/dt):

$dA/dt = -(K1 + K3)*A$

$$Dose^{Res} = (CL_1 + CL_3)* (AUC)^{Res}_{Res} \quad (1)$$

Rate of change of R3S (dB/dt):

$dB/dt = K_1*A – (K_2)*B$

$$0 = CL_1*(AUC)^{Res}_{Res} – (CL_2) *(AUC)^{Res}_{R3S}$$

$$CL_1 = (CL_2) *[(AUC)^{Res}_{R3S} / (AUC)^{Res}_{Res}] \quad (2)$$

Rate of change of R3G (dC/dt):

$dC/dt = K3*A - K4*C$

$$0 = CL_3*(AUC)_{Res}^{Res} - CL_4*(AUC)_{R3G}^{Res} \quad (3)$$

2) When R3S is dosed:

Rate of change of R3S (dB/dt):

$dB/dt = K_1*A - (K_2)*B$

$$- Dose^{R3S} = CL_1 *(AUC)_{Res}^{R3S} - (CL_2)*(AUC)_{R3S}^{R3S}$$

Since,$(AUC)_{Res}^{R3S}$ is zero, as per our assumption, no RES formed after R3S administration.

$$CL_2 = Dose^{R3S}/(AUC)_{R3S}^{R3S} \quad (4)$$

3) Similarly, when R3G is dosed:

Rate of change of R3G (dC/dt):

$dC/dt = K3*A - K4*C$

$$- Dose^{R3G} = CL_3*(AUC)_{Res}^{R3G} - CL_4*(AUC)_{R3G}^{R3G}$$

Since the amount of RES formed from IA R3G dosing is assumed to be zero,

$$CL_4 = Dose^{R3G} / (AUC)_{R3G}^{R3G} \quad (5)$$

Now,

$fm_{R3S} = CL1/(CL1+CL3)$

So, using equations 2 and 4 we get,

$$CL_1 = [Dose^{R3S}/(AUC)^{R3S}_{R3S}] * [(AUC)^{Res}_{R3S} / (AUC)^{Res}_{Res}] \quad (6)$$

Now using equation,

$$(CL_1 + CL_3) = Dose^{Res} / (AUC)^{Res}_{Res} \quad (7)$$

Using equations 6 and 7,

$$fm_{R3S} = [AUC)^{Res}_{R3S} / AUC)^{R3S}_{R3S}] / [Dose^{R3S} / Dose^{Res}] \quad (8)$$

Similarly,

$fm_{R3G} = CL3/(CL1+CL3)$

So, using equations 3 and 5 we get,

$$CL3 = [Dose^{R3G} / (AUC)^{R3G}_{R3G}] * [(AUC)^{Res}_{R3G} / (AUC)^{Res}_{Res}] \quad (9)$$

So, now using equations 9 and 7 we get,

$$fm_{R3G} = [AUC)^{Res}_{R3G} / (AUC)^{R3G}_{R3G}] / [Dose^{R3G} / Dose^{Res}] \quad (10)$$